FINAL REPORT
U.S. Department of Energy

COLLOID-FACILITATED TRANSPORT OF RADIONUCLIDES THROUGH THE VADOSE ZONE

Principal Investigator:

Markus Flury
Department of Crop and Soil Sciences
Washington State University

Collaborators:

James B. Harsh
Department of Crop and Soil Sciences
Washington State University

Yan Jin
Department of Plant and Soil Sciences
University of Delaware

John M. Zachara
Environmental Molecular Science Laboratory
Pacific Northwest National Laboratories

Project Number:
70135

Grant Number:
DE-FG07-99ER62882

Grant Project Officers:
Francis J. Wobber
Chester E. Miller
Kara Twitchell

Project Duration:
September 15, 1999 to September 14, 2002
(no-cost extension until September 14, 2003)

Contents

1 Executive Summary **3**

2 Research Objectives **6**

3 Methods and Results **7**

3.1 Experimental Methods . . . 7

3.1.1 General Scheme of Experiments . . . 7

3.1.2 Sediments . . . 7

3.1.3 Colloid Formation . . . 7

3.1.4 Cs Sorption to Colloids . . . 8

3.1.5 Colloid Mobilization and Transport . . . 8

3.1.6 Cs Transport through Hanford Sediments . . . 9

3.1.7 Colloid-Facilitated Cs Transport . . . 9

3.2 Principal Results . . . 10

3.2.1 Colloid Formation . . . 10

3.2.2 Cs Sorption to Colloids . . . 15

3.2.3 Colloid Mobilization and Transport . . . 15

3.2.4 Cs Transport through Hanford Sediments . . . 17

3.2.5 Colloid-Facilitated Cs Transport . . . 17

4 Relevance, Impact, and Technology Transfer **20**

5 Project Productivity **22**

6 Personnel Supported **22**

7 Publications **23**

7.1 Published in Peer-reviewed Journals . . . 23

7.2 Published in Unreviewed Publications . . . 23

7.3 Submitted for Publication . . . 23

8 Interactions **23**

9 Transitions **26**

10 Patents **26**

Literature Cited **27**

Appendix: Reprints and Preprints of Publications **28**

1 Executive Summary

The main purpose of this project was to advance the basic scientific understanding of colloid and colloid-facilitated Cs transport of radionuclides in the vadose zone. We focused our research on the hydrological and geochemical conditions beneath the leaking waste tanks at the USDOE Hanford reservation. Specific objectives were (1) to determine mineral alterations and transformations under the extreme geochemical conditions occurring during leakage of tank waste, (2) to characterize interactions between colloids (particles with diameter less than 2 μm, which remain suspended in an aqueous solution for an extended period of time), sediments, and the radionuclide Cs, (3) to evaluate mobility of colloids beneath Hanford waste tanks, and (4) to determine whether colloids can enhance the movement of the radionuclide Cs.

We have shown that upon contact with simulated waste tank solutions, Hanford sediments change their mineralogical composition. Certain minerals, i.e., quartz, smectite, and kaolinite, are partially dissolved, and new mineral phases, i.e., the feldspathoids cancrinite and sodalite, are formed. We have extensively characterized these mineral transformations. The new minerals were mainly in the colloidal size fraction (diameter less than 2 μm) and had a negative surface charge. The new minerals sorbed the radionuclide Cs strongly. Transport experiments under water saturated and unsaturated conditions showed that the colloids were mobile in Hanford sediments. As the water saturation of the sediments decreased, the amount of colloids transported also decreased. The colloids had the ability to enhance the migration of the radionuclide Cs; however, Cs initially sorbed to colloids was desorbed during transport through uncontaminated Hanford sediments. The finding that Cs was stripped off the colloids during the transport through uncontaminated sediments implies that colloids will likely not be an effective carrier for Cs, unless the Cs is incorpo-

rated into the mineral structure of the colloids such that the radionuclide cannot desorb from the colloids. Nevertheless, it appears that the amount of Cs that can be transported by mobile colloids beneath Hanford waste tanks is limited. Colloids will not be able to move the bulk mass of Cs through the vadose zone at Hanford.

The results of this project are relevant for remediation and long-term environmental management of Cs contamination beneath the Hanford waste tanks. Our results indicate that mobile colloidal particles may exist in the sediments below the waste tanks, and that these particles may enhance the movement of a small fraction of the Cs residing below the tanks. However, it is unlikely that a significant amount of Cs can be mobilized with the colloids, unless the present geochemical and hydrological conditions change in a way that would mobilize a large amount of particles. Large amounts of colloids could be mobilized through artificial recharge of low ionic strength water, i.e., flooding of the area. Under present conditions, however, it appears that the main mass of Cs located in the vadose zone will not migrate much further. Even if colloids are sorbing the Cs and moving downward, much of the sorbed Cs will be stripped off the colloids as the colloids move through uncontaminated sediments, and deep migration of Cs is unlikely. These results support findings from other EMSP projects that show that the current depth distribution of Cs beneath Hanford waste tanks can be explained by ion exchange reactions, and further downward movement of Cs is unlikely.

The project has supported, in part, three graduate students. One MS student has graduated and the results of his thesis have been published (Cherrey, K.D., M. Flury, and J.B. Harsh, Nitrate and colloid transport through coarse Hanford sediments under steady-state, variably-saturated flow, *Water Resour. Res.*, *39*, 1165, doi:10.1029/2002WR001944, 2003). One PhD student is graduating in December 2003, and her dissertation is being

written up. This dissertation will contain three chapters, the first of which has been submitted for publication (Mashal, K., J.B. Harsh, M. Flury, and A. Felmy, Colloid formation in Hanford sediments reacted with simulated tank waste, *Environ. Sci. Technol.*, submitted, 2003). The second PhD student will graduate in Summer 2004, and only preliminary results from his dissertation are available to date. Results of all three theses are incorporated into the executive summary provided above. The project has also supported, in part, three postdoctoral scientists.

2 Research Objectives

Contaminants have leaked into the vadose zone at the USDOE Hanford reservation. It is important to understand the fate and transport of these contaminants to design remediation strategies and long-term waste management plans at the Hanford reservation. Colloids may play an important role in fate and transport of strongly sorbing contaminants, such as Cs or Pu.

This project seeks to improve the basic understanding of colloid and colloid-facilitated transport of contaminants in the vadose zone. The specific objectives addressed are:

1. Determine the structure, composition, and surface charge characteristics of colloidal particles formed under conditions similar to those occurring during leakage of waste typical of Hanford tank supernatants into soils and sediments surrounding the tanks.

2. Characterize the mutual interactions between colloids, contaminant, and soil matrix in batch experiments under various ionic strength and pH conditions. We will investigate the nature of the solid-liquid interactions and the kinetics of the reactions.

3. Evaluate mobility of colloids through soil under different degrees of water saturation and solution chemistry (ionic strength and pH).

4. Determine the potential of colloids to act as carriers to transport the contaminant through the vadose zone and verify the results through comparison with field samples collected under leaking tanks.

5. Improve conceptual characterization of colloid-contaminant-soil interactions and colloid-facilitated transport for implementation into reactive chemical transport models.

This project was in part supported by an NSF-IGERT grant to Washington State University. The IGERT grant provided funding for graduate student research and education, and two graduate students were involved in the EMSP project. The IGERT program also supported undergraduate internships.

The project is part of a larger EMSP program to study fate and transport of contaminants under leaking Hanford waste tanks. The project has close relations to the following EMSP projects:

- Project: 70126, Interfacial Soil Chemistry of Radionuclides in the Unsaturated Zone (PI: Jon Chorover)

- Project: 70070, Reactivity of Primary Soil Minerals and Secondary Precipitates (PI: Kathy Nagy)

- Cesium Transport in Hanford Sediments: Application of an Experimentally Based Cation Exchange Model (PI: Susan Carroll and Carl Steefel)

3 Methods and Results

3.1 Experimental Methods

3.1.1 General Scheme of Experiments

A series of batch and transport experiments were carried out, and the experimental methods are summarized below for each of these experiments. The experiments aimed at fractionating native colloidal materials found in Hanford sediments and at identifying transformation products formed after contact of sediments with simulated Hanford waste tank solutions. Native colloids and transformation products were then used to study Cs sorption, colloid transport, and colloid-facilitated Cs transport.

3.1.2 Sediments

Sediments used in this study were collected from the submarine pit (218-E-12B) at the Hanford site in January 2000. These sediments are representative, both in texture and mineralogy, of the material underlying the immediate vicinity of the S-SX (single-shell) tank farm at Hanford. The sediments were air dried and sieved through a 2 mm square screen. These sediments were used for reaction studies with simulated Hanford tank solutions and for transport studies to investigate transport of colloids and Cs-137. These sediments have been used by other EMSP investigators and extensive characterization data are given elsewhere [*Serne et al.,* 2002].

3.1.3 Colloid Formation

We reacted the Hanford sediments with different simulated tank waste (STW) solutions in a series of batch experiments (Table 1). The STW solutions mimic conditions in the Hanford waste tanks. One kilogram of sediment (diameter < 2 mm) and 1 L of simulated waste tank solutions were placed into air-tight capped 2 L polyethylene bottles. Temperature was controlled at 50°C by an electric oven and the reaction times were 25 and 40 days. After the specified time periods, sediments and liquids were separated by centrifugation and the colloidal fraction of the reacted sediments was characterized with x-ray diffraction (XRD), FTIR spectroscopy, NMR, scanning and transmission electron microscopy, electrophoretic mobility, and BET surface area. Supernatant chemical composition was determined and used for chemical modeling with the GMIN code.

We studied the kinetics of the mineral transformations by examining transformation products after 1, 10, 25, and 50 days reaction time. Colloid formation was also studied under column flow through conditions, whereby a tank leak was simulated by infiltrating STW solutions into columns packed with Hanford sediments, followed by leaching with low-ionic strength water.

Pure reference clay minerals were also reacted with the simulated tank solutions to test which minerals are most susceptible to Hanford waste solution attack. We reacted kaolinite, illite, quartz, and micas with simulated tank waste. Reaction products were extensively characterized with XRD, FTIR, NMR, and SEM/TEM. We also used Cs in the

Table 1. Composition of simulated tank waste (STW), prepared at room temperature (20 to 22°C), and experimental conditions of batch experiments.

Designation of solution	NaOH	$NaAlO_4$ (mol/kg)	$NaNO_3$	pH	Temperature[a] (°C)	Time[a] (days)	Designation of colloids formed
Control[b]	0	0	0	7.1[b]	50	40	colloid 0
STW1	1.4	0.125	3.7	14.2[c]	50	25, 40	colloid 1
STW2	2.8	0.125	3.7	14.5[c]	50	40	colloid 2
STW3	1.4	0.25	3.7	14.2[c]	50	40	colloid 3
STW4	2.8	0.25	3.7	14.5[c]	50	40	colloid 4

[a]Temperature and duration of batch reactions with sediments.
[b]Distilled water.
[c]Determined by titration which measures non-carbonate alkalinity (NCA).

simulated tank waste to see whether Cs can be incorporated into the new mineral phases upon precipitation of the feldspathoid minerals.

3.1.4 Cs Sorption to Colloids

We studied the interactions of the newly formed minerals with the radionuclide Cs. Cesium sorption to unreacted and reacted colloids was studied in a series of batch adsorption and desorption experiments. Adsorption isotherms were constructed and sorption kinetics was investigated over time sequences ranging from 0.25 to 336 hours. Sorption experiments were conducted with standard batch shaking studies. Different cations (Na, K, Ca) were used to investigate their potential to compete with Cs for sorption sites. We determined cation exchange capacity and sorption kinetics of Cs with isotopic exchange experiments using Cs-137 and Na-22.

3.1.5 Colloid Mobilization and Transport

To mimic a Hanford tank leak, we setup a packed column which was initially leached with a high ionic strength simulated tank waste solution (1000 mM $NaNO_3$) followed by a low ionic strength solution (1 mM $NaNO_3$) which represents meteoric water displacing the tank waste. The tank waste contained Cs as contaminant. Column outflow was monitored as function of time for colloidal particles and Cs. Cesium concentrations were determined separately in solution phase and as sorbed species on colloids. Solid material leached out of the column was characterized with SEM, XRD, electrophoretic mobility, and dynamic light scattering. These column experiments were conducted under water-saturated conditions.

Native, unreacted colloids from Hanford sediments and colloids found after reactions of sediments with simulated tank waste solutions were used to investigate the transport potential of these colloids in unsaturated Hanford sediments. A column system was developed with which we could control volumetric water contents with accuracy better than 0.01 effective saturation and the water potentials to better than 0.06 cm-H_2O (Figure 1). Inflow

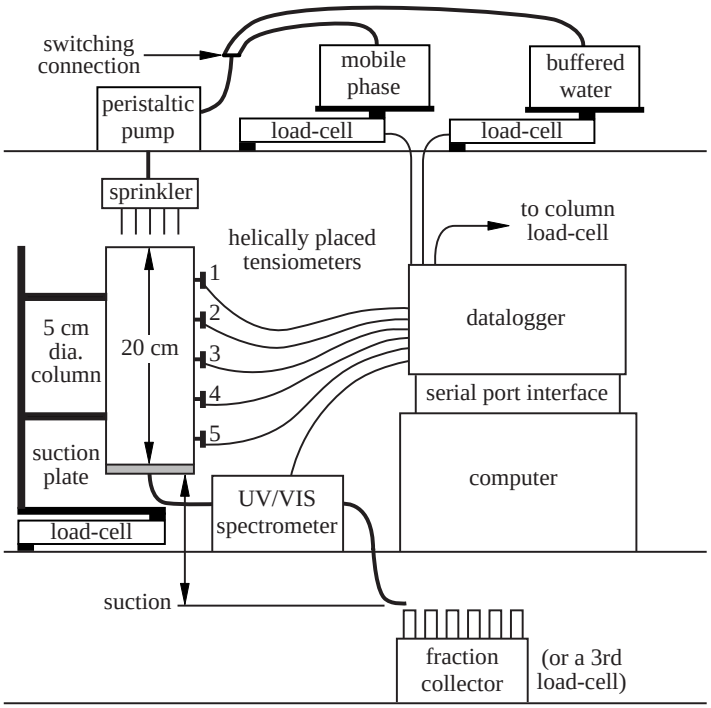

Fig. 1. Schematic of experimental column setup for unsaturated flow experiments.

and outflow boundary conditions had to be meticulously controlled to ensure uniformity of water contents and water potentials inside the column. Colloid breakthrough curves were determined under a series of water contents ranging from 0.2 to 1.0 effective water saturation.

3.1.6 Cs Transport through Hanford Sediments

We investigated the effect of ionic strengths on Cs migration through two types of porous media: silica sand and Hanford sediments. Cesium sorption and transport was studied in 1, 10, 100, and 1000 mM NaCl electrolyte solutions at pH 10. Sorption isotherms were constructed from batch equilibrium experiments and the batch-derived sorption parameters were compared with column breakthrough curves. Column transport experiments were analyzed with a two-site equilibrium-nonequilibrium model.

3.1.7 Colloid-Facilitated Cs Transport

The ability of colloids to facilitate the transport of Cs was investigated with packed column experiments. A series of saturated column experiments were conducted to investigate effects of colloids on Cs transport in two types of porous media (Hanford sediment characteristic of 2:1 clay minerals and silica Ottawa sand). The silica sand medium was used for comparative purposes, as most colloid-facilitated Cs transport experiments have been conducted with

silica sand matrices so far. The colloids used were obtained by reacting Hanford sediment with simulated tank waste solutions as described above. These transport experiments were conducted under water-saturated conditions.

The colloid-facilitated Cs transport experiments were then extended to study colloid-facilitated Cs transport under variably-saturated flow conditions. Transport experiments were conducted under variably-saturated, steady-state flow conditions, with effective water saturations ranging from 0.2 to 1.0 varied in increments of 0.1. The experimental setup developed and used previously for colloids alone was used for these studies (Figure 1).

Nuclear magnetic resonance (NMR) was used to determine whether colloid transport can be visualized in columns filled with Hanford sediments. Colloids were tagged with Cu to make them paramagnetic and colloid-sediment mixtures were tested in the NMR facility of the Pacific Northwest National Laboratory.

3.2 Principal Results

3.2.1 Colloid Formation

The x-ray diffraction pattern of the untreated Hanford sediments indicated that the $< 2\ \mu$m fraction consisted of four major layered aluminosilicates, such as chlorite, smectite, kaolinite and illite, and primary minerals, including quartz, christobalite, albite, and microcline. Upon reaction with tank waste solutions, native minerals released Si and other elements into the solution phase. This Si precipitated with the Al present in the waste solutions to form secondary minerals, identified as the feldspathoids cancrinite and sodalite (Figure 2). The FTIR spectra corroborate the results from the XRD patterns. Electron micrographs of colloids formed from sediment after 25 days of reaction time with STW1 illustrate how the secondary minerals are formed (Figure 3). The spherical structures, associated with sodalite, clearly grow out of the plate-like structures of the original clay minerals (Figure 3b). This indicates that sodalite and cancrinite are the product of secondary nucleation and not the result of a direct solid state transformation [*Barnes et al.,* 1999]. A similar observation has been reported from reactions of simulated tank liquors with pure quartz [*Bickmore et al.,* 2001]. The amount of colloidal material in the sediments increased upon reaction with waste solutions. At the natural pH found in Hanford sediments (pH 8) the newly-formed minerals are negatively charged, similar to the unreacted colloidal material present in the sediments. The formation of colloidal material in Hanford sediments upon reaction with tank waste solutions is an important aspect to consider in the characterization of Hanford tank leaks, and may affect fate and transport of hazardous radionuclides present in the tank waste.

The electrophoretic mobility of the colloidal particles changed considerably after reaction with STW (Figure 4). The unreacted colloids have a negative electrophoretic mobility for pH values ranging from 2.5 to 11, typical for aluminosilicate clays, like smectite, illite, and chlorite [*McBride,* 1989]. The mobility becomes less negative at low pH due to protonation of edge sites or dissolution-exchange reactions with Al [*Swartzen-Allen and Matijevic,*

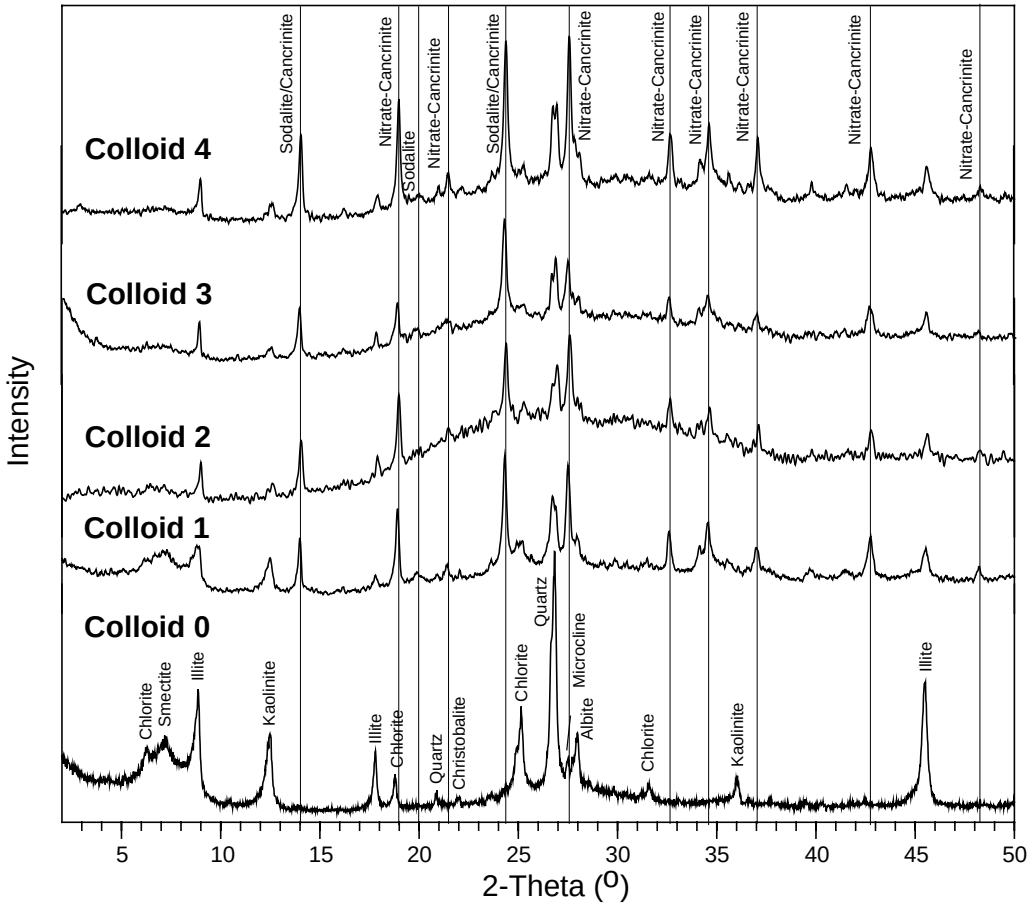

Fig. 2. XRD patterns of unreacted and reacted Hanford sediments at 50°C after 40-days reaction time. Vertical lines are characteristic spacings for nitrate-cancrinite and sodalite.

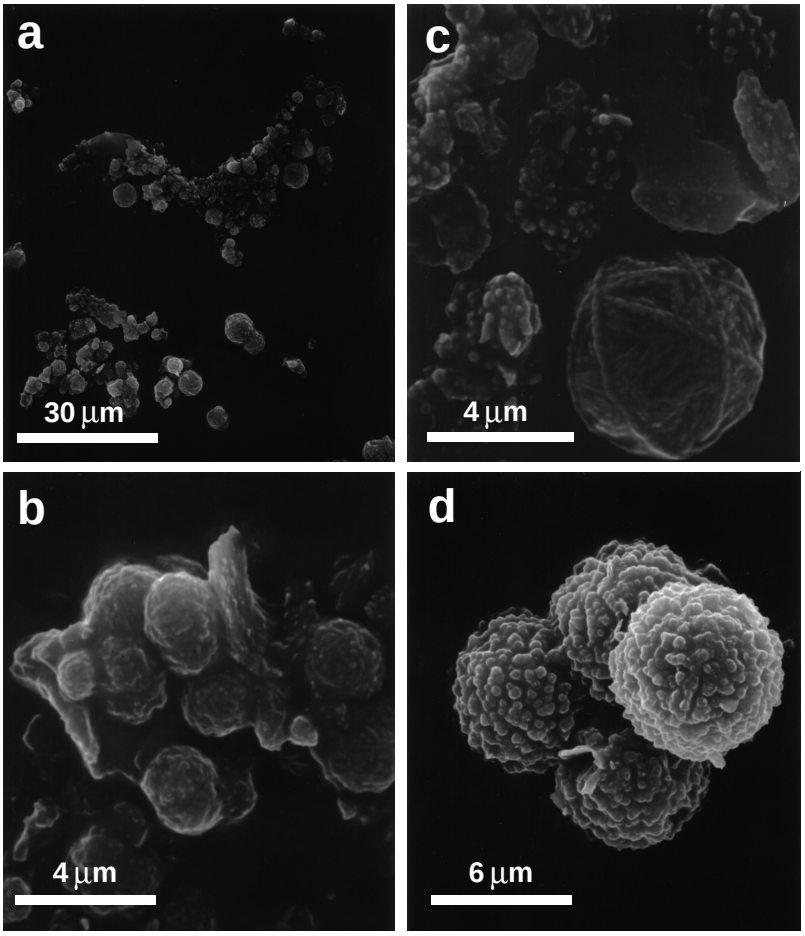

Fig. 3. Scanning electron images of colloidal material in reacted Hanford sediments with STW1 following 25-days reaction time at 50°C. The ball-like structures are cancrinite/sodalite mixtures. Plate-like structures are aluminosilicates originally present in the Hanford sediments.

1974]. The charge reversal observed between pH 6 and 8 is probably due to an artifact resulting from dissolution of the feldspathoids and formation of poorly crystalline aluminosilicates (allophane) and/or aluminum hydroxide. At higher pH, the particles remain negatively charged and have a similar electrophoretic mobility to the unreacted colloids, although slightly more negative. Based on the results from XRD, FTIR, and electron microscopy, we know that the reacted colloids are a composite of unreacted, native minerals, altered native minerals, and secondary mineral phases. The electrophoretic mobility measured is an average of these composite samples, and does not represent the mobility of any individual mineral phase.

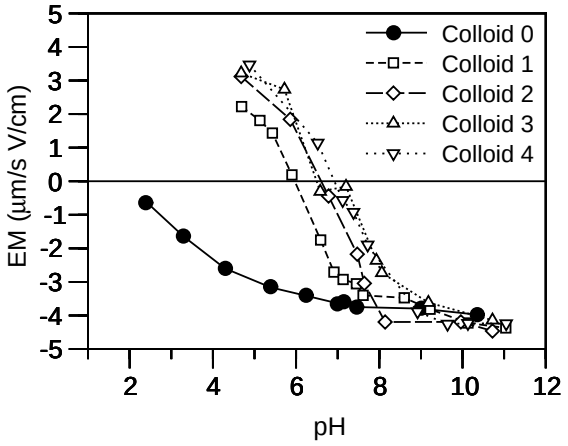

Fig. 4. Electrophoretic mobility of colloidal material in unreacted and reacted Hanford sediments following 40-days reaction time at 50°C.

The negative charge on the colloids at pH values typical for the vadose zone at Hanford (pH > 7.5) suggests that the colloids (1) are likely to form relatively stable suspensions, (2) are not electrostatically attracted to the predominantly negatively charged surfaces of Hanford sediments, and (3) cations such as Cs^{+} and Sr^{2+} will be electrostatically attracted to the colloids.

Pure mineral reaction indicated that there were considerable differences in the reactivity of different minerals. Kaolinite, smectite, and quartz were highly susceptible to waste solution attack. Tank solutions almost completely transformed kaolinite into the feldspathoids cancrinite and sodalite. Time sequences showed that the dissolution of kaolinite and reprecipitation to feldsphatoids was affected by reaction time and by temperature (Figure 5). The feldspathoid products sorbed nearly an order of magnitude more Cs than the unaltered kaolinite. Quartz was partially dissolved and cancrinite and sodalite formed. Illite and the micas seemed to be more resistant against waste solution attack.

The presence of Cs in the simulant solutions did not affect the types of minerals formed in 1 M NaOH solutions until the Cs concentration was greater than 0.1 M, a concentration that is not likely to occur in the sediment underlying the Hanford tanks. Elemental mapping indicated that incorporated Cs was homogeneously distributed in cancrinite and sodalite. High concentrations of Cs promoted the formation of highly crystalline cancrinite. The presence of Cs in solutions precluded the influence anions have shown in the non-cesium system. The presence of chloride anion was favorable for the formation of pure sodalite in a non-cesium solution, yet no sodalite was found in the precipitates formed at high Cs concentration (0.5 M). Adsorption experiments indicated that Cs could access the internal parts of cancrinite and sodalite, but the diffusion appeared more difficult than that of Na and K. Cesium exchange in cancrinite and sodalite caused structural disordering of the minerals as reflected by the XRD patterns.

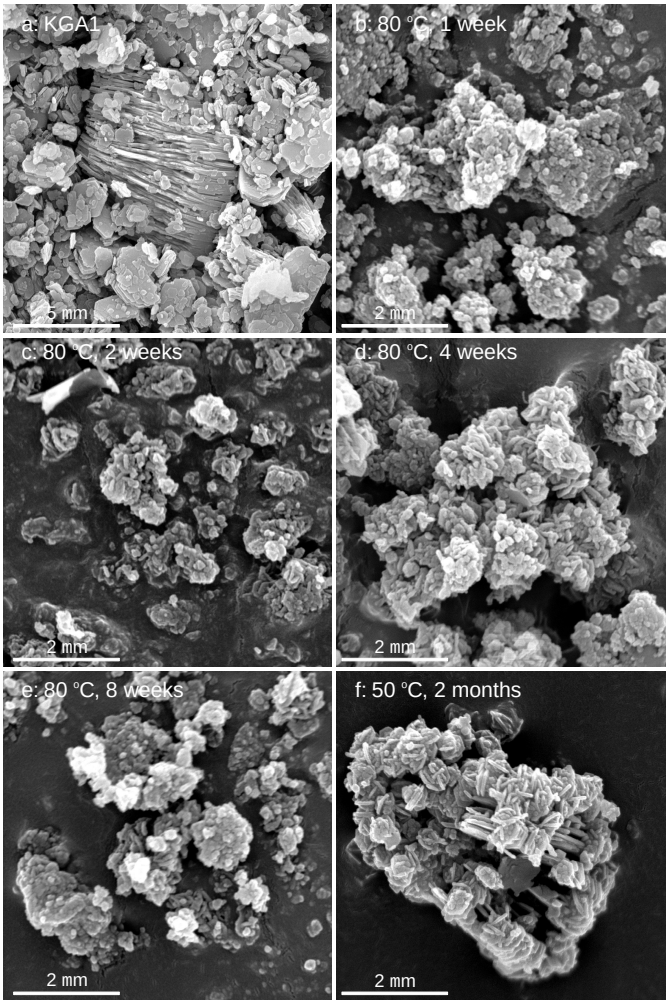

Fig. 5. Mineral morphology change of KGa-1-kaolinite after reacting with STW1 for different times. (a). starting KGa-1 kaolinite with vermiform structure; (b to e). after 1, 2, 4, 8 weeks of reaction at 80°C, respectively; (f). after 2 months of reaction at 50°C.

3.2.2 Cs Sorption to Colloids

The Hanford colloids had sites of different affinity for Cs sorption. The results support the finding from others [*Zachara et al.,* 2002*; Steefel et al.,* 2003] that there are high affinity and low affinity sorption sites for Cs. The fraction of Cs desorbed from colloids strongly depended on the initial Cs loading. The higher the initial Cs loading, the higher was the fraction of Cs that could be desorbed from the colloids (Figure 6).

3.2.3 Colloid Mobilization and Transport

Colloids were mobilized and transported through the Hanford sediment column as the ionic strength was lowered from 1000 to 1 mM $NaNO_3$. The breakthrough occurred one pore volume after change of the inflow solution, basically following the normality front (Figure 7a). Whereas the shape of the colloid breakthrough curve shows a sharp peak, the elution portion shows a pronounced tailing and indicates two different rates of colloid release. The colloids mobilized were identified as kaolinite, quartz, mica-vermiculite-illite, chlorite, and smectite. There was no separation of mineral types occurring during the mobilization event, although there appears to be less smectite and chlorite in the later stages of the colloid mobilization. After change of the ionic strength to induce colloid mobilization, the eluted colloids carried some Cs with them, and the Cs was associated mostly with the colloidal phase (Figure 7b). Total concentrations of Cs in the outflow varied between 0.5 and 0.8 μmol/L, and dropped to below 0.03 μmol/L after 110 pore volumes. Based on studies of contaminated sediments from the Hanford site, it is likely that the Cs was mainly carried by biotite and to a lesser degree by vermiculite [*McKinley et al.,* 2001]. The amount of Cs mobilized with colloids was 3.1 μmol or, related to the mass of sediments in the column, 5.59×10^{-8} mol/g. This number is similar to the concentration of poorly exchangeable Cs, reported as 3.45×10^{-8} mol/g, calculated from batch sorption studies with Hanford sediments under high Na background (5 M $NaNO_3$) [*Zachara et al.,* 2002].

Unsaturated flow experiments showed that colloids were mobile in Hanford sediments. Native, as well as colloids reacted with simulated waste tank solutions, moved through the sediments at practically the same speed as a conservative nitrate tracer. Colloids were mobile under all water saturations, but the total amount of colloids transported decreased with decreasing water saturation (Figure 8). Native as well as modified colloids moved through the sediments at practically the same speed as the conservative nitrate tracer; however, the inflow concentrations were not reached during the injection pulse and the breakthrough curves show a plateau-like behavior. The results also indicated that under unsaturated conditions, a portion of the water became immobile and did not contribute to the flow anymore. The experimental data support the concept of mobile-immobile water zones.

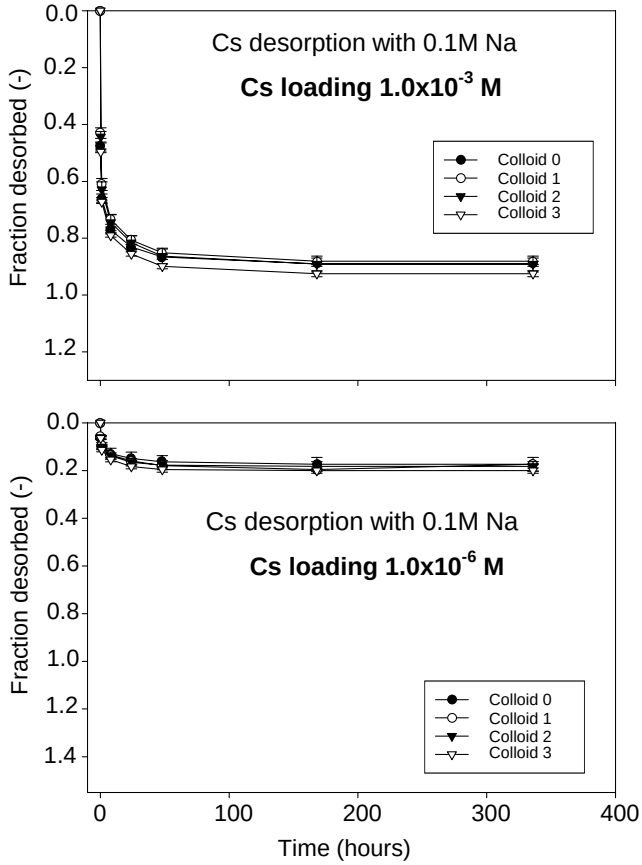

Fig. 6. Cesium desorption from reacted and unreacted Hanford colloids.

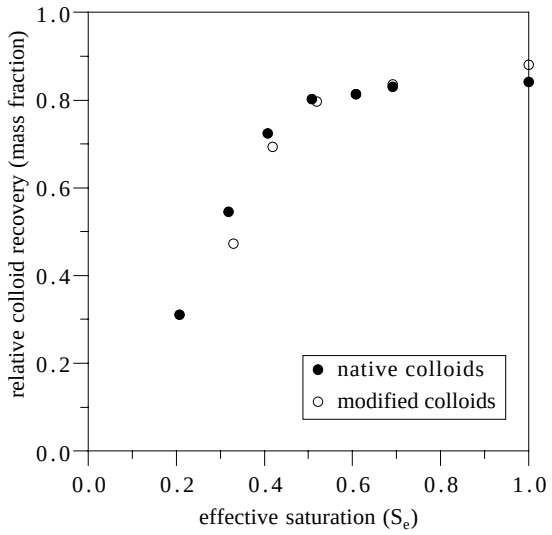

Fig. 8. Mass of colloids recovered in outflow from Hanford sediments under different water saturations.

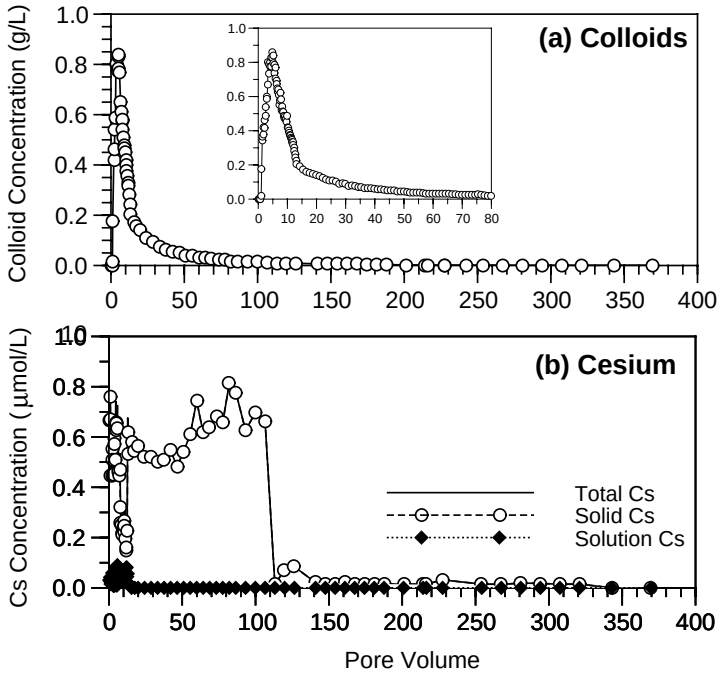

Fig. 7. Column outflow after eluent change from 1 M to 1 mM $NaNO_3$.

3.2.4 Cs Transport through Hanford Sediments

Cesium sorption to the silica sand in batch experiments showed a linear sorption isotherm for all ionic strengths, which matched well with the results from the column experiments at 100 and 1000 mM ionic strength; however, the column experiments at 1 and 10 mM ionic strength indicated a nonlinear sorption behavior of Cs to the silica sand. Transport through silica sand occurred under one-site sorption and equilibrium conditions. Cesium sorption to Hanford sediments in both batch and column experiments was best described with a nonlinear Freundlich isotherm. The column experiments indicated that Cs transport in Hanford sediments occurred under two-site equilibrium and nonequilibrium sorption. The effect of ionic strength on Cs transport was much more pronounced in Hanford sediments than in silica sands. Effective retardation factors of Cs during transport through Hanford sediments were reduced by a factor of 10 when the ionic strength increased from 100 to 1000 mM; for silica sand, the effective retardation was reduced by a factor of 10 when ionic strength increased from 1 to 1000 mM. A two order of magnitude change in ionic strength was needed in the silica sand to observe the same change in Cs retardation as in Hanford sediments.

3.2.5 Colloid-Facilitated Cs Transport

Transport experiments with Cs showed that the presence of colloids facilitated the transport of Cs through both Hanford sediment and Ottawa sand via association of Cs with mobile colloidal particles. Due to the non-linearity of the Cs sorption, the colloid-facilitated Cs transport was more pronounced at the low Cs concentration (1.4×10^{-8} M Cs) than at the

high concentration (7.5×10^{-5} M Cs) when expressed relative to the inflow Cs concentration (Figure 9). In absence of colloids, no Cs moved through the 10-cm long columns during the experiment within about 20 pore volumes, except for the high Cs concentration in the Ottawa sand where a complete Cs breakthrough was obtained. Also, it was found that colloid-associated Cs could be partially stripped from colloids during the transport. The stripping effect was controlled by both Cs concentration and sorption capacity of the transport matrix. The results show that colloid-facilitated Cs transport at the Hanford site is likely not an effective mechanism for Cs movement. At Hanford, it can be expected that Cs would be stripped from colloidal carriers as the colloids move through the 27 to 33 m thick uncontaminated vadose zone and only a very small fraction of initially sorbed Cs would move with mobile colloids. Furthermore, under the conditions at the Hanford site (pore water chemistry, degree of water saturation) colloids are less likely to be stable in suspension than under our experimental conditions, further limiting the possibility for colloid-facilitated transport. Our results can be interpreted as a worst-case scenario for colloid-facilitated Cs transport at the Hanford site, but even in this case, the quantitative amount of Cs that can be co-transported appears to be limited.

Similar results were found under variably-saturated flow. The higher the water flow rates, the less Cs was stripped off, indicating, in part, a rate-limited desorption of Cs from the carrying colloids. Depending on flow rate, up to 70% of the initially sorbed Cs desorbed from the colloidal carriers and was captured in the stationary sediments. Less Cs was stripped off colloids under unsaturated than under saturated flow conditions at similar flow rates. This phenomenon was likely due to the reduced availability of sorption sites for Cs on the sediments as the water content decreased and water flow was partitioned between mobile and immobile regions. As the water saturation decreased, more and more colloids were being retained inside the column, and consequently colloid-facilitated Cs transport became less pronounced (Figure 10).

In order to use H-NMR to track colloid movement through columns, we performed Cu sorption studies to obtain optimal Cu concentrations on colloidal materials. Kinetic adsorption and desorption experiments indicate that colloids can be tagged with up to 175 mmol/kg non-Ba-extractable Cu. Copper loading on colloids decreased proton T-1 relaxation times. Between 19 and 81 mmol/kg Cu concentrations, the T-1 decreased, but the decrease was small. There was insufficient change in T-1 relaxation times (about 15%) due to the presence of colloids to allow accurate visualization in the porous materials. Particularly, the high paramagnetic background in Hanford sediments makes the use of H-NMR for Hanford sediments unsuitable. We are currently exploring the use of F-NMR to overcome these difficulties.

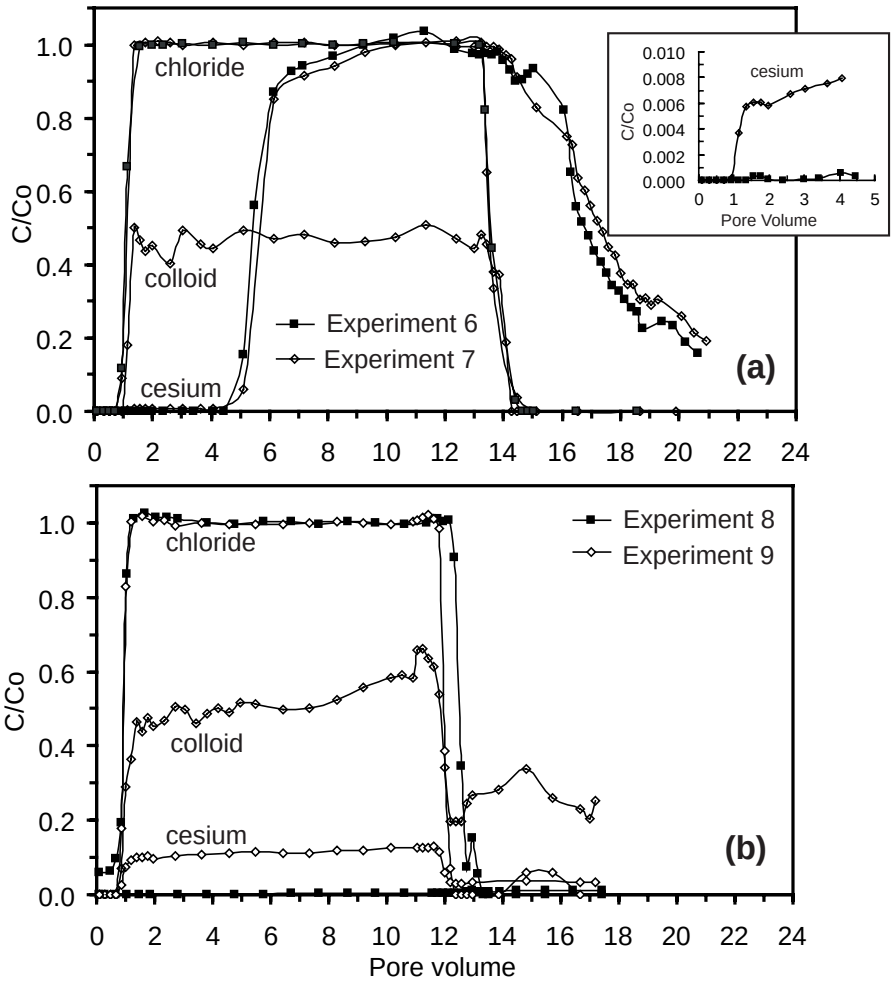

Fig. 9. Breakthrough curves of Cs, Cl, and colloids in Hanford sediment at various colloid concentrations at (a) high Cs loading (7.5×10^{-5} M) and (b) low Cs loading (1.4×10^{-8} M). The insert shows a magnified view of the Cs breakthrough.

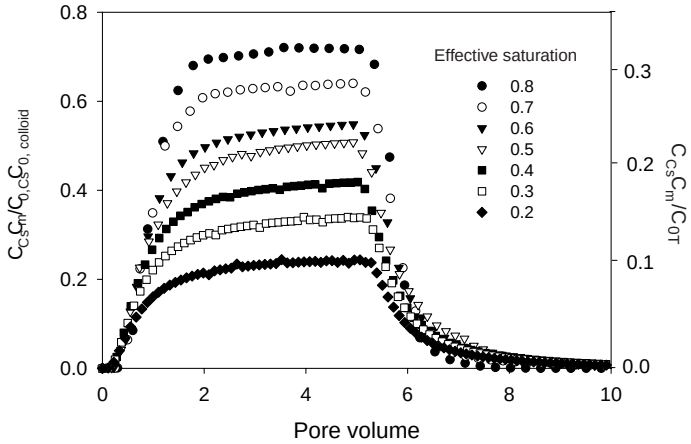

Fig. 10. Cesium breakthrough data under unsaturated conditions. Cesium concentrations are related to initially sorbed Cs on colloids ($C_{\mathrm{Cs}}C_m/C_{0,\mathrm{Cs}}C_{0,\mathrm{colloid}}$) and total amount of Cs in inflow ($C_{\mathrm{Cs}}C_m/C_{0T}$). All Cs is associated with colloidal particles.

4 Relevance, Impact, and Technology Transfer

a. *How does this new scientific knowledge focus on critical DOE environmental management problems?*
The Hanford waste tanks are a critical DOE environmental management problem. The main focus of this project was to investigate whether the transport of contaminants present in Hanford tank waste (i.e., Cs) can be facilitated by colloids. We have investigated the role of colloids and their ability to transport Cs under conditions representative for the vadose zone beneath Hanford tank farms.

b. *How will the new scientific knowledge that is generated by this project improve technologies and clean-up approaches to significantly reduce costs, schedules, and risks and meet DOE compliance requirements?*
An important question regarding the Hanford tank farms is how the current depth distribution of Cs in the vadose can be explained. Will the Cs stay in place or does it constitute a future threat to the groundwater? Our project focused on the role of colloids in facilitating the movement of Cs. Based on the results of our project, it is unlikely that colloids can enhance the movement of Cs to a significant degree. While we found that colloids can move through the vadose zone at Hanford, under saturated, as well as under unsaturated conditions, the amount of Cs that can be transported with the colloids is limited. Furthermore, Cs sorbed to colloidal particles will be desorbed from colloids and sorbed to the stationary sediment matrix as colloids move through uncontaminated sediments. Our results support findings from others [*Zachara et al.*, 2002; *Knepp*, 2002; *Steefel et al.*, 2003] that show that the bulk of the Cs very likely will stay in place and does not move much further in the vadose zone. Cesium will therefore decay in place before it will reach the groundwater. The best remediation strategy for the Cs contamination beneath the Hanford waste tanks may therefore be leaving the Cs in place and letting it decay. This suggests that

no costly remediation actions have to be taken to reduce risks of Cs contamination of groundwater. It is, however, possible that small amounts of Cs can migrate far distances associated with colloids.

c. *To what extent does the new scientific knowledge bridge the gap between broad fundamental research that has wide-ranging applications and the timeliness to meet needs-driven applied technology development?*
This project has produced new scientific knowledge regarding mineral transformations and colloid and colloid-facilitated Cs transport in the Hanford vadose zone. We have shown that new minerals can form upon contact of sediments with Hanford tank waste and that these minerals can be mobile in the subsurface. The results confirmed that Cs will likely stay in place in the vadose zone, unless the geochemical and hydrological conditions currently existing at the site change significantly. If the current geochemical and hydrological conditions are maintained, then no considerable movement of Cs in the vadose zone is expected.

d. *What is the project's impact on individuals, laboratories, departments, and institutions? Will the result be used? If so, how will they be used, by whom, and when?*
The results of this project support the findings from other EMSP projects that the bulk of Cs leaked beneath the Hanford waste tanks will likely stay in place and does not pose a threat to groundwater. This finding will help the DOE in assessing the risk of Cs in the vadose zone at Hanford.

e. *Are large scale trials warranted? What differences has the project made? Now that the project is complete, what new capacity, equipment or expertise has been developed?*
This project has assessed Cs fate and transport in packed laboratory columns. The next step would be the validation of these results in larger scale, undisturbed sediment columns. The results of the project have contributed to an advancement of the understanding of fate and transport of Cs in the vadose zone. See also items a to d.

f. *How have the scientific capabilities of collaborating scientists been improved?*
During this project, we have steadily expanded our expertise in surface and colloid science as related to the vadose zone at the Hanford site. We have considerably advanced experimental and theoretical understanding of mineral transformations and colloid fate and transport. We have intensified the link between physical and chemical processes relevant to study colloid-facilitated transport of radionuclides in the vadose zone. We have considerably improved our capabilities to study variably-saturated flow phenomena in porous media.

g. *How has the research advanced our understanding of the area?*
As a result of this project, we have made several significant scientific contributions. We have demonstrated that mineral transformations can take place under conditions of a Hanford tank leak and we have characterized the mineral transformations and its impact on Cs sorption. We have, for the first time, shown a very detailed investigation of the effect of water saturation on colloid transport in porous media. We

have demonstrated that Cs can be stripped off colloidal carriers as Cs-loaded colloids move through uncontaminated sediments. Overall, we have advanced the fundamental understanding of Cs fate and transport under conditions similar to Hanford waste tank leaks.

h. *What additional scientific or other hurdles must be overcome before the results of this project can be successfully applied to DOE Environmental Management problems?*
The results of this project support the conclusion that the Cs beneath the Hanford waste tanks does not pose an environmental threat to groundwater. This conclusion is supported by various other findings [*Zachara et al.,* 2002*; Knepp,* 2002*; Steefel et al.,* 2003]. A small fraction of Cs, however, may be transported via colloids. The results of this project were obtained from packed sediment columns only. Undisturbed column experiments should be conducted to quantify the amount of Cs that can be mobilized with colloids.

i. *Have any other government agencies or private enterprises expressed interest in the project? Please provide contact information?*
The Idaho National Engineering and Environmental Laboratory (INEEL) has expressed interest in this project. We have had numerous contacts with scientists from INEEL (Larry Hull, George Redden, Jenn-Tai Liang, Robert Fox).

5 Project Productivity

The project accomplished all of the proposed goals. The project was on schedule, but due to the unexpected departure of the postdoctoral scientist (Hongting Zhao), who took a new position at Sandia National Laboratories, some delay was caused. The hiring of a new postdoctoral scientist took some time. We consequently applied for a one-year no cost extension and have completed the project within this one-year extension.

6 Personnel Supported

The following personnel was fully or partially supported by and/or associated with the project:

- Washington State University: Markus Flury (Assistant, and later Associate Professor), James Harsh (Professor), Hongting Zhao (Postdoctoral Researcher, now at Sandia National Laboratory), Gang Chen (Postdoctoral Researcher), Youjun Deng (Postdoctoral Researcher), Kholoud Mashal (PhD student), Szabolcs Czigany (PhD student), Kelly Cherry (MS student), Emily Volkmar (Undergraduate Student), Jessica Auman (Undergraduate Student), Jon Mathison (Research Technician), Jeff Boyle (Research Technician).

- University of Delaware: Yan Jin (Associate Professor), Joe Zhuang (Postdoctoral Researcher), Nicole Romisch (Undergraduate Student).

- Pacific Northwest National Laboratory: John Zachara (Lead Scientist), Kevin Minard (NMR Facility), Andy Felmy (Lead Scientist).

7 Publications

7.1 Published in Peer-reviewed Journals

- Zhao, H., Y. Deng, J. B. Harsh, M. Flury, and J. Boyle, Alteration of kaolinite to cancrinite and sodalite by simulated Hanford Tank Wastes and its impact on cesium retention, *Clays Clay Miner.*, (in press), 2004.

- Zhuang, J., M. Flury, and Y. Jin, Colloid-facilitated Cs transport through water-saturated Hanford sediment and Ottawa sand, *Environ. Sci. Technol.*, *37*, (in press), 2003.

- Flury, M., S. Czigany, G. Chen, and J. B. Harsh, Cesium migration in saturated silica sand and Hanford sediments as impacted by ionic strength, *J. Contam. Hydrol.*, (in press), 2003.

- Cherrey, K. D., M. Flury, and J. B. Harsh, Nitrate and colloid transport through coarse Hanford sediments under steady-state, variably-saturated flow, *Water Resour. Res.*, *39*, 1165, doi:10.1029/2002WR001944, 2003.

- Flury, M., J. B. Mathison, and J. B. Harsh, *In situ* mobilization of colloids and transport of cesium in Hanford sediments, *Environ. Sci. Technol.*, *36*, 5335–5341, 2002.

7.2 Published in Unreviewed Publications

- Hendrickx, J. M. H., and M. Flury, Uniform and preferential flow mechanisms in the vadose zone, in *Conceptual Models of Flow and Transport in the Fractured Vadose Zone*, edited by National Research Council, pp. 149–187, National Academy Press, Washington DC, 2001.

7.3 Submitted for Publication

- Mashal, K., J. B. Harsh, M. Flury, and A. Felmy, Colloid formation in Hanford sediments reacted with simulated tank waste, *Environ. Sci. Technol.*, (submitted), 2003.

- Zhuang, J., Y. Jin, and M. Flury, Comparison of natural colloid and kaolinite transport in porous media, *Vadose Zone J.*, (submitted), 2003.

8 Interactions

a. Participation/presentations at meetings, workshops, conferences.

- Chen, G., M. Flury, and J. B. Harsh. *Colloid-facilitated Transport of Cesium.* American Geophysical Union Annual Meeting, San Francisco, December 6–10, 2002.
- Jin, Y., *Colloid retention and transport in saturated and unsaturated porous media.* Western Regional Soil Physics Committee (W-188) Meeting, Las Vegas, NV, 2003.
- Deng, Y., J. B. Harsh, M. Flury, J. Boyle, J. Young, J. Ford, *Mineral Phase Transformation in Conditions Mimicking Sediment Solutions Underlying Leaked Hanford Waste Tanks.* Mineralogical Society of America Spring Meeting, Athens, Georgia, June 7–12, 2003.
- Deng, Y., J. B. Harsh, M. Flury, J. Boyle, J. Young, J. Ford, *Incorporation and Adsorption of Cs in Zeolitic Minerals Formed in Conditions Similar to the Underlying Hanford Waste Tanks.* Mineralogical Society of America Spring Meeting, Athens, Georgia, June 7–12, 2003.
- Jin, Y, J. Zhuang, and M. Flury. 2002. *Colloid-facilitated Cs transport through Ottawa sand and Hanford sediment*, In: International Workshop on Colloids and Colloid-Facilitated transport of Contaminants in Soils and Sediments. Lis Wollesen de Jonge et al. (eds.). DIAS Report 80: 253-260. Danish Institute of Agricultural Sciences, Denmark, 2002.
- Flury, M., K. D. Cherrey, and J. B. Harsh. *Colloid Transport through Hanford Sediments under Steady-State, Variably-Saturated Flow.* American Geophysical Union Annual Meeting, San Francisco, December 6–10, 2002.
- Zhuang, J., M. Flury, and Y. Jin. *Effect of colloid type and porous medium properties on colloid transport.* Agronomy Abstract, Annual Meeting of the Soil Science Society of America, Indianapolis, IN, 2002.
- Zhuang, J., Y. Jin, and M. Flury. *Colloid-facilitated cesium transport through Hanford sediment.* Agronomy Abstract, Annual Meeting of the Soil Science Society of America, Indianapolis, IN, 2002.
- Flury, M., J. B. Harsh, Y. Jin, and J.M. Zachara. *Colloid-facilitated Transport of Radionuclides through the Vadose Zone.* Environmental Management and Science Program, Department of Energy, Workshop, Richland, November 5–7, 2001.
- Flury, M., J. B. Mathison, and J. B. Harsh. *Cesium Transport via In Situ Mobilized Colloids from Hanford Sediments.* Soil Science Society of America Annual Meeting, Charlotte, NC, October 21–25, 2001.
- Romisch N., J. Zhuang, and Y. Jin. *Colloid and colloid-facilitated Cs transport through sand columns.* Agronomy Abstract, Annual Meeting of the Soil Science Society of America, Charlotte, NC, 2001.
- Flury, M., K. Mashal, H. Zhao, J. B. Harsh, Y. Jin, and J. M. Zachara. *Colloid-Facilitated Transport of Cesium during Leaking of Hanford Waste Tanks.* INRA/INEEL Subsurface Science Symposium, Idaho Falls, September 6–7, 2001.

- Flury, M., K. Mashal, H. Zhao, J. B. Harsh, Y. Jin, and J.M. Zachara. *Colloid Formation in the Vadose Zone Contaminated with Hanford Tank Waste.* Unsaturated Zone Interest Group Meeting, Idaho Falls, July 30–August 2, 2001.
- Hanson, L. A., J. B. Harsh, M. Flury, K. Minard, and D. G. Strawn. *Tracking the Movement of Copper-Saturated Colloidal Silica through Packed Soil Columns Using 1H-NMR.* American Chemical Society Annual Meeting, Chicago, August 26–30, 2001.
- Mashal, K. Y., H. Zhao, J. B. Harsh, M. Flury. *Colloid Formation in Hanford Sites contaminated with Tank Waste.* American Chemical Society Annual Meeting, Chicago, August 26–30, 2001.
- Zhao, H., K. Y. Mashal, J. B. Harsh, and M. Flury. *Alteration of Mineralogical and Surface Properties of Hanford Sediments Contaminated with Tank Waste.* American Chemical Society Annual Meeting, Chicago, August 26–30, 2001.
- Jin, Y. *Colloid-facilitated Cs Transport in Sand.* Western Regional Soil Physics Committee (W-188) Meeting, Las Vegas, NV, 2001.
- Mashal, K., H. Zhao, J. B. Harsh, and M. Flury. *Formation and Characterization of Colloids in Hanford Sediments during Tank Leakage.* American Geophysical Union Annual Meeting, San Francisco, December 14–18, 2000.
- Flury, M. and J. B. Harsh. *In situ Mobilization of Colloids in Hanford Sediments.* American Geophysical Union Annual Meeting, San Francisco, December 14–18, 2000.
- Flury, M., J. B. Harsh, Y. Jin, and J. M. Zachara. *Colloid-facilitated Transport of Radionuclides through the Vadose Zone.* Environmental Management and Science Program, Department of Energy, Workshop, Richland, November 25–28, 2000.
- Harsh, J. B., M. Flury, H. Zhao, K. Mashal, Y. Jin, and J. M. Zachara. *Colloid-facilitated Transport of Radionuclides through the Vadose Zone.* Environmental Management and Science Program, Department of Energy, National Workshop, Atlanta, April 24–28, 2000.
- Flury, M., J. B. Harsh, Y. Jin, and J. M. Zachara. *Colloid-facilitated Transport of Radionuclides through the Vadose Zone.* Environmental Management and Science Program, Department of Energy, Workshop, Richland, November 16–18, 1999.

b. Consultative and advisory functions to other laboratories and agencies, especially DOE and other government laboratories.

- Markus Flury, Advisory Panel, US Department of Energy, Remediation Challenges and Research Opportunities at the Savannah River Site, Aiken, SC, 2003.
- James Harsh, Review Panel, US Department of Energy, Environmental Management Science Program Proposal Review, 2002.

- Markus Flury, Member, DOE Vadose Zone Science and Technology Roadmap Workgroup, "Characterization, Modeling, and Simulation of Subsurface Contaminant Fate and Transport", March–September 2000.
- Markus Flury and James Harsh, Consultation on colloid-facilitated transport of Pu and Am to the Idaho National Engineering and Environmental Laboratory, 2001–2002.

c. Collaborations.

- Los Alamos National Laboratory, Peter Lichtner, Modeling of Colloid-facilitated Cs Transport.
- Idaho National Engineering and Environmental Laboratory, Larry Hull, Colloid-facilitated Transport of Pu and Am.
- Oregon State University, John Selker, Surface Properties of Colloids.
- Pacific Northwest National Laboratory, Kevin Minard, NMR Studies for Colloid Visualization.
- Pacific Northwest National Laboratory, Glendon Gee, PhD Committee Member of Szabolcs Czigany, student supported by the EMSP grant.

9 Transitions

The project did not result in a new technology or technique. Purpose of this research was to provide fundamental scientific understanding of fate and transport of Cs in the vadose zone at the Hanford site, and not primarily the development of new technologies.

10 Patents

No patents have been resulted from this project.

Literature Cited

Barnes, M. C., J. Addai-Mensah, and A. R. Gerson, The mechanism of the sodalite-to-cancrinite phase transformation in synthetic spent Bayer liquor, *Microporous Mesoporous Mat.*, *31*, 287–302, 1999.

Bickmore, B. R., K. L. Nagy, J. S. Young, and J. W. Drexler, Nitrate-cancrinite precipitation on quartz sand in simulated Hanford tank solutions, *Environ. Sci. Technol.*, *35*, 4481–4486, 2001.

Knepp, A. J., *Field Investigation Report for Waste Management Area S-SX*, RPP-7884, Rev. 0, CH2M HILL Hanford Group, Inc., Richland, Washington, 2002.

McBride, M. B., Surface chemistry of soil minerals, in *Minerals in the Soil Environment*, edited by J. B. Dixon, and S. B. Weed, pp. 35–88, Soil Science Society of America, Madison, WI, 1989.

McKinley, J. P., C. J. Zeissler, J. M. Zachara, R. J. Serne, R. M. Lindstrom, H. T. Schaef, and R. D. Orr, Distribution and retention of Cs-137 in sediments at the Hanford Site, Washington, *Environ. Sci. Technol.*, *35*, 3433–3441, 2001.

Serne, R. J., B. N. Bjornstad, H. T. Schaef, B. A. Williams, D. C. Lanigan, D. G. Horton, R. E. Clayton, A. V. Mitroshkov, V. L. LeGore, M. J. O'Hara, C. F. Brown, K. E. Parker, I. V. Kutnyakov, J. N. Serne, G. V. Last, S. C. Smith, C. W. Lindenmeier, J. M. Zachara, and D. S. Burke, *Characterization of Vadose Zone Sediment: Uncontaminated RCRA Borehole Core Samples and Composite Samples*, Pacific Northwest National Laboratory, US Department of Energy, PNNL-13757-1, Richland, Washington, 2002.

Steefel, C. I., S. Carroll, P. Zhao, and S. Roberts, Cesium migration in Hanford sediment: a multisite cation exchange model based on laboratory experiments, *J. Contam. Hydrol.*, , in press, 2003.

Swartzen-Allen, S. L., and E. Matijevic, Surface and colloid chemistry of clays, *Chem. Rev.*, *74*, 385–400, 1974.

Zachara, J. M., S. C. Smith, C. Liu, J. P. McKinley, R. J. Serne, and P. L. Gassman, Sorption of Cs^+ to micaceous subsurface sediments from the Hanford Site, USA, *Geochim. Cosmochim. Acta*, *66*, 193–211, 2002.

Appendix: Reprints and Preprints of Publications

- Flury, M., J. B. Mathison, and J. B. Harsh, *In situ* mobilization of colloids and transport of cesium in Hanford sediments, *Environ. Sci. Technol.*, *36*, 5335–5341, 2002.
- Cherrey, K. D., M. Flury, and J. B. Harsh, Nitrate and colloid transport through coarse Hanford sediments under steady-state, variably-saturated flow, *Water Resour. Res.*, *39*, 1165, doi:10.1029/2002WR001944, 2003.
- Zhuang, J., M. Flury, and Y. Jin, Colloid-facilitated Cs transport through water-saturated Hanford sediment and Ottawa sand, *Environ. Sci. Technol.*, *37*, (in press), 2003.
- Zhao, H., Y. Deng, J. B. Harsh, M. Flury, and J. Boyle, Alteration of kaolinite to cancrinite and sodalite by simulated Hanford Tank Wastes and its impact on cesium retention, *Clays Clay Miner.*, (in press), 2004.
- Flury, M., S. Czigany, G. Chen, and J. B. Harsh, Cesium migration in saturated silica sand and Hanford sediments as impacted by ionic strength, *J. Contam. Hydrol.*, (in press), 2003.
- Mashal, K., J. B. Harsh, M. Flury, and A. Felmy, Colloid formation in Hanford sediments reacted with simulated tank waste, *Environ. Sci. Technol.*, (submitted), 2003.
- Zhuang, J., Y. Jin, and M. Flury, Comparison of natural colloid and kaolinite transport in porous media, *Vadose Zone J.*, (submitted), 2003.

Environ. Sci. Technol. **2002**, *36,* 5335−5341

In Situ Mobilization of Colloids and Transport of Cesium in Hanford Sediments

MARKUS FLURY,*
JON B. MATHISON, AND
JAMES B. HARSH

Department of Crop and Soil Sciences, Center for Multiphase Environmental Research, Washington State University, Pullman, Washington 99164-6420

Radioactive waste, accumulated during Pu production, has leaked into the subsurface from underground storage tanks at the U.S. Department of Energy's Hanford site. The leaking solutions contained ^{137}Cs and were of high ionic strength. Such a tank leak was simulated experimentally in steady-state flow experiments with packed Hanford sediments. The initial leak was simulated by a 1 M $NaNO_3$ solution, followed by a decrease of ionic strength to 1 mM $NaNO_3$. Cesium breakthrough curves were determined in both 1 M and 1 mM $NaNO_3$ background. Colloidal particles were mobilized during the change of ionic strength. Mobilized colloids consisted mainly of quartz, mica, illite, kaolinite, and chlorite. Electrophoretic mobilities of colloids in the eluent solution were −3(μm/s)(V/cm) and increased to less negative values during later stages of mobilization. Mobilized colloids carried a fraction of the cesium along. While transport of cesium in 1 M $NaNO_3$ background was much faster than in 1 mM $NaNO_3$, cesium attached to colloids moved almost unretarded through the sediments. Cesium attached to mobilized colloids was likely associated with high affinity sorption sites on micas and illites.

Introduction

Radioactive and hazardous waste stored at in the underground tanks at the Hanford site, Washington, has leaked into the vadose zone (*1*). Tank waste supernatants consist of solutions of high pH and ionic strength and contain radioactive contaminants such as Cs. When such a waste plume contacts subsurface sediments and migrates through the vadose zone, its ionic strength will decrease, a scenario which can lead to in situ colloid mobilization and transport (*2*−*5*). If strongly sorbing contaminants are present, the leak scenario can also lead to colloid-facilitated contaminant transport (*6*).

In situ mobilization and transport of colloidal material in natural porous media has been demonstrated for various subsurface materials, such as noncalcareous silt loam soil (*4*, *6*), sand soil (*7*), highly weathered aquifer sand (*8*, *9*), and soils at groundwater recharge facilities (*10*). The major factors inducing mobilization and subsequent transport are a change in solution ionic strength and pH; however, pH is often not that important for permanently charged clay minerals (*4*). Concentrations of mobilized particles can be large, up to a few hundreds of milligrams per liter have been reported for laboratory column outflow (*4*). The experimental evidence suggests that, upon disturbance of ionic strength, in situ colloid mobilization can be an important transport mechanism for colloidal particles. If the disturbance of ionic strength occurs in combination with the presence of sorbing contaminants, the mobilized particles can also act as vectors for accelerated contaminant movement (*6*).

A contaminant of major concern at Hanford is radioactive ^{137}Cs. Initially, ^{137}Cs contributed about 40% of the radioactivity present in the tanks (*11*). Presently, ^{137}Cs and ^{90}Sr together constitute about 99% of the tank's radioactivity (*1*). Whereas ^{90}Sr is believed to remain mostly in the sludge of the tanks, ^{137}Cs is contained in the liquid supernatant that can and has leaked out (*1*). Concentrations of ^{137}Cs in the tanks vary considerably. When the leaks occurred, ^{137}Cs concentrations in tanks SX-108, SX-111, and SX-115 are estimated to have ranged between 0.02 and 0.19 mmol/L (*12*). Ionic strength of the tank supernatants is dominated by NaOH and $NaNO_3$; the latter is estimated to reach up to 5 M $NaNO_3$ (*12*).

We hypothesize that during a tank leak at the Hanford Reservation, in situ colloidal particles are initially immobilized because of the high ionic strength of the leaking solutions. At the same time, Cs sorbs only weakly to the sediments due to the high competition of Na ions. As the ionic strength of the solution is decreased by dispersion and dilution, colloids become mobilized, and at the same time, Cs sorbs much stronger to the stationary sediments as well as to the mobile colloids. Colloid-facilitated transport of Cs is likely under such conditions. To test this hypothesis and to quantify the effects, we simulate a tank leak scenario in a saturated laboratory column experiment. The objectives of this study are to determine (1) whether native colloids can be mobilized in situ during a Hanford tank leak and (2) to what extent Cs transport is affected by colloid mobilization.

Materials and Methods

Sediments and Sediment Characterization. Uncontaminated sediments were obtained from the Hanford Reservation, Submarine Site (218-E−12B). The material consists of a pebbly coarse sand belonging to the Hanford Formation, deposited during the cataclysmic events of the Missoula floods. The sediments were taken from a trench wall in January 2000. The sediments are texturally and mineralogically similar to the material underlying the immediate vicinity of the S−SX (single-shell) tank farm at Hanford (personal communication, Bruce N.Bjornstad, September 2001, Pacific Northwest National Laboratories, Richland, WA). The material was air-dried, dry-sieved through a 2-mm square screen, and stored in five-gallon plastic buckets. The pH, measured in a 1:1 w/w water extract, was 8.0.

For particle size analysis, the sediments were treated with 30% w/w H_2O_2 and 0.5 M Na-acetate to remove organic matter and calcium carbonate. For these treatments, samples were placed on a hot plate (65 °C) for 120 min. Samples were then centrifuged at 48 400 g for 120 min, dried at 105 °C, redispersed in a 0.5 g/L Na-hexametaphosphate solution, and wet-sieved through 1-mm and 0.5-mm square sieves. The material passing through the screens was measured with static light scattering (MasterSizer S, Malvern Instruments Ltd., Malvern, UK). The instrument was equipped with reverse Fourier optics and a Helium−Neon laser of 633 nm wavelength. Particle size distribution was obtained by fitting full Mie scattering functions for spheres. The mineralogy of the sand and silt fraction was determined by preparing thin-sections and examination with a petrographic microscope (*13*). For mineralogical analysis of the clay fraction, sediments

* Corresponding author phone: (509)335-1719; fax: (509)335-8674; e-mail: flury@mail.wsu.edu.

10.1021/es025638k CCC: $22.00 © 2002 American Chemical Society
Published on Web 11/07/2002

TABLE 1. Experimental Conditions for Column Experiments

column parameters	values
length and diameter	$L = 21.4$ cm, i.d. = 2.5 cm
bulk density	1.69 g/cm^3
saturated water content	0.36 cm^3/cm^3
pore volume	37.8 cm^3
flow rate Q	25.8 cm^3/h
water flux J	5.25 cm/h
temperature	20−22 °C
eluent solutions	1000 mM $NaNO_3$, pH 10 (1 mM Na_2CO_3/$NaHCO_3$)
	1 mM $NaNO_3$, pH 10 (0.1 mM Na_2CO_3/$NaHCO_3$)
Cs pulse	0.1 mM $CsNO_3$

were dispersed in deionized water and the size fraction <2 μm was separated by centrifugation. Potassium saturated and air-dried, K-saturated and 550-heated, Mg-saturated and air-dried, and Mg-saturated and glycerol-solvated samples were analyzed as random powder by X-ray diffraction (Philips XRG 3100, Philips Analytical Inc., Mahwah NJ) with Cu−Kα radiation (*14*). Operating conditions for X-ray diffraction were 35kV and 30mA, with scanning at 0.02 degrees 2-theta/sec. The scans were collected using Datascan and processed with Jade (Materials Data, Inc.). Jade was used to smooth and locate peak positions.

Column Experiments. Hanford sediments were packed into a 2.5-cm i.d., 21.4-cm long glass column equipped with Teflon end-pieces (Omnifit, Cambridge, UK). Dry sediments were filled in 1-cm increments under a CO_2 atmosphere into the column, and each increment was then saturated with a 1 M $NaNO_3$ solution by pumping from the bottom before the next increment was added. The strong electrolyte solution kept the fine particles flocculated and allowed a uniform filling of the entire column. After packing, a steady-state flow rate was established using a peristaltic pump (Ismatec IP4, Glattbrugg, Switzerland). All connections and tubings were made of Teflon, except for the peristaltic pump tubing piece, which was of Tygon. A 20 μm pore-size Teflon frit was used at the column inflow end, no frit was used at the outflow end. Column outflow was collected with a fraction collector in 9-mL increments. Four hundred pore volumes of 1 M $NaNO_3$ were initially pumped through the column to equilibrate the material with the electrolyte solution. All eluent solutions were degassed under vacuum, buffered at pH 10 with Na_2CO_3/$NaHCO_3$, and filtered through a 0.1 μm filter (Millipore, polyvinylidene fluoride membrane filter). The ionic strength of the buffer electrolytes was kept at least one order of magnitude smaller than that of the $NaNO_3$ solution. Inflow and outflow pH were monitored periodically to ensure constant pH conditions. Direction of flow during the experiments was from top to bottom. The column was wrapped in aluminum foil to prevent light-induced growth of algae. The foil was periodically removed to visually inspect the column for uniformity of packing and water content during the course of the experiment. Relevant column parameters are summarized in Table 1.

After equilibration of the column with $NaNO_3$, the eluent was changed for about 40 pore volumes to a NaCl solution keeping the same ionic strength and pH. The NaCl was then replaced with a step input of the original $NaNO_3$ to measure the NO_3^- breakthrough. Thirty pore volumes following the $NaNO_3$ input, a 0.1 mM $CsNO_3$ pulse in the same $NaNO_3$ eluent background was introduced. After Cs had eluted from the column, we changed the eluent solution to 1 mM $NaNO_3$ to initiate colloid mobilization. When no more colloids were detected in the outflow, a second Cs pulse was introduced, followed by another NO_3^- breakthrough after initial replacement of $NaNO_3$ with NaCl. The eluent was then changed back to 1 M $NaNO_3$ to obtain a third Cs breakthrough curve. For all Cs breakthrough curves, Cs was added as a pulse in the inflow until the outflow concentration had reached the inflow concentration. Figure 1 shows a synopsis of the column history.

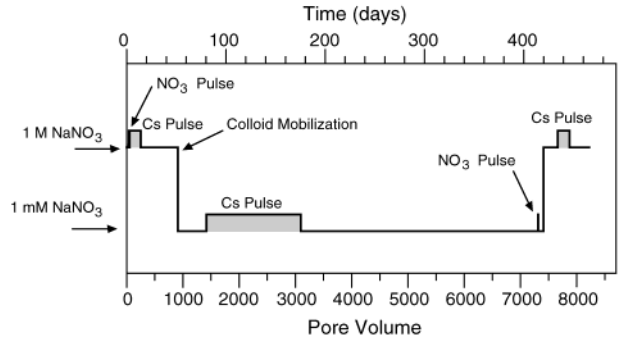

FIGURE 1. Summary of events during the column study.

In summary, the column study consists of a sequence of four experiments: (1) First a Cs breakthrough experiment was conducted in high ionic strength where colloidal material is aggregated and does not move. Due to the presence of micaceous minerals, we expect that a portion of the Cs will not elute and remain inside the column. (2) During the change of ionic strength from high to low, colloidal material will be dispersed and mobilized, and thereby carrying a fraction of the remaining Cs with it. (3) A second Cs breakthrough experiment was measured at low ionic strength, after colloids had eluted from the column. In this phase, no colloids are present in the eluent anymore. (4) Finally a Cs breakthrough experiment was conducted at high ionic strength again, to compare with the initial Cs breakthrough. Again, in this phase, no colloids will be mobile.

Analysis of Nitrate Breakthrough Curves. Column Peclet numbers (Pe) were determined by fitting an analytical solution of the advection-dispersion equation to the conservative tracer breakthrough curve, before and after colloid mobilization following standard procedures (*15*). A Dirichlet boundary condition was employed at the top and a Neumann boundary condition at the bottom of the column. Peclet numbers were estimated using the Levenberg−Marquardt optimization algorithm (*16*).

Colloid Characterization. The outflow samples containing colloidal material were vibrated with a vortex mixer, sonicated for 20 min, and then split in three aliquots. The first aliquot was used to determine colloid concentrations, electrophoretic mobility, and particle morphology. Electrophoretic mobilities were measured with dynamic light scattering using a Zetasizer 3000HSA with a Helium−Neon laser of 633 nm wavelength (Malvern Instruments Ltd., Malvern, UK). For the dynamic light scattering measurements, the background electrolyte concentration used was the same as the one eluted from the column, and the particle concentrations were adjusted to be between 0.1 and 20 mg/L to obtain optimal count rates. The second aliquot was flocculated with a few drops of 1 M $NaNO_3$ and centrifuged at 9200 g for 5 min (this will settle out aggregates with equivalent radii larger than $\sim 7.1 \times 10^{-8}$m). The supernatant was then analyzed for solution phase Cs. The third aliquot was evaporated on a hot plate, and colloids were digested as follows: Colloids were treated overnight with 2 mL of H_2O_2 (30% w/w) at room temperature and then heated to 85 for 2 h. Five mL of aqua regia, consisting of HNO_3 (70%), HCl (37%) and H_2O in a 1:3:1 (w/w/w) ratio, were added, heated on a hot plate to 90 °C, and refluxed for 5 to 6 h. The liquid was then evaporated, and five mL of HNO_3 (5%) was added and stirred with a vortex stirrer. Colloids were allowed to settle and supernatant siphoned off for Cs analysis. It was

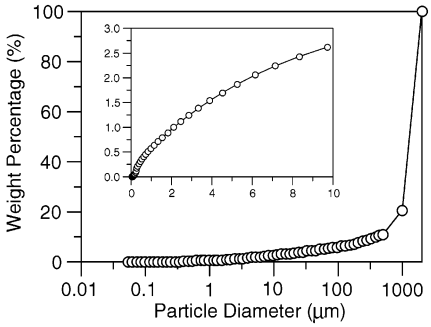

FIGURE 2. Particle size distribution of Hanford sediments used in this study. The inset shows a magnification of the small particle sizes on a linear scale.

assumed that this digestion yields total Cs concentrations in the samples, and using mass balance considerations, concentrations of Cs attached to the colloidal phase were then calculated based on the solution phase concentration from the second aliquot (*6*). The Cs extraction procedure was tested with colloids spiked with known amounts of Cs and a standard soil sample. Cesium recovery of the procedure was between 97 and 103%. For XRD measurements, several samples were combined to obtain sufficient material and analyzed as described above. Insufficient colloidal material was available to measure a complete suite of XRD treatments; only K-saturated and air-dried, K-saturated and heated, and Mg-saturated and glycerol-solvated spectra were determined. Scanning electron microscope (SEM) images were taken with a Hitachi S-570 electron microscope. Colloidal dispersions, containing 0.15% w/w tertbutylamine to reduce surface tension, were added to carbon-coated electron microscopy stubs, evaporated in a laminar-flow hood, gold-coated, and examined with SEM. Particles tended to aggregate during evaporation of the suspensions on the microscopy stubs, and to minimize aggregation, we diluted the suspensions by factors of ten.

Nitrate, Cesium, and Colloid Concentration Analysis. Nitrate and colloid concentrations were measured with a spectrophotometer (HP 8452A, Hewlett-Packard) at a wavelength of 220 and 380 nm, respectively. For colloid measurements, the calibration curve was established with a series of samples that were oven-dried and colloid mass determined gravimetrically. Cesium from the breakthrough curves was measured by atomic emission spectroscopy (Varian 220 Flame Atomic Absorption Spectrometer, Varian Ltd., Mulgrave, Australia) in a 1000 mg/L K background. Cesium concentrations from the colloid mobilization experiment were measured with ICP-MS (Sciex Elan model 250 ICP-MS).

Results and Discussion

Sediment Characterization. The Hanford sediments used are very coarse, with 89% of the mass larger than 0.5 mm and only 1% smaller than 2 μm (Figure 2). The sand and silt fractions are dominated by quartz, amphibole, plagioclase, K-feldspar, mica, and magnetite. Among the micas, both muscovite and biotite are common. The clay-size fraction consists mainly of chlorite, smectite, vermiculite, kaolinite, illite, and quartz.

Column Hydrodynamics. Colloid mobilization, induced by the change in ionic strength, can potentially lead to an alteration of the hydrodynamic properties of the porous medium. The column hydrodynamics was assessed by a series of conservative tracer breakthrough experiments. The results showed that the hydrodynamics of the column did not change during the course of the experiment. The mobilization and elution of colloidal material did not significantly affect the

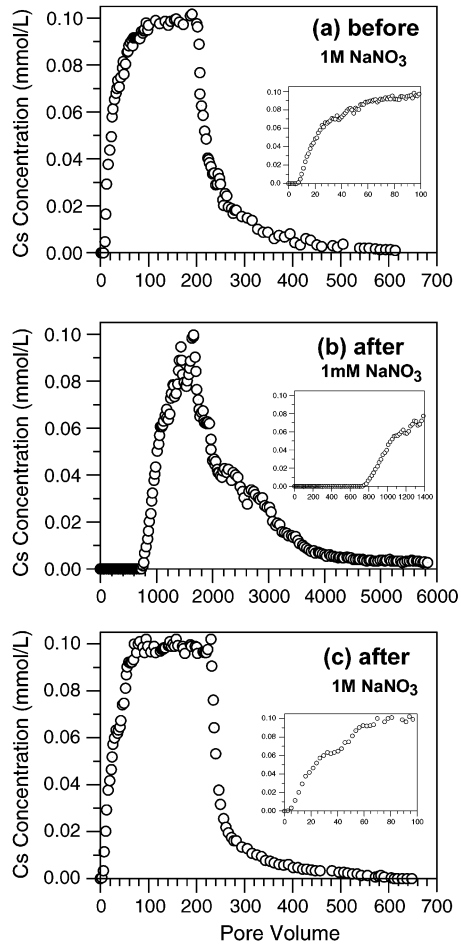

FIGURE 3. Cesium breakthrough curves in Hanford sediments in absence of colloid-facilitated transport. (a) Before colloid mobilization (1 M $NaNO_3$), (b) after colloid mobilization (1 mM $NaNO_3$), (c) after colloid mobilization (1 M $NaNO_3$). Insets show detail from the initial part of the breakthrough. In all cases, colloid concentrations in the eluent were below the analytical detection limit.

column Peclet number (Table 2), and the tracer breakthrough curves were not distinguishable. The hydrodynamic dispersion in our system appears to be determined largely by the coarse sediment material.

Cesium Transport. We are expecting two counteracting phenomena governing the transport of Cs in our column experiment. At the high ionic strength, Cs sorption to Hanford sediments is suppressed because of competition with Na for sorption sites. At the low ionic strength, Cs sorbs more strongly, but the sediment matrix has lost some of its fine material during the colloid mobilization, and consequently Cs sorption will decrease because fewer sorption sites are available. Which effect will dominate is difficult to assess a priori. The experiments showed that the ionic strength effect clearly dominated the transport of Cs. At 1 M $NaNO_3$, Cs breakthrough, defined as $C/C_0 = 0.5$, where C_0 is the concentration of the Cs pulse, occurred after 25 pore volumes, whereas at 1 mM $NaNO_3$, Cs breakthrough occurred after 950 pore volumes (Figure 3). The two breakthrough curves differed not only in breakthrough time but also in shape. Compared to the 1 M $NaNO_3$ case, the 1 mM $NaNO_3$ breakthrough curve has a steeper breakthrough front and a more pronounced tailing. This indicates that the sorption process is more nonlinear at the low ionic strength than at the high ionc strengths. The Cs breakthrough in 1 M $NaNO_3$ after colloid mobilization (Figure 3c) is almost identical to the Cs breakthrough in 1 M $NaNO_3$ before colloid mobilization. However, there is somewhat less tailing in the desorption

TABLE 2. Peclet Numbers and Experimental Cesium Mass Recoveries

parameters	units	1 M $NaNO_3$	1 mM $NaNO_3$	1 M $NaNO_3$
colloids eluted		no	yes	yes
Peclet no.[a] Pe = VL/D		76.9 ± 9.8	67.7 ± 5.7	67.7 ± 6.2
exptl mass recovery	%	99.43	98.24	97.57

[a] Column Peclet number based on pore water velocity V, column length L, and hydrodynamic dispersion coefficient D; determined from NO_3 breakthrough curves.

part of the breakthrough curve after colloids have eluted from the column.

The mass recovery indicates that most of the Cs was eluted from the columns (Table 2). The mass recovery of the second Cs pulse in 1 M $NaNO_3$ was likely the least accurate because the measured high concentration values were variable.

Colloid Mobilization. Colloids were mobilized and transported through the column as the ionic strength was lowered from 1000 to 1 mM $NaNO_3$. The breakthrough occurred one pore volume after change of the inflow solution, basically following the normality front (Figure 4a). It is expected that the pH of the eluent solution will increase during the displacement of the high with the low ionic strength solution (*17*), but because of the pH buffering, the equilibrium pH should be attained again within a few pore volumes (*4*).

The peak colloid concentration was reached at five pore volumes, and colloids kept eluting from the column for about 250 pore volumes, after which the concentrations fell below the analytical detection limit. The concentrations of colloidal particles in the outflow reached up to 900 mg/L. Obviously, the maximum concentrations observed are a function of the solution composition, in particular the ionic strength and valence of the electrolytes, but, nevertheless, values in the same order of magnitude have been reported from other in situ colloid mobilization experiments in natural porous media (*4, 18−20*). These colloid concentrations are 2 to 4 orders of magnitude larger than concentrations found in geochemically stable subsurface systems; however, it is known that during geochemical disturbance, colloid concentrations can increase several orders of magnitude compared to the stable geochemical conditions (*2*). Whereas the shape of the colloid breakthrough curve shows a sharp peak, the elution portion shows a pronounced tailing and indicates two different rates of colloid release (Figure 4a,b).

The electrophoretic mobility of the eluted particles was initially constant at −3 (μm/s)(V/cm) (Figure 4c). After about 100 pore volumes, the electrophoretic mobilities became more variable and increased to −2.5 to −1.8 (μm/s)(V/cm). The colloid concentrations at that time were already small, i.e., less than 10 mg/L. We believe that the change in electrophoretic mobility is caused because the most mobile colloids (with the most negative electrophoretic mobility) are eluted first and the colloids with the less negative electrophoretic mobility lag behind. After 300 pore volumes, colloid concentrations were so small that no electrophoretic mobility measurements were possible.

The SEM images indicated that the colloids were polydisperse and of irregular shape and, interestingly, also showed that relatively large particles (up to 15 μm diameter) were eluted from the column (Figure 5). Individual particle diameters determined with SEM ranged from 0.2 to 15 μm. In the SEM images, individual smaller particles were often forming larger aggregates, which probably formed during the drying process on the SEM stubs. Larger aggregates consisted of crystalline particles resembling kaolinite and illite (upper left in Figure 5), whereas smaller aggregates often appeared to consist of smectite (lower left in Figure 5). The

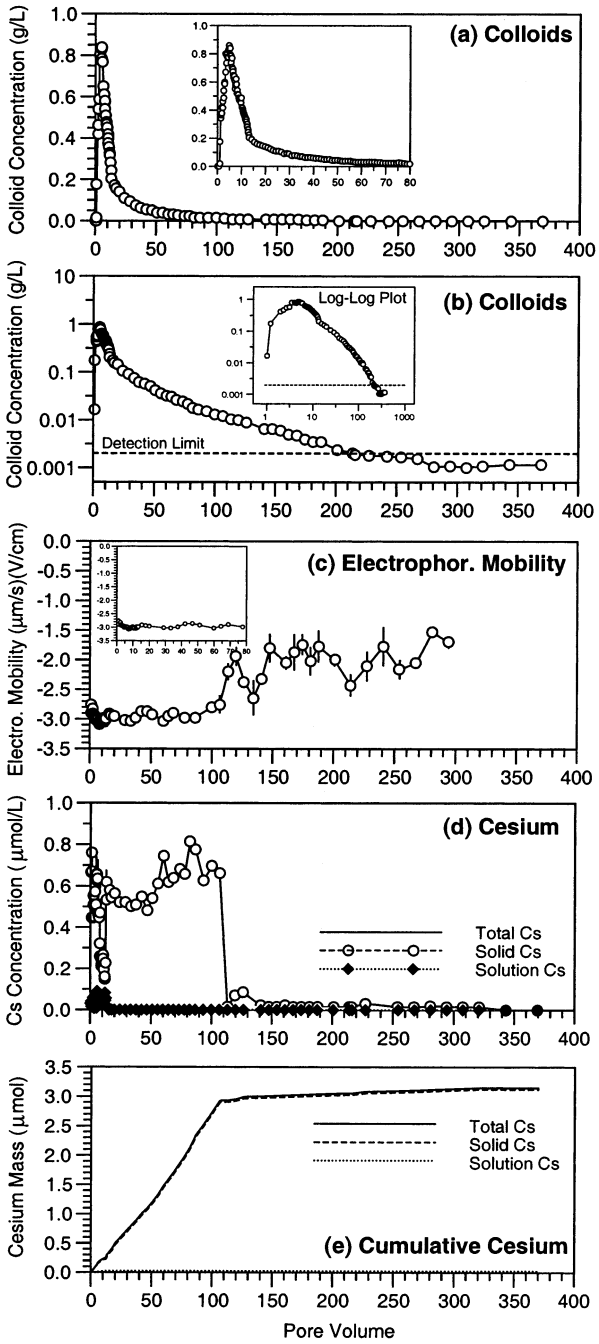

FIGURE 4. Column outflow after eluent change from 1 M to 1 mM $NaNO_3$. The pore volume axis starts when the ionic strength of the inflow was changed. (a) Colloid concentration breakthrough curve, (b) colloid breakthrough curve in semi-log scale, (c) electrophoretic mobility measured at pH 10 and 1 mM $NaNO_3$, (d) Cs concentration breakthrough, and (e) cumulative Cs breakthrough. The vertical bars in (c) indicate ± one standard deviation. The insets show a closeup of the breakthrough portion.

SEM analysis did not show any systematic shape and size pattern as a function of pore volume.

The colloids mobilized were identified as kaolinite, quartz, mica-vermiculite-illite, chlorite, and smectite (Figure 6). The smectite was identified with the Mg-saturated, glycerol-solvated samples. The mineralogical composition of the mobilized colloids is consistent with the composition of the <2 μm-particle fraction of the sediments and with published analyses of sediments from the Hanford formation (*11*). There was no separation of mineral types occurring during the

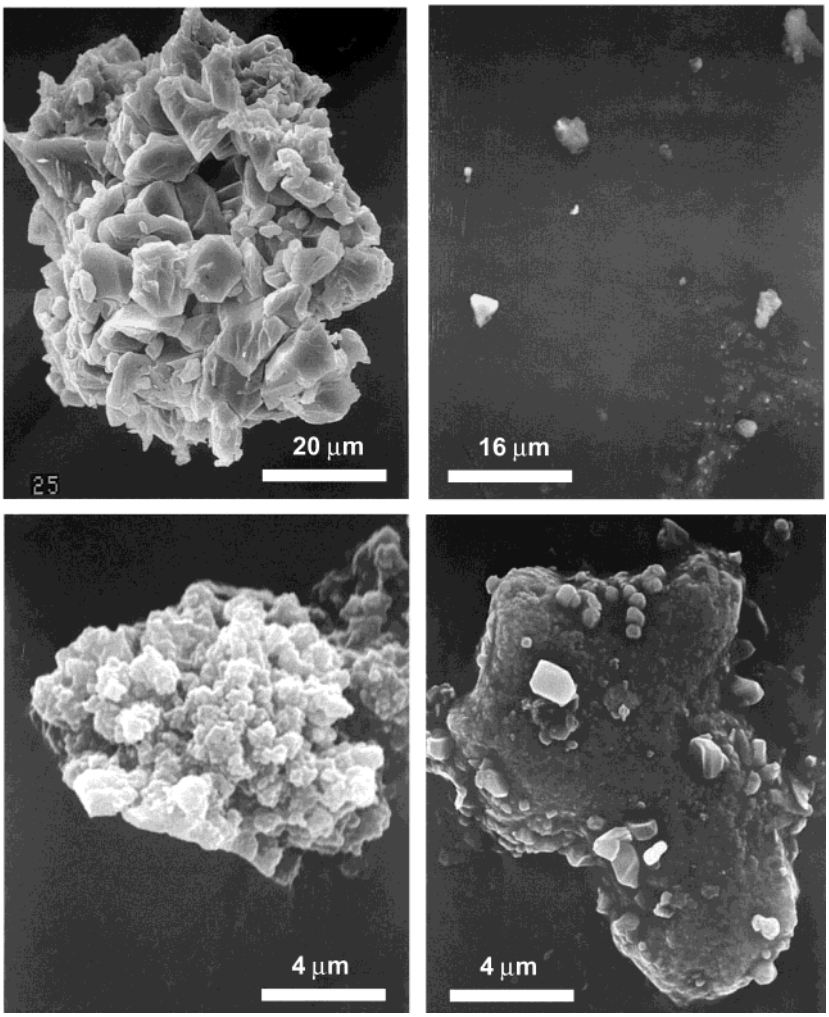

FIGURE 5. Representative SEM images of colloids eluted from the column. Images were taken at 20 kV. Upper right image is taken from a diluted sample to minimize aggregation.

mobilization event, although there appears to be less smectite and chlorite in the later stages of the colloid mobilization. It is noteworthy that minerals usually accounted to the silt and sand fraction, like mica and quartz, were eluted along with the clay minerals kaolinite, smectite, illite, and chlorite.

Colloid-Facilitated Cs Transport. The first Cs pulse introduced at 1 M $NaNO_3$ was eluted for the most part (99.43%); however some Cs still remained in the column. Cesium is known to sorb to high and low affinity sites in sediments such as ours (*11*, *21*). High affinity sorption sites are frayed edge sites and interlayer sites of nonexpansible 2:1 phyllosilicates, such as micas and illites (*22*, *23*). The low-affinity sites are mainly the planar surfaces of phyllosilicate clay minerals. Iron oxyhydroxides and quartz do not sorb Cs to a significant amount (*23*), nor does organic matter (*22*). It is likely, during the Cs breakthrough in 1 M $NaNO_3$, the Cs had saturated all high- and low-affinity sorption sites during the adsorption part, but during the desorption part, only the Cs at the low-affinity sorption sites has been desorbed via cation exchange with Na. In addition, Cs desorption from high-affinity sites is much slower than from the low-affinity sites (*24*, 25). Therefore, some Cs at high-affinity sites will have remained in the column, likely attached to micas and nonexpansible clay minerals. Indeed, after change of the ionic strength to induce colloid mobilization, the eluted colloids carried some Cs with them, and the Cs was associated mostly with the colloidal phase (Figure 4d,e). Total concentrations of Cs in the outflow varied between 0.5 and 0.8 μmol/L and dropped to below 0.03 μmol/L after 110 pore volumes. There is a sudden drop in colloid-associated Cs concentrations after 110 pore volumes, which coincides with an increase of electrophoretic mobility of colloidal particles. Attempts to identify a possible change in mineralogy of the colloids associated with this drop failed because of insufficient amount of colloidal material available for XRD.

Some Cs was detected in the solution phase, but the concentrations were small (<0.01 μmol/L). The only significant concentrations in the solution phase were measured within the first 15 pore volumes following colloid elution when solution phase concentrations reached up to 0.1 μmol/L. The bulk portion of the Cs was associated with the colloidal phase. Based on studies on contaminated sediments from the Hanford Site, it is likely that the Cs was mainly carried by biotite and to a lesser degree by vermiculite (*11*); however, we have not specifically identified the Cs-carrying phases in our experiment.

We calculated the mass balance of Cs for the mobilization experiment based on the concentrations measurements in the outflow (Figure 7). Most of the Cs introduced into the column was eluted during the Cs breakthrough experiment (1 M $NaNO_3$), accounting to 99.43% of the Cs mass. After the change in ionic strength, an additional 0.432% of the Cs was eluted. The colloid-associated Cs amounted to 0.428%. A negligible amount of Cs (0.004%) was detected in the solution phase during the colloid mobilization experiment. Based on the mass balance calculation, the 0.428% of colloid-associated Cs might not seem like much; however, considering the portion of Cs remaining inside the column after the first Cs

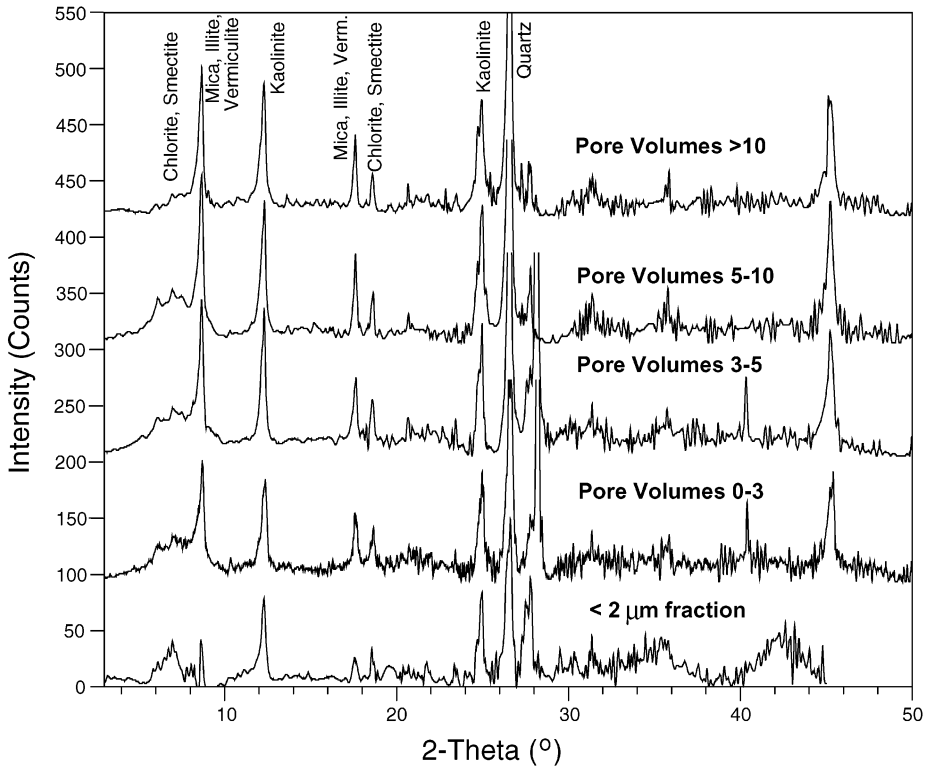

FIGURE 6. X-ray diffraction patterns (K-saturated, air-dried) of <2 μm-fraction of the sediments (bottom curve) and the mobilized colloids for different portions of the breakthrough curve (four upper curves).

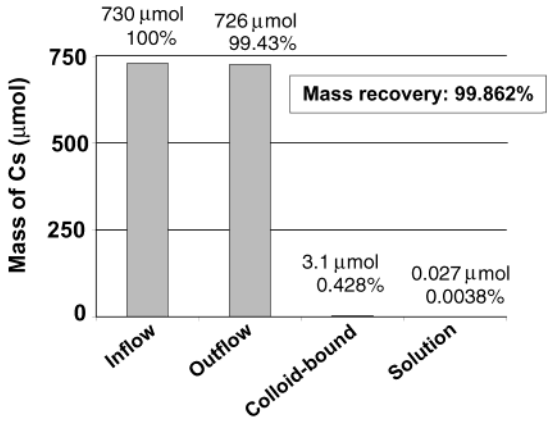

FIGURE 7. Mass balance calculations from Cs breakthrough curves and colloid mobilization experiment.

breakthrough curve, the eluted colloid-associated Cs accounts for 75.09% of the Cs remaining in the column. A considerable amount of the Cs remaining in the column was therefore mobilized via colloidal particles.

The amount of Cs mobilized with colloids was 3.1 μmol or, related to the mass of sediments in the column, 5.59×10^{-8} mol/g (Figure 7). This number is similar to the concentration of poorly exchangeable Cs, reported as 3.45×10^{-8} mol/g, calculated from batch sorption studies with Hanford sediments under high Na background (5 M $NaNO_3$) (*21*). Zachara et al. (*21*) also estimated the concentration of frayed edge sites using the AgTU-method, which, at 4.92×10^{-8} mol/g, was similar to the concentration of poorly exchangeable Cs. Considering the experimental errors involved in the mass balance calculations and the variability of Hanford sediments, this agreement is remarkable. It is therefore plausible that the Cs attached to the mobilized colloids was mainly poorly exchangeable and associated with frayed edge sites.

Implications for Radionuclide Transport. The results of this column experiment can be applied to the situation of Hanford tank leakage. Chemical conditions in our experiment were chosen to mimic a tank leak at Hanford. It is known that colloid mobilization is dependent on the water flow rate (*7*, *19*). The flow rate in our experiment (1.26 m/d) is well within the range of saturated and unsaturated hydraulic conductivities measured in sediments from the Hanford formation (*26*). We have demonstrated that in situ colloid mobilization from Hanford sediments is possible and that the mobilized colloids can facilitate the transport of sorbed Cs. Although Cs is mobile at high ionic strength, the mobility of colloid-bound Cs is much better. Colloid-bound Cs traveled almost unretarded through our column. The colloids mobilized from the sediments consisted of minerals that are known to sorb Cs strongly, including micas and illites, and which are also known to retain some of the ^{137}Cs that has leaked from the waste tanks. At this time, however, we do not know how far the mobilized colloidal material will travel through the vadose zone and what the conditions would be under unsaturated flow.

Acknowledgments

This work was supported by the Environmental Management Science Program, U.S. Department of Energy under contract DE-FG07-99ER62882, Project Officers Drs. Frank Wobber and Chester Miller. We thank Jeff Boyle (Washington State University, WSU) for his help with XRD and cesium measurements, the Electron Microscopy Center at WSU for use of their facility, and John Zachara and Jeff Serne (Pacific Northwest National Laboratory) for providing us with the Hanford sediments. We thank three anonymous reviewers for helpful suggestions.

Literature Cited

(1) Gephart, R. E.; Lundgren, R. E. *Hanford Tank Cleanup: A Guide to Understanding the Technical Issues*, 4th ed.; Battelle Press: Columbus, 1998.

(2) McCarthy, J. F.; Degueldre, C. In *Environment Particles*; Buffle, J., van Leeuwen, H., Eds.; Lewis Publisher: Boca Raton, FL, 1993; Vol. II, pp 247−315.
(3) Ryan, J. N.; Elimelech, M. *Colloids Surf.* **1996**, *107*, 1−56.
(4) Grolimund, D.; Borkovec, M. *Environ. Sci. Technol.* **1999**, *33*, 4054−4060.
(5) Kretzschmar, R.; Borkovec, M.; Grolimund, D.; Elimelech, M. *Adv. Agron.* **1999**, *66*, 121−193.
(6) Grolimund, D.; Borkovec, M.; Barmettler, K.; Sticher, H. *Environ. Sci. Technol.* **1996**, *30*, 3118−3123.
(7) Kaplan, D. I.; Bertsch, P. M.; Adriano, D. C.; Miller, W. P. *Environ. Sci. Technol.* **1993**, *27*, 1193−1200.
(8) Seaman, J. C.; Bertsch, P. M.; Miller, W. P. *Environ. Sci. Technol.* **1995**, *29*, 1808−1815.
(9) Seaman, J. C.; Bertsch, P. M.; Strom, R. N. *Environ. Sci. Technol.* **1997**, *31*, 2782−2790.
(10) Nightingale, H. I.; Bianchi, W. C. *Ground Water* **1977**, *15*, 146−152.
(11) McKinley, J. P.; Zeissler, C. J.; Zachara, J. M.; Serne, R. J.; Lindstrom, R. M.; Schaef, H. T.; Orr, R. D. *Environ. Sci. Technol.* **2001**, *35*, 3433−3441.
(12) Serne, R. J.; Zachara, J. M.; Burke, D. S. *Chemical Information on Tank Supernatants, Cs Adsorption from Tank Liquids onto Hanford Sediments, and Field Observations of Cs Migration from Past Tank Leaks*; Pacific Northwest National Laboratory, PNNL-11495/UC-510: Richland, WA, 1998.
(13) Cady, J. G.; Wilding, L. P.; Drees, L. R. *In Methods of Soil Analysis. Part 1. Physical and Mineralogical Methods*; Klute, A., Ed.; American Society of Agronomy: Madison, Wisconsin, 1986; 2nd ed., pp 185−218.
(14) Whittig, L. D.; Allardice, W. R. *In Methods of Soil Analysis. Part 1. Physical and Mineralogical Methods*; Klute, A., Ed.; American Society of Agronomy: Madison, Wisconsin, 1986; 2nd ed., pp 331−362.
(15) Fortin, J.; Flury, M.; Jury, W. A.; Streck, T. *J. Contam. Hydrol.* **1997**, *25*, 219−234.
(16) Press, W. H.; Teukolsky, S. A.; Vetterling, W. T.; Flannery, B. P. *Numerical Recipes. The Art of Scientific Computing*, 2nd ed.; Cambridge University Press: Cambridge, 1992.
(17) Scheidegger, A.; Bürgisser, C. S.; Borkovec, M.; Sticher, H.; Meeussen, H.; van Riemsdijk, W. *Water Resour. Res.* **1994**, *30*, 2937−2944.
(18) Jacobsen, O. H.; Moldrup, P.; Larson, C.; Konnerup, L.; Petersen, L. W. *J. Hydrol.* (Amsterdam) **1997**, *196*, 185−203.
(19) Ryan, J. N.; Illangasekare, T. H.; Litaor, M. I.; Shannon, R. *Environ. Sci. Technol.* **1998**, *32*, 476−482.
(20) Grolimund, D.; Elimelech, M.;Borkovec, M.; Barmettler, K.; Kretzschmar, R.; Sticher, H. *Environ. Sci. Technol.* **1998**, *32*, 3562−3569.
(21) Zachara, J. M.; Smith, S. C.; Liu, C.; McKinley, J. P.; Serne, R. J.; Gassman, P. L. *Geochim. Cosmochim. Acta* **2002**, *66*, 193−211.
(22) Cremers, A.; Elsen, A.; de Preter, P.; Maes, A. *Nature* **1988**, *335*, 247−249.
(23) Cornell, R. M. *J. Radioanal. Nuclear Chem.* **1993**, *171*, 483−500.
(24) Comans, R. N. J.; Haller, M.; de Preter, P. *Geochim. Cosmochim. Acta* **1991**, *55*, 433 −440.
(25) Comans, R. N. J.; Hockley, D. E. *Geochim. Cosmochim. Acta* **1992**, *56*, 1157−1164.
(26) Khaleed, R.; Freeman, E. J. *Variability and Scaling of Hydraulic Properties for 200 Area Soils, Hanford Site*; Westinghouse Hanford Company, WHC-EP-0883: Richland, WA, 1995.

Received for review March 9, 2002. Revised manuscript received July 26, 2002. Accepted September 17, 2002.

ES025638K

Nitrate and colloid transport through coarse Hanford sediments under steady state, variably saturated flow

Kelly D. Cherrey, Markus Flury, and James B. Harsh

Department of Crop and Soil Sciences, Center for Multiphase Environmental Research, Washington State University, Pullman, Washington, USA

Received 27 December 2002; revised 18 February 2003; accepted 17 March 2003; published 24 June 2003.

[1] At the U.S. Department of Energy's Hanford Reservation, colloid-facilitated transport is a potential mechanism for accelerated movement of radionuclides like Cs-137. Here we investigate the transport of colloids through Hanford sediments under steady state, unsaturated flow conditions. We isolated colloids from Hanford sediments by dispersion and sedimentation and determined colloid breakthrough curves in packed sediment columns. A column system was developed with which we could control volumetric water contents with accuracy better than 0.01 effective saturation and the water potentials to better than 0.06 cm-H_2O. Inflow and outflow boundary conditions had to be meticulously controlled to ensure uniformity of water contents and water potentials inside the column. Colloid breakthrough curves were determined under a series of water contents ranging from 0.2 to 1.0 effective saturation. Colloids were mobile under all water saturations, but the total amount of colloids transported decreased with decreasing water saturation. Colloid behavior was described with the mobile-immobile model concept, including first-order deposition from the mobile phase only. *INDEX TERMS:* 1831 Hydrology: Groundwater quality; 1832 Hydrology: Groundwater transport; 1866 Hydrology: Soil moisture; 1875 Hydrology: Unsaturated zone; *KEYWORDS:* colloids, unsaturated flow, vadose zone

Citation: Cherrey, K. D., M. Flury, and J. B. Harsh, Nitrate and colloid transport through coarse Hanford sediments under steady state, variably saturated flow, *Water Resour. Res.*, *39*(6), 1165, doi:10.1029/2002WR001944, 2003.

1. Introduction

[2] Colloidal particles have been suspected and, in some cases shown, to facilitate the movement of contaminants through the subsurface [*McCarthy and Zachara*, 1989; *Kretzschmar et al.*, 1999]. While much information is available about colloid transport under water saturated conditions [*Kersting et al.*, 1999], much less is known about the behavior of colloids in the vadose zone. Results from the few studies conducted indicate that colloid movement under unsaturated conditions is less effective than under saturated conditions, with more and more colloids being removed from the fluid phase as the water content of the soil and sediments decreases. This has been demonstrated for inorganic silica colloids [*Lenhart and Saiers*, 2002], as well as organic colloidal bacteria [*Wan et al.*, 1994; *Schäfer et al.*, 1998; *Jewett et al.*, 1999] and viruses [*Chu et al.*, 2001].

[3] During saturated and unsaturated flow, colloids are deposited at the solid-liquid interface. For unsaturated flow, colloids are also removed from the fluid phase by two other major mechanisms: (1) attachment to the liquid-gas interface and (2) straining in liquid films that have thickness smaller than colloid diameters [*Wan and Tokunaga*, 1997; *Lenhart and Saiers*, 2002]. With decreasing water saturation, the liquid-gas interfacial area increases and the film thickness decreases, and consequently colloids are more likely to be deposited inside the porous medium. It has been postulated that capillary-based liquid pathways are effective conduits for colloid movement as long these conduits form connected pathways, and that at low water saturations these conduits become discontinuous causing an abrupt decrease in colloid transport [*Wan and Tokunaga*, 1997].

[4] Contaminants of particular concern for colloid-facilitated movement are the strongly sorbing radionuclides cesium, plutonium, and americium. At the Hanford Reservation in south-central Washington state, cesium-137 has been released to the vadose zone from leaking underground waste storage tanks [*Gephart and Lundgren*, 1998; *McKinley et al.*, 2001]. Cesium-137 is the major contributor to the radioactivity released by leaking waste tanks. The current depth distribution of cesium indicates that cesium has, at least in part, moved in accordance with a chromatographic model [*Zachara et al.*, 2002], but colloid-facilitated transport as an important transport mechanism cannot be ruled out. The geochemical conditions under leaking Hanford waste tanks is conducive to in situ colloid alteration and formation [*Bickmore et al.*, 2001; *Zhao et al.*, 2001]. It has been shown that the displacement of high ionic strength solutions by water of low ionic strength can induce in situ mobilization of native colloids from the Hanford sediments [*Blume et al.*, 2002; *Flury et al.*, 2002]. If these colloids can move large distances through the vadose zone at Hanford, there is a possibility for colloid-facilitated transport of radionculides. It has also been shown that mobilized colloids can be trapped by fine-textured sediment layers, resulting in a permeability reduction of the fine-textured sediments [*Blume et al.*, 2002]. In this study, we focus on colloid transport within a single, coarse-textured sediment layer only.

Copyright 2003 by the American Geophysical Union.
0043-1397/03/2002WR001944$09.00

[5] The goal of this study was the accurate measurement of colloid transport in unconsolidated Hanford sediments under well controlled saturated and unsaturated water contents at steady state fluxes. The experimental objective was the development of a laboratory column apparatus to control levels of effective saturation (S_e) at better than 0.01 error (σ_{S_e}). S_e is defined as

$$S_e = \frac{\theta_v - \theta_r}{\theta_s - \theta_r} \quad (1)$$

where θ_v is the volumetric water content, θ_r is the residual water content, and θ_s is the saturated water content. Breakthrough curves were done with a conservative $NaNO_3$ tracer, and two types of colloids: those removed from Hanford sediments and those modified by a simulated Hanford tank-waste solution [*Zhao et al.*, 2001].

2. Materials and Methods

2.1. Column Setup

[6] The experimental apparatus was designed [*Cherrey*, 2002] to accurately measure unsaturated colloid transport under steady state flux and unit hydraulic gradient (Figure 1). The column (acrylic, with internal diameter and length of 5 and 20 cm, respectively) was selected to minimize flow alterations around the tensiometers and along the wall edge. Five porous ceramic tensiometers (652X03-B1M3, 1 bar high flow, Soilmoisture Equipment Inc., Santa Barbara, CA) were equally spaced vertically and radially (i.e., equally on a helix). The water tension within each tensiometer was monitored by an electronic strain gauge pressure transducer (PX170-28DV, Omega Engineering, Stamford, CT). The average water content of the column was monitored gravimetrically with an electronic strain gauge load cell (PT1002, Precision Transducers Ltd., Castle Hill, Australia). This average water content was then transformed to effective saturation using equation (1).

[7] A sprinkler and peristaltic pump were used to supply influent to the column upper boundary. Flow through the sprinklers was controlled by a four channel peristaltic pump (Ismatec ISM760, Glattbrugg, Switzerland). Two different sprinkler heads were designed for high and low flow rate applications. Using three, two, or one of the pump channels, a high-flow sprinkler provided uniform flow rates from 90 mL min^{-1} down to 2–3 mL min^{-1}. A low-flow sprinkler was used for lower flow rates. Both sprinklers were designed with a low dead volume (≈0.2 mL) to minimize dispersion during influent switch-over. Tubing to the peristaltic pump and between the pump and the sprinkler was 1/16″ (1.6 mm) I.D. Tygon.

[8] The lower boundary condition was controlled at constant potential using a hanging water column [*Hillel*, 1998, *p. 167*] with a custom porous glass frit. The custom glass frit (ACE glass fiber disc, porosity C, 2.8 mm thick, 59.7 mm diameter, ACE Glass Inc., Vineland, NJ) was selected after testing against a porous stainless steel frit and nylon membranes. In contrast to the glass frit, colloids were captured in a stainless steel frit with pore diameter of ≈10 μm. The nylon membranes were susceptible to puncturing by the jagged Hanford sediments. The ACE frit carrys a negative charge, provides adequate mechanical support, has high hydraulic conductivity, and minimizes

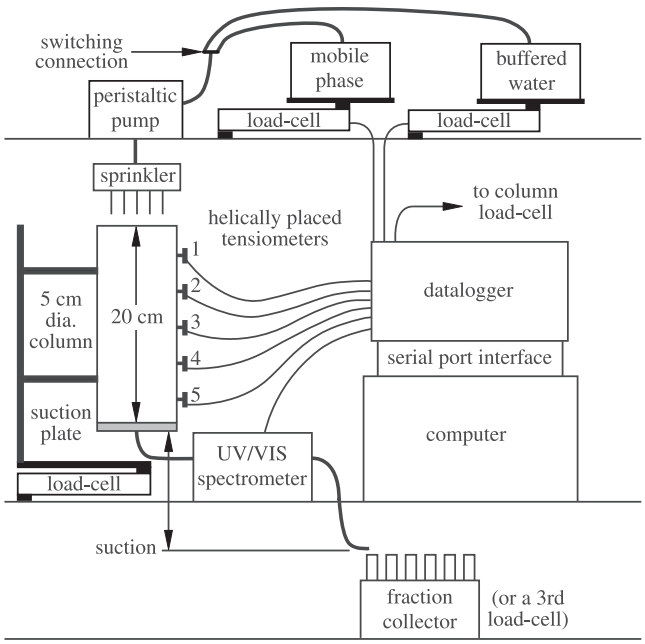

Figure 1. Schematic of experimental column setup.

colloid capture. The ACE frit had a bubbling pressure of ≈45 cm-H_2O (pressure when air bubbling begins) corresponding to a pore diameter of 65 μm. Saturated hydraulic conductivity of the ACE frit, measured by the falling head method [*Hillel*, 1998], was 0.11 cm min^{-1}. The ACE frit was epoxied to a Teflon sealing ring treated with FluoroEtch (Acton Technologies, Pittston, PA). This assembly was mated to acrylic column surfaces with flat Buna-N O-rings. When saturated, the ACE frit held 3.2 mL of water.

[9] The column outflow was measured in real-time using a Perkin Elmer LC95 UV/VIS spectrometer. The LC95 flow cell was modified for high flow rates (up to ≈90 mL min^{-1}). The flow cell (1/16″ I.D. = 1.6 mm) was constructed using a Torlon flow cylinder with quartz lenses and stainless steel tubing connections. All outflow tubing was 1/8″ (3.2 mm) I.D. Tygon.

[10] The weight of inflow, column, and outflow was monitored with electronic load cells. Within a laboratory temperature fluctuation of 21 to 25°C, the standard deviation of calibrated load cells (σ_w) was less than 0.4 g, and the standard deviation of calibrated pressure transducers (σ_h) was typically less than 0.02 cm-H_2O. These measurement errors were less than the design goals of $\sigma_w \approx 1.3$ g and $\sigma_h \approx 0.06$ cm-H_2O for $\sigma_{S_e} = 0.01$. Load cells and pressure transducers were calibrated prior to experimentation. Load cells, pressure transducers, and spectrometer were interfaced to a data logger (CR-7X, Campbell Scientific, Logan, UT).

2.2. Sediments and Sediment Treatment

[11] Sediments from the Hanford formation were obtained from the Submarine Site (218-E-12B) at the U.S. DOE Hanford Reservation in south-central Washington state. These coarse, unconsolidated sediments were air dried and filled into plastic buckets. These sediments are representative of the material underlying the S-SX (single-shell) tank farm in the 200 East Area (personal communication,

Bruce N. Bjornstad, September 2001, Pacific Northwest National Laboratories, Richland, WA). Detailed characterization data are reported by *Serne et al.* [2002a]. A 2-mm-square sieve was used to remove coarse particles from the sediments.

[12] To prevent colloid mobilization of residual colloids during the transport experiments, the sediments were treated to reduce the colloid fraction. Before treatment, Na^+ cation exchange was done to minimize cation exchange during breakthrough experiments. About 1 kg of sediment was packed into an acrylic column with internal diameter and length of 5 and 30 cm, respectively. Seven pore volumes of 1 M NaCl buffered at pH 10 (1.67 mM $NaHCO_3$ + 1.67 mM Na_2CO_3) were pumped through the column, followed only by pH 10 buffered water until the electrical conductivity of the outflow was less than 1 dS m^{-1}. The sediment was then removed from the column and simultaneously agitated and sonicated for at least five minutes in pH 10 buffered water. After settling through 10 cm of this pH 10 buffered water for about 16 hours the suspension was decanted and saved for the native colloid source. This process was repeated daily for 2 weeks, after which the sediment was packed into a column and additional colloids were removed by pumping through about 300 pore volumes of pH 10 buffered water. Approximately 6.5 g of colloids per kg of sediment were removed by sonication and sedimentation. Column mobilization removed another 3.5 g per kg of sediment.

[13] The solutions used for pretreatment and the following transport experiments were all buffered at pH 10 to prevent carbonate dissolution and to mimic Hanford tank farm conditions. The pH of the sediments used was 7.8 (in 1:1 w/w H_2O) and under the S-SX tank farm, the pH is in the range of 9 to 10 [*Serne et al.*, 2002b]. Our solutions were buffered to maintain a stable pH throughout the experiments.

[14] The particle size distribution of the treated sediment was determined by dry sieving. Petrographic thin sections were prepared and the primary minerals were determined with a petrographic microscope [*Cady et al.*, 1986].

2.3. Tracer and Colloidal Material

[15] Sodium nitrate ($NaNO_3$, 0.2 mM) was used as a conservative tracer to determine column parameters before infusing colloids. Colloid transport was measured with two types of colloids: native and modified. Native colloids were obtained from the colloid suspensions decanted during sediment treatment. Modified colloids were separated after reacting Hanford sediment with a simulated Hanford tank waste solution (1.4 *m* NaOH, 0.25 *m* $NaAlO_4$, and 3.7 *m* $NaNO_3$) at 50°C for 40 days [*Zhao et al.*, 2001]. This procedure was designed to mimic the reactions taking place in the subsurface after a Hanford tank leak [*Zhao et al.*, 2001]. Modified colloid suspensions were decanted from the reacted sediment after ≈16 hours of gravity sedimentation through a depth of 10 cm of suspension. Solids of both types of colloids were resuspended by sonication and decanted after settling for 2 weeks. The concentration of these suspensions (≈10 mg L^{-1}) remained stable for at least three days.

[16] Colloid mineralogy was characterized by X-ray diffraction (Philips XRG 3100, Philips Analytical Inc., Mahwah NJ) with Cu-Kα radiation [*Whittig and Allardice*, 1986]. Colloid particle size was determined by static light scattering (MasterSizer S, Malvern Instruments Ltd., Malvern, UK) and dynamic light scattering (Zetasizer 3000HSa, Malvern Instruments Ltd., Malvern, UK with a Helium-Neon laser at 633 nm wavelength). Electrophoretic mobility of the colloids was measured by the Zetasizer 3000HSa. All light scattering experiments were made with colloids suspended in 1.67 mM $NaHCO_3$ + 1.67 mM Na_2CO_3 pH 10 buffers (I = 6.67 mM).

2.4. Spectrometer Measurements

[17] Nitrate (NO_3^-) and colloid breakthrough concentrations were measured with a Perkin Elmer LC95 single wavelength UV/VIS spectrometer. Optimal wavelength for nitrate measurement was determined with the aid of an HP8452A full spectrum diode-array UV/VIS spectrometer. The HP8452A spectrometer showed uniform, monomodal peak shapes with regard to wavelength at nitrate concentrations lower than 0.2 mM. The LC95 spectrometer reproducibly detected these nitrate peaks when dialed to 204 nm from below. For reproducible colloid detection, the LC95 spectrometer was dialed to 300 nm from below. The wavelength of 300 nm was found to be optimal based on the absorption spectrum of the colloids; nitrate was essentially undetectable at 300 nm. Reproducible operation of the LC95 at these two wavelengths is necessary during the course of experimentation since nitrate, native colloid, and modified colloid breakthroughs were done in sequence at each water content. Calibration curves showed that nitrate concentration versus spectrometer response was slightly nonlinear and we fitted a quadratic function as calibration curve. Colloid concentration versus spectrometer response was linear. Analytical detection limits were 0.002 mM for nitrate and 0.2 mg L^{-1} for colloids.

2.5. Hydraulic Properties and Transport Experiments

[18] The column was packed by incrementally filling moistened sediments under flowing CO_2 gas. The background electrolyte solution (pH 10 buffered water) was pumped from the bottom to keep the sediments saturated. After the column was packed, about 20 pore volumes of pH 10 buffered water were pumped through to dissolve CO_2 gas bubbles and remove the dissolved CO_2. The pore volume of the saturated column was determined based on identically packed smaller cylinders, and independently verified by analysis of nitrate breakthrough curves. Saturated hydraulic conductivity of the packed sediments was measured by the constant head method, taking into account the saturated conductivity of the porous frit [*Hillel*, 1998]. Unsaturated hydraulic conductivities were obtained from the water flux and water potential measurements during the nitrate breakthroughs. The moisture characteristic of the sediments was measured by the hanging water column technique and confirmed during the nitrate breakthroughs.

[19] Nitrate and colloid breakthroughs were all buffered at pH 10 (1.67 mM $NaHCO_3$ + 1.67 mM Na_2CO_3). The experiments were run in a specific sequence, starting with the saturated column followed by incrementally lowering the water content. The column was uniformly desaturated by adjusting the inlet flow rate and the outlet suction. The

experimental goal was to uniformly decrease the effective water saturation S_e = 1.0, 0.9, 0.8, . . ., 0.1; however, it was not possible to uniformly desaturate the column at S_e = 0.9, 0.8, and 0.1.

[20] Water potential was predicted by fitting the van Genuchten equation, $S_e = [1 + (\alpha h)^n]^{(1/n-1)}$ [*van Genuchten*, 1980], to the measured moisture characteristic, where h is the water potential, α is the inverse of the air-entry potential, and n is a parameter related to the pore size distribution. Uniform water flux, water content, and water potential along the column was established at each water content. The high-flow sprinkler was used for $S_e \geq 0.3$, the low-flow sprinkler was used for $S_e < 0.3$.

[21] At each water content, first a nitrate breakthrough was performed, followed by a native colloid breakthrough, and finally a modified colloid breakthrough. The amount of colloid infused was minimized to prevent loading the column with colloids. The pH 10 buffered water was used to elute the nitrate and colloids, and to adjust the column to the next water content. Breakthroughs were reproducible and neither colloid breakthrough influenced subsequent breakthroughs.

2.6. Data Analysis

[22] The nitrate and colloid breakthroughs are modeled using the physical nonequilibrium mobile-immobile model (MIM). Steady state unsaturated flow has often been found to correspond to the MIM physical nonequilibrium concept [*Gaudet et al.*, 1977; *De Smedt and Wierenga*, 1984; *Bond and Wierenga*, 1990; *Padilla et al.*, 1999; *Gamerdinger and Kaplan*, 2000]. We assume that colloid deposition only occurs from the mobile water phase and is negligible in the immobile phase. First-order deposition coefficients are often found directly proportional to the pore water velocity [*Kretzschmar et al.*, 1999], so that deposition in the immobile phase will vanish. Under these assumptions, the dimensionless form of the MIM can be written as [*Toride et al.*, 1995]:

$$\beta\frac{\partial C_m}{\partial T} + (1-\beta)\frac{\partial C_{im}}{\partial T} = \frac{1}{Pe}\frac{\partial^2 C_m}{\partial Z^2} - \frac{\partial C_m}{\partial Z} - \mu_m C_m \qquad (2)$$

$$(1-\beta)\frac{\partial C_{im}}{\partial T} = \omega(C_m - C_{im}) \qquad (3)$$

where C_m and C_{im} are the scaled solute concentrations in the mobile and immobile water phases, respectively, $\beta = \theta_m/(\theta_m + \theta_{im}) = \theta_m/\theta$ is the ratio of mobile water content to total water content, $Pe = vL/D$ is the Peclet number, where v is the pore water velocity and L is the length of the column, $\omega = \alpha L/(\theta_m v)$ is a Dahmköhler number expressing the ratio of the mass transfer coefficient to the pore water velocity, $T = vt\theta_m/(\theta L)$ is the dimensionless time where t is the time, $Z = z/L$ is the dimensionless depth where z is the depth, and μ_m is the first-order deposition coefficient for colloids in the mobile region. The dimensionless deposition coefficient μ_m is defined as $\mu_m = L\theta_m\mu/(\theta v)$, where μ is the deposition coefficient with dimensions one over time. Scaled concentrations are defined as absolute concentrations divided by the concentration in the inlet. An analytical solution of (2) and (3) for a semi-infinite column with Dirichlet boundary conditions was fitted to the experimental data using CXTFIT 2.1 [*Toride et al.*, 1995]. For nitrate, we assumed that $\mu_m = 0$.

Table 1. Particle Size Distribution of Treated Hanford Sediments

Diameter, mm	Concentration, % (by weight)	Standard Deviation, % (by weight)
2.0–1.0	74.99	3.65
1.0–0.5	19.37	3.09
0.5–0.25	3.57	1.08
0.25–0.124	0.91	0.19
0.124–0.053	0.80	0.13
<0.053	0.33	0.10

3. Results and Discussion

3.1. Sediments and Colloid Characterization

[23] Treated sediments show a highly skewed particle size distribution peaked between 1 and 2 mm (Table 1). The primary minerals were mainly quartz, plagioclase, K feldspar, amphibole, sericite, pyroxene, magnetite, biotite, and muscovite. Native colloids consisted mainly of chlorite, smectite, vermiculite, kaolinite, illite, and quartz. Modified colloids were composed of similar mineral phases as the native colloids and contained new mineral phases. For modified colloids, the native mineral phases kaolinite and quartz have been partially or completely dissolved in the high alkaline environment of simulated Hanford tank waste, and the new mineral phases cancrinite and sodalite have been detected [*Zhao et al.*, 2001]. The resulting colloids consisted of a mixture of: (1) newly-formed phases (e.g., cancrinite and sodalite), (2) partially dissolved native soil minerals, and (3) unaltered native soil minerals. Electrophoretic mobilities were typically −4.0 and −4.5 (μm s^{-1})/(V cm^{-1}) for native and modified colloids, respectively. Particle size distributions of the two types of colloids were similar, with a mean Z-averaged diameter of 348 ± 14 nm for the native and 368 ± 16 nm for the modified colloids (Figure 2).

3.2. Hydraulic Properties

[24] The coarse-textured sediments show a pronounced air-entry pressure of about 7 cm-H_2O suction and reach their residual water content at suctions larger than about 30 cm-H_2O (Figure 3a). The narrow range of suctions needed to drain the sediments was explicitly considered in the design of the column system, and in particular for the accuracy needed for pressure transducers and load cells as well as for the selection of the porous plate (glass frit) to control the lower boundary condition. The hydraulic conductivities of the column are large, but decrease considerably as the column desaturates (Figure 3b). The parameters of the van Genuchten equation are α = 0.136, n = 4.776, θ_r = 0.06, and θ_s = 0.394.

3.3. Water Contents and Water Potentials

[25] Water contents and water potentials need to be meticulously controlled and monitored to ensure uniform and constant hydraulic conditions during unsaturated transport experiments. Hydraulic conditions were generally more variable during colloid breakthroughs than during nitrate breakthroughs, possibly because of colloid capture in the sediment matrix and the porous plate. Water contents

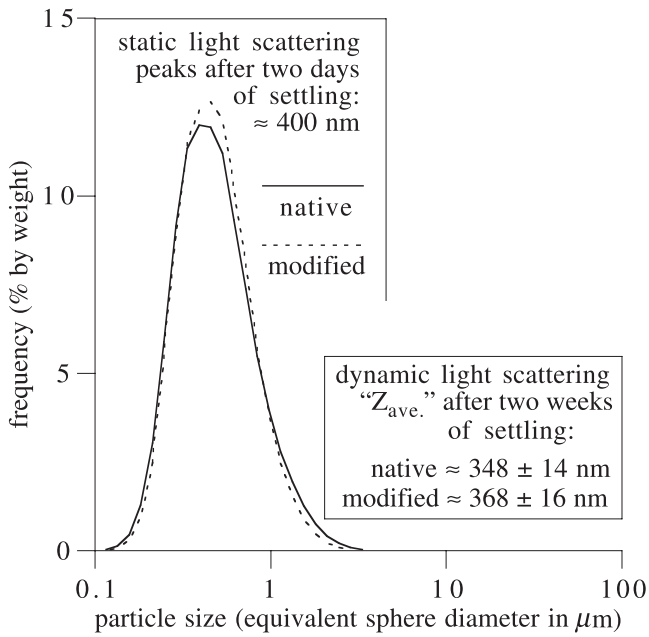

Figure 2. Particle size distribution of native and modified colloids in the inflow suspensions used for transport experiments.

remained constant during nitrate breakthroughs, and slightly increased during colloid breakthroughs (Figure 4). This effect was more pronounced as the water content of the sediments decreased. The weight increase with time (or pore volume) was clearly due to an increase in water content and not due to the mass of colloids captured inside the column. The mass of colloids captured inside the column (at most 1.5 mg during a colloid breakthrough curve) could not be resolved with our apparatus.

[26] The water potential measurements confirmed the observations from the water content measurements. During nitrate breakthrough, water potentials remained constant and very uniform, especially between tensiometers 2 and 4. For $S_e = 0.7$, the bottom tensiometer (tensiometer 5) indicated wetter conditions near the bottom plate than at the other parts of the column (Figure 5a), whereas for $0.7 > S_e \geq 0.2$, the water potentials were more uniformly distributed ($S_e = 0.3$ shown in Figure 5b is representative of the uniformity). During colloid breakthrough, the water potentials changed to slightly wetter conditions. This was most pronounced near the bottom of the column and with native colloids. After colloid breakthrough, tensiometer readings showed that the bottom of the column becomes drier again. This suggests colloid capture in the porous plate with some colloids released after influent is switched back to the colloid-free solution. These results show that it was not possible to maintain a unit hydraulic gradient mainly near the bottom of the column at all times and for all water saturations. Between tensiometers 2 and 4 the hydraulic gradient was no worse than 0.95, and typically much closer to one.

[27] Effective water saturations for the nitrate breakthroughs were S_e = 1.0, 0.69, 0.60, 0.50, 0.40, 0.30, 0.20, and 0.16. Uniform water contents were not achieved at S_e = 0.9 and 0.8 because of outflow restrictions, mainly due to the hydraulic conductivity and bubbling pressure of the suction plate. Effective saturations during the colloid breakthroughs were slightly higher, namely S_e = 1.0, 0.69, 0.61, 0.51–0.52, 0.41–0.42, 0.32–0.33, and 0.21–0.22, where, if a range is given, the first number denotes the native colloid breakthrough and the second number the modified colloid breakthrough. Mainly during colloid breakthrough, the bottom of the column (indicated by tensiometer 5) had a higher water content than the remainder of the column, but the water content between tensiometers 1 to 4 was uniform. Colloid breakthroughs at $S_e = 0.16$ are not reported because of highly variable colloid detection, possibly because of suction plate colloid mobilization and variable colloid concentration in the sprinkler.

3.4. Nitrate Transport

[28] Nitrate breakthrough curves under saturated conditions followed the classical advection-dispersion behavior

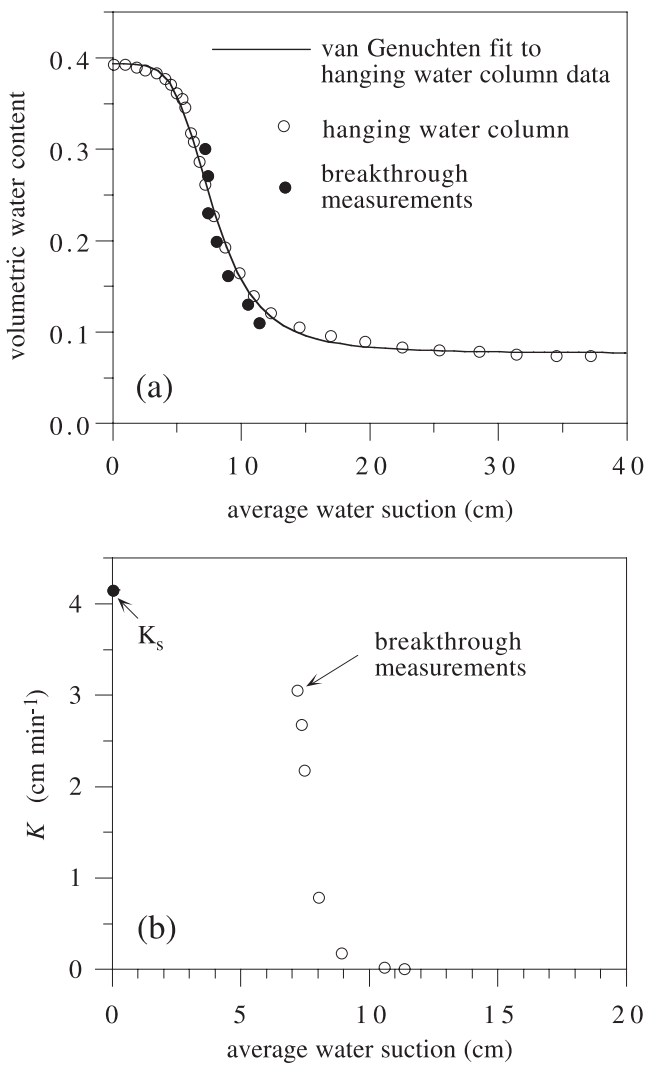

Figure 3. Hydraulic properties of sediments: (a) Moisture characteristic from sediments determined with hanging water column technique (open circles) and fitted van Genuchten equation (solid line); solid circles represent measurements obtained from column transport experiments. (b) Hydraulic conductivities measured during unsaturated transport experiments (open circles) and at saturation (solid circle).

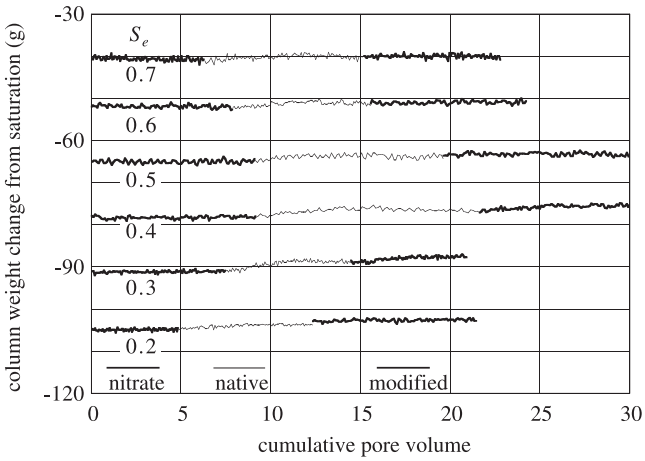

Figure 4. Column weight change during transport experiments at different water saturations. Ordinate indicates weight change referenced to the completely water-saturated column.

and the data were well described by the equilibrium advection-dispersion equation (ADE). Under unsaturated conditions, nitrate breakthrough curves show characteristic behavior in regard to initial tracer breakthrough and variance, as reported from other unsaturated tracer transport experiments [*Krupp and Elrick*, 1968; *Gaudet et al.*, 1977; *De Smedt and Wierenga*, 1984; *Padilla et al.*, 1999]: with decreasing water content, initial tracer breakthrough occurs earlier and breakthrough curve variance became larger (Figure 6). The unsaturated breakthrough data were well fitted with the MIM physical nonequilibrium model; measured and model parameters are summarized in Table 2. There was a substantial amount of immobile water present, which varied nonlinearly with the water saturation of the sediments. Whereas in the literature it was often reported that the fraction of immobile water increases with decreasing water content [*Gaudet et al.*, 1977; *Maraqa et al.*, 1997; *Griffioen et al.*, 1998; *Padilla et al.*, 1999], our analysis shows this was true only at high saturations—at low saturations the immobile water fraction decreased with decreasing water saturation (Figure 7). The increase in immobile water is usually attributed to the increase in film water and stagnant regions relative to the total water content [*Griffioen et al.*, 1998]. It appears that in our coarse sediments, immobile water regions develop as the system desaturates at high water contents, and that these regions themselves desaturate as the water content drops below $S_e = 0.5$.

[29] Model comparison showed that the mobile-immobile model was superior to the simple advection-dispersion model. As illustrated in Figure 8, the advection-dispersion equation was similar to the mobile-immobile model, and high-quality experimental data are necessary to distinguish between the two models. The conceptual difference between the two cases in Figure 8, however, is significant: the mobile-immobile model indicates that 27% of the water phase was immobile. Only one unsaturated result is shown

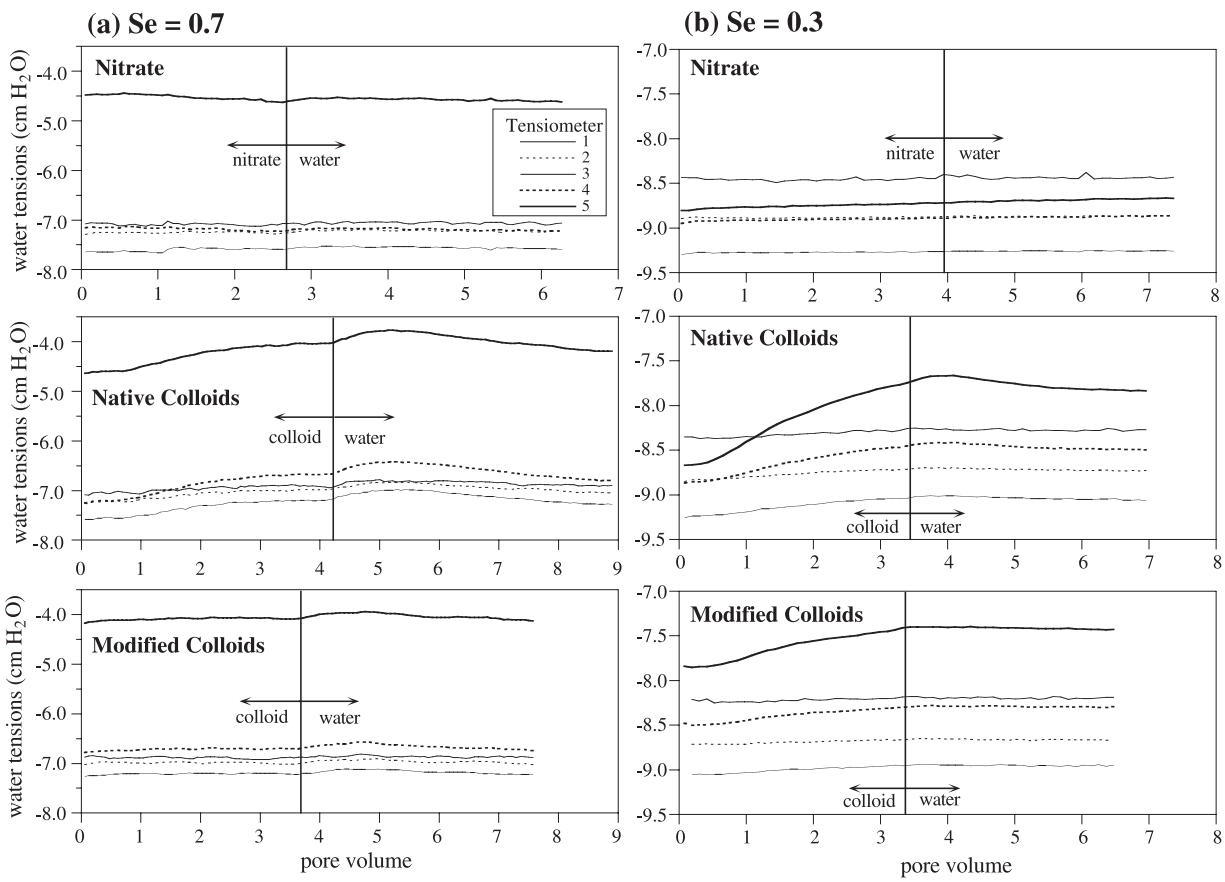

Figure 5. Tensiometer readings during transport experiments at effective water saturations of (a) S_e = 0.7 and (b) S_e = 0.3.

Table 2. Experimental and Modeling Summary for Nitrate Breakthroughs[a]

Measured Values				Mobile-Immobile Model Parameters					
S_e	θ, m^3 m^{-3}	J_w, cm min^{-1}	v, cm min^{-1}	v, cm min^{-1}	D, cm^2 min^{-1}	Pe	β	ω	Model R^2
1.0	0.40	4.107	10.16	10.08	5.857	33.2	–	–	0.999747
0.69	0.30	3.04	10.25	10.60	3.68	55.2	0.878	0.356	0.999952
0.60	0.27	2.68	10.05	10.41	4.05	49.2	0.810	0.487	0.999941
0.50	0.23	2.17	9.40	9.80	5.98	31.4	0.728	0.587	0.999885
0.40	0.20	0.783	3.99	4.19	3.34	34.0	0.730	0.623	0.999906
0.30	0.16	0.184	1.13	1.182	1.214	18.6	0.793	0.457	0.999885
0.20	0.13	0.022	0.178	0.183	0.184	19.0	0.804	0.392	0.998961
0.16	0.11	0.005	0.040	0.0368	0.054	13.1	0.841	0.184	0.996591

[a] S_e, effective saturation; θ, volumetric total water content; J_w, water flux; $v = J_w/\theta$, pore water velocity; D, hydrodynamic dispersion coefficient; Pe, Peclet number; β, fraction of mobile water content; ω, Dahmköhler number. Saturated water content θ_s = 0.40; residual water content θ_r = 0.06; column pore volume is 152.2 mL; column length is 19.15 cm.

in Figure 8; the remaining saturations gave very similar results.

3.5. Colloid Transport

[30] Native as well as modified colloids moved through the sediments at practically the same speed as the conservative nitrate tracer; however, the inflow concentrations were not reached during the injection pulse and the breakthrough curves show a plateau-like behavior (Figure 9). The modified colloid breakthrough plateau has a near-zero slope, but the native colloid breakthroughs show a more positive slope. Between S_e = 1 and 0.2, all breakthrough curves showed a smooth shape with monotonically increasing colloid concentrations during inflow and monotonically decreasing colloid concentrations during elution. At the lowest saturation for the modified colloids (S_e = 0.22), the elution portion of the breakthrough curve indicates that colloids were being eluted from the column and the concentrations did not return to zero as for the higher water saturations. This behavior is attributed either to in situ colloid mobilization or to release of colloids from the porous plate at the bottom of the column.

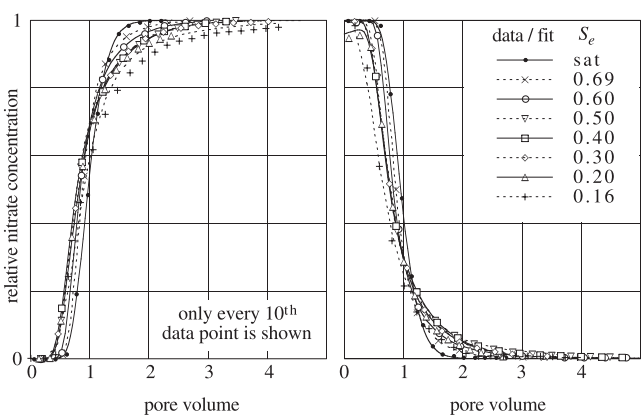

Figure 6. Breakthrough and elution limbs for the conservative tracer nitrate in Hanford sediments (2–2000 μm) under different effective water saturations S_e. Symbols are measured data; lines are model fits. The origin of each plot, i.e., pore volume = 0, indicates when nitrate was infused (breakthrough limb) and nitrate infusion was stopped (elution limb).

[31] All colloid breakthrough curves, except those at the lowest water saturation, were analyzed with the MIM. Fitted model parameters are listed in Table 3. The modified colloid behavior was well described with the MIM (Figure 9). The native colloid behavior, however, showed a more gradual increase of colloid concentration in the breakthrough limb than described by the MIM. This difference indicates that colloid deposition deviated from a first-order process, and is likely governed by a second-order process where colloid attachment sites are being blocked or filled up [*Chu et al.*, 2001; *Lenhart and Saiers*, 2002]. We attribute the different behavior of native and modified colloids to their different mineralogical composition and different electrophoretic mobility.

[32] The mass of colloids eluted from the column decreased in a nonlinear fashion with decreasing water saturation (Figure 10). At water saturations greater than S_e = 0.5, more than 80% of the infused colloids were eluted, but at S_e < 0.5, a considerable amount of colloids remained in the column. The increased colloid retention as the water

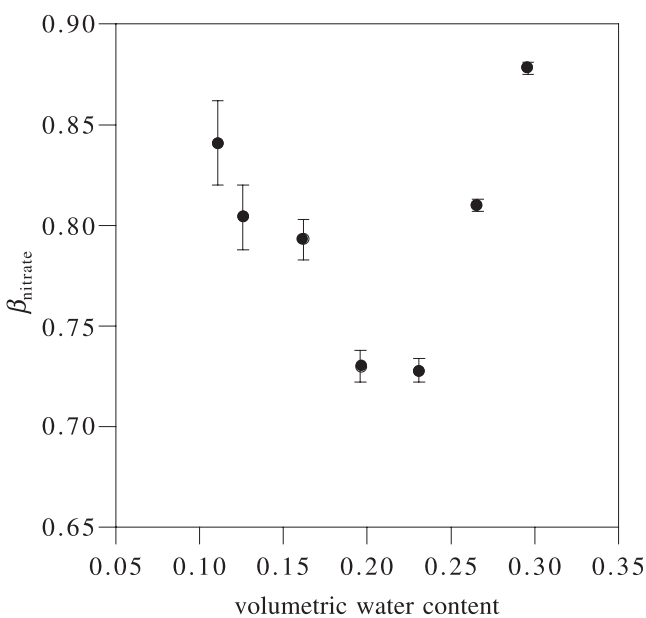

Figure 7. Fraction of mobile water $\beta = \theta_m/(\theta_m + \theta_{im})$ as a function of water content determined from nitrate data. Vertical bars represent ±1 standard deviation.

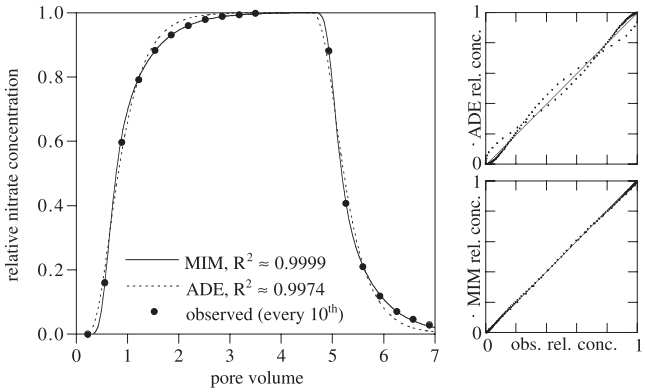

Figure 8. Comparison between fits of advection-dispersion equation (ADE) and mobile-immobile model (MIM) to nitrate breakthrough curve at $S_e = 0.5$. The subplots show the relation between ADE and MIM breakthrough data; the solid line is the 1:1 relation, shown as a guide to the eye.

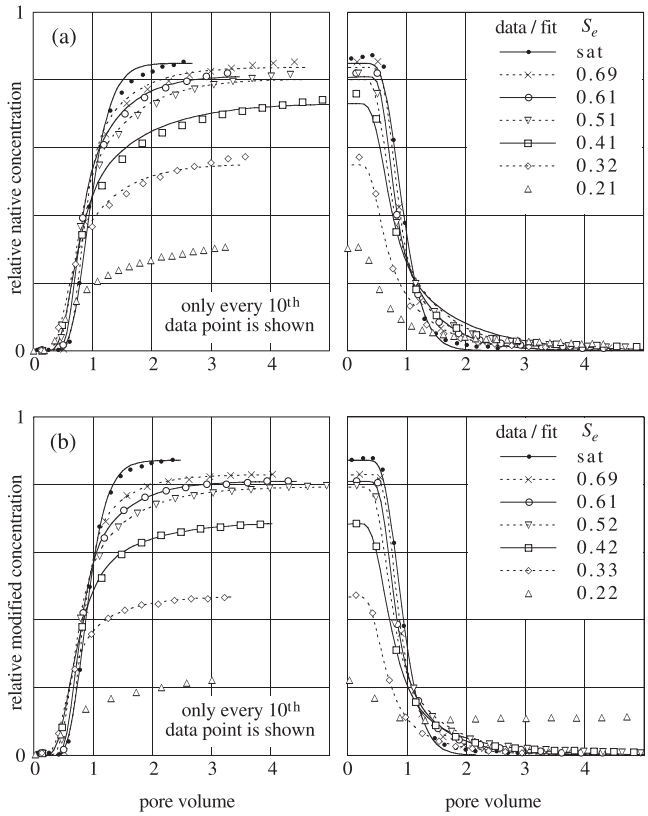

Figure 9. Breakthrough curves for (a) native and (b) modified colloids in Hanford sediments under different water saturations. Symbols are measured data; lines are MIM model fits. Data for the lowest water saturations were not fitted due to residual turbidity. The origin of each plot, i.e., pore volume = 0, indicates when colloids were infused (breakthrough limb) and colloid infusion was stopped (elution limb).

saturation decreases has been consistently observed by others [*Wan et al.*, 1994; *Wan and Tokunaga*, 1997; *Schäfer et al.*, 1998; *Lenhart and Saiers*, 2002]. The major mechanisms postulated for the enhanced colloid removal under unsaturated flow are attachment to the gas-liquid interface and straining in water films that have thickness smaller than the colloid diameters [*Wan and Tokunaga*, 1997; *Lenhart and Saiers*, 2002]. While our experiments do not determine the exact mechanisms of colloid removal inside the column, they do show a considerable change in colloid removal for both native and modified colloids as the water saturation drops below $S_e = 0.5$. This may be related to a change in the dominant colloid removal mechanism.

4. Implications

[33] At the Hanford Reservation, where radioactive materials have leaked from underground waste tanks, an ultimate concern is the mobility of the radionuclide Cs-137. Colloidal particles can potentially facilitate the movement of

Table 3. Experimental and Modeling Summary for Colloid Breakthroughs[a]

Measured Values				Mobile-Immobile Model Parameters						
S_e	θ, m³ m⁻³	J_w, cm min⁻¹	v, cm min⁻¹	v, cm min⁻¹	D, cm² min⁻¹	Pe	β	ω	μ_m	Model R^2
				Native Colloids						
1.0	0.40	4.09	10.12	9.89	7.78	24.0	–	–	0.085	0.99782094
0.69	0.30	3.02	10.16	9.57	3.61	50.8	0.805	0.408	0.178	0.99889992
0.61	0.27	2.67	9.98	9.71	3.99	46.6	0.750	0.600	0.208	0.99915235
0.51	0.23	2.17	9.25	8.60	5.26	31.3	0.686	0.615	0.221	0.99882561
0.41	0.20	0.78	3.89	3.33	3.49	18.3	0.688	0.473	0.318	0.99728774
0.32	0.17	0.18	1.10	1.10	1.07	19.6	0.673	0.694	0.612	0.99702499
0.21	0.13	0.022	0.17	NF	NF	NF	NF	NF	NF	NF
				Modified Colloids						
1.0	0.40	4.05	10.01	10.48	8.32	24.1	–	–	0.076	0.99924566
0.69	0.30	3.01	10.10	10.27	4.48	43.9	0.848	0.305	0.187	0.99984646
0.61	0.27	2.67	9.93	10.02	5.16	37.2	0.789	0.415	0.212	0.99980308
0.52	0.24	2.17	9.18	9.12	7.61	23.0	0.740	0.413	0.234	0.99971373
0.42	0.20	0.78	3.84	3.71	5.37	13.2	0.774	0.285	0.380	0.99969106
0.33	0.17	0.18	1.07	1.16	1.77	12.5	0.773	0.365	0.799	0.99981479
0.22	0.13	0.021	0.163	NF	NF	NF	NF	NF	NF	NF

[a] S_e, effective saturation; θ, volumetric total water content; J_w, water flux; v, pore water velocity; D, hydrodynamic dispersion coefficient; Pe, Peclet number; β, fraction of mobile water content; ω, Dahmköhler number; μ_m, deposition coefficient. Saturated water content $\theta_s = 0.40$; residual water content $\theta_r = 0.06$; column pore volume is 152.2 mL; column length is 19.15 cm. NF indicates not fitted because of residual turbidity.

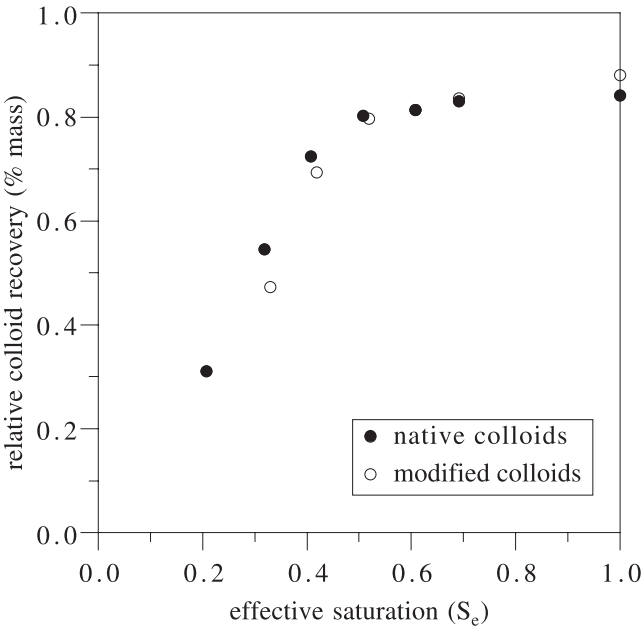

Figure 10. Mass of colloids recovered in outflow from Hanford sediments under different water saturations.

radionuclides like Cs-137, and colloid movement needs to be considered in long-term risk assessment and management of the waste at Hanford. In this study, we demonstrate that native colloids can move through natural Hanford sediments, but the amount of colloids transported strongly depends on the water saturation of the sediments. The presence of immobile water during steady state unsaturated flow leads to an earlier breakthrough and a larger dispersion of colloidal particles as compared to when immobile water is absent. No pore size exclusion, which results in increasing transport velocities, was observed for the colloids in the Hanford sediments.

[34] Analyses of boreholes drilled at the S-SX tank farm at Hanford indicate that the gravimetric water saturations in sediments of the Hanford formation in the vicinity the S-SX waste tanks range from 0.05 to 0.15 kg kg^{-1} [*Serne et al.*, 2002a]. These gravimetric water contents correspond to effective saturations S_e of 0 to 0.5 in our sediment column. Under these conditions colloid transport is possible, but not as effective as under higher water saturations.

[35] At the Hanford site, where the subsurface sediments consist of layered flood-deposits, it is possible that colloids released by a salinity change in the pore water are captured in finer-textured sediment layers as the colloids migrate downward [*Blume et al.*, 2002]. Such an effect would counteract colloid-facilitated transport if the trapped colloids are not remobilized at a later stage.

[36] **Acknowledgments.** This work was supported by the Environmental Management Science Program, U.S. Department of Energy under contract DE-FG07-99ER62882, Project Officers Frank Wobber and Chester Miller. We thank John Zachara and Jeff Serne (Pacific Northwest National Laboratory) for providing us with the Hanford sediments, Hongting Zhao for XRD analysis, and Szabolcs Czigány for the petrographic sediment characterization.

References

Bickmore, B. R., K. L. Nagy, J. S. Young, and J. W. Drexler, Nitrate-cancrinite precipitation on quartz sand in simulated Hanford tank solutions, *Environ. Sci. Technol.*, *35*, 4481–4486, 2001.

Blume, T., N. Weisbrod, and J. S. Selker, Permeability changes in layered sediments: Impact of particle release, *Groundwater*, *40*, 466–474, 2002.

Bond, W. J., and P. J. Wierenga, Immobile water during solute transport in unsaturated sand columns, *Water Resour. Res.*, *26*, 2475–2481, 1990.

Cady, J. G., L. P. Wilding, and L. R. Drees, Petrographic microscope techniques, in *Methods of Soil Analysis*, part 1, *Physical and Mineralogical Methods*, edited by A. Klute, pp. 185–218, Am. Soc. of Agron., Madison, Wis., 1986.

Cherrey, K. D., Laboratory column technique for the measurement of colloidtransport in variability-saturated porous media, M.S. thesis, Wash. State Univ., Pullman, Wash., 2002.

Chu, Y., Y. Jin, M. Flury, and M. V. Yates, Mechanisms of virus removal during transport in unsaturated porous media, *Water Resour. Res.*, *37*, 253–263, 2001.

De Smedt, F., and P. J. Wierenga, Solute transfer through columns of glass beads, *Water Resour. Res.*, *20*, 225–232, 1984.

Flury, M., J. B. Mathison, and J. B. Harsh, In situ mobilization of colloids and transport of cesium in Hanford sediments, *Environ. Sci. Technol.*, *36*, 5335–5341, 2002.

Gamerdinger, A. P., and D. I. Kaplan, Application of a continuous-flow centrifugation method for solute transport in disturbed, unsaturated sediments and illustration of mobile-immobile water, *Water Resour. Res.*, *36*, 1747–1755, 2000.

Gaudet, J. P., H. Jegat, G. Vachaud, and P. J. Wierenga, Solute transport, with exchange between mobile and stagnant water, through unsaturated sand, *Soil Sci. Soc. Am. J.*, *41*, 665–671, 1977.

Gephart, R. E., and R. E. Lundgren, *Hanford Tank Cleanup: A Guide to Understanding the Technical Issues*, 4th ed., Battelle, Columbus, Ohio, 1998.

Griffioen, J. W., D. A. Barry, and J. Y. Parlange, Interpretation of two-region model parameters, *Water Resour. Res.*, *34*, 373–384, 1998.

Hillel, D., *Environmental Soil Physics*, Academic, San Diego, Calif., 1998.

Jewett, D. G., B. E. Logan, R. G. Arnold, and R. C. Bales, Transport of Pseudomonas fluorescence strain P17 through quartz sand columns as a function of water content, *J. Contam. Hydrol.*, *36*, 73–89, 1999.

Kersting, A. B., D. W. Efurd, D. L. Finnegan, D. J. Rokop, D. K. Smith, and J. L. Thompson, Migration of plutonium in ground water at the Nevada Test Site, *Nature*, *397*, 56–59, 1999.

Kretzschmar, R., M. Borkovec, D. Grolimund, and M. Elimelech, Mobile subsurface colloids and their role in contaminant transport, *Adv. Agron.*, *66*, 121–193, 1999.

Krupp, H. K., and D. E. Elrick, Miscible displacement in an unsaturated glass bead medium, *Water Resour. Res.*, *4*, 809–815, 1968.

Lenhart, J. J., and J. E. Saiers, Transport of silica colloids through unsaturated porous media: Experimental results and model comparisons, *Environ. Sci. Technol.*, *36*, 769–777, 2002.

Maraqa, M. A., R. B. Wallace, and T. C. Voice, Effects of degree of water saturation on dispersivity and immobile water in sandy soil columns, *J. Contam. Hydrol.*, *25*, 199–218, 1997.

McCarthy, J. F., and J. M. Zachara, Subsurface transport of contaminants, *Environ. Sci. Technol.*, *23*, 496–502, 1989.

McKinley, J. P., C. J. Zeissler, J. M. Zachara, R. J. Serne, R. M. Lindstrom, H. T. Schaef, and R. D. Orr, Distribution and retention of Cs-137 in sediments at the Hanford Site, Washington, *Environ. Sci. Technol.*, *35*, 3433–3441, 2001.

Padilla, I. Y., T.-C. J. Yeh, and M. H. Conklin, The effect of water content on solute transport in unsaturated porous media, *Water Resour. Res.*, *35*, 3303–3313, 1999.

Schäfer, A., P. Ustothal, H. Harms, F. Stauffer, T. Dracos, and A. J. B. Zehnder, Transport of bacteria in unsaturated porous media, *J. Contam. Hydrol.*, *33*, 149–169, 1998.

Serne, R. J., et al., Characterization of vadose zone sediment: Uncontaminated RCRA borehole core samples and composite samples, *PNNL-13757-1*, Pac. Northwest Natl. Lab., U.S. Dep. of Energy, Richland, Wash., 2002a.

Serne, R. J., et al., Characterization of vadose zone sediment: Slant borehole SX-108 in the S-SX Waste Management Area, *PNNL-13757-4*, Pac. Northwest Natl. Lab., U.S. Dep. of Energy, Richland, Wash., 2002b.

Toride, N., F. J. Leij, and M. T. van Genuchten, The CXTFIT code for estimating transport parameters from laboratory or field tracer experiments, version 2.1, *Res. Rep. 137*, U.S. Salinity Lab., Riverside, Calif., 1995.

van Genuchten, M. T., A closed-form equation for predicting the hydraulic conductivity of unsaturated soils, *Soil Sci. Soc. Am. J.*, *44*, 892–898, 1980.

Wan, J. M., and T. K. Tokunaga, Film straining of colloids in unsaturated porous media: Conceptual model and experimental testing, *Environ. Sci. Technol.*, *31*, 2413–2420, 1997.

Wan, J. M., J. L. Wilson, and T. L. Kieft, Influence of the gas-water interface on transport of microorganisms through unsaturated porous media, *Appl. Environ. Microbiol.*, *60*, 509–516, 1994.

Whittig, L. D., and W. R. Allardice, X-ray diffraction techniques, in *Methods of Soil Analysis*, part 1, *Physical and Mineralogical Methods*, edited by A. Klute, pp. 331–362, Am. Soc. of Agron., Madison, Wis., 1986.

Zachara, J. M., S. C. Smith, C. Liu, J. P. McKinley, R. J. Serne, and P. L. Gassman, Sorption of Cs^+ to micaceous subsurface sediments from the Hanford Site, USA, *Geochim. Cosmochim. Acta*, *66*, 193–211, 2002.

Zhao, H., J. B. Harsh, M. Flury, and K. Mashal, Alteration of mineralogical and surface properties of Hanford sediments contaminated with tank waste, paper presented at 222nd ACS National Meeting, Am. Chem. Soc., Chicago, Ill., 26–30 August 2001.

K. D. Cherrey, M. Flury, and J. B. Harsh, Department of Crop and Soil Sciences, Center for Multiphase Environmental Research, Washington State University, Pullman, WA 99164, USA. (flury@mail.wsu.edu)

Colloid-Facilitated Cs Transport through Water-Saturated Hanford Sediment and Ottawa Sand

JIE ZHUANG,[†] MARKUS FLURY,[‡] AND YAN JIN*,[†]

Department of Plant and Soil Sciences, University of Delaware, Newark, Delaware 19717, and Department of Crop and Soil Sciences, Center for Multiphase Environmental Research, Washington State University, Pullman, Washington 99164

In this study, a series of saturated column experiments were conducted to investigate effects of colloids on Cs transport in two types of porous media (Hanford sediment characteristic of 2:1 clay minerals and silica Ottawa sand). The colloids used were obtained by reacting Hanford sediment with simulated tank waste solutions. Because of the highly nonlinear nature of Cs sorption found in batch experiments, we used two different concentrations of Cs (7.5×10^{-5} M and 1.4×10^{-8} M) for the transport experiments. The presence of colloids facilitated the transport of Cs through both Hanford sediment and Ottawa sand via association of Cs with mobile colloidal particles. Due to the nonlinearity of the Cs sorption, the colloid-facilitated Cs transport was more pronounced at the low Cs concentration (1.4×10^{-8} M) than at the high concentration (7.5×10^{-5} M) when expressed relative to the inflow Cs concentration. In the absence of colloids, no Cs moved through the 10-cm long columns during the experiment within about 20 pore volumes, except for the high Cs concentration in the Ottawa sand where a complete Cs breakthrough was obtained. Also, it was found that colloid-associated Cs could be partially stripped off from colloids during the transport. The stripping effect was controlled by both Cs concentration and sorption capacity of the transport matrix.

Introduction

In the waste tanks at the former plutonium production site at Hanford in eastern Washington State, U.S.A., a major portion of the radioactivity is contributed by the radionuclides ^{137}Cs and ^{90}Sr. It is reported that 67 of the 177 single-shell tanks have leaked, discharging ~3800 m^3 (more than 1 million gallons) of mixed wastes and ~4×10^{16} Bq (1 million Ci) of ^{137}Cs to the vadose zone (*1*). The directly measured activity from the contaminated sediments under Hanford tanks was as high as 10^5 Bq/g, and indirect field estimates were as high as 10^8 Bq/g (*2*).

The fate and transport of Cs in natural systems depend, to a large degree, on its partitioning behavior between aqueous and immobile solid phases and the factors affecting the partitioning (*3*, *4*). Many studies conducted during the past decades indicate that Cs is preferentially sorbed by phyllosilicate minerals, e.g., expansible layer silicates such as smectite and vermiculite, and nonexpansible micas, such as biotite and muscovite (*5*−*12*). In particular, Cs sorbs in a highly selective fashion to wedge or frayed edge sites (FES) that develop along the weathered periphery of micas (e.g., biotite and muscovite) and their immediate weathering products (hydrous-mica and illite) (*13*). Therefore, the materials containing these 2:1 layer-silicates have generally been chosen as candidates for radioactive waste depositories (*14*−*16*). In contrast, Cs sorption onto quartz, apatite, calcite, or iron oxides is low (K_d < 5 L/kg), due to low ion exchange capacity of the minerals (*17*, *18*).

At the Hanford site, the sediments are coarse-textured, and micaeous 2:1 phyllosilicates play a significant role in sorbing radiocesium and limiting its vertical migration to groundwater (*2*, *12*, *19*). The radiocesium at the SX Tank Farm has reached depths of 20−25 m below surface, with maximum depths possibly reaching 38 m (*20*, *21*). Modeling results using cesium sorption parameters measured in Hanford sediments indicate that the current depth distribution of cesium at Hanford can be explained by chromatographic solute transport in high electrolyte solutions and that cesium movement is slowed considerably at present due to strong sorption to micaeous minerals and decreased ionic strength of the pore water (*22*).

While solution phase cesium movement at present and in the future appears unlikely at Hanford (*22*), cesium can potentially move facilitated by colloidal particles. At the Hanford tank farms, alkaline tank waste that has leaked into the subsurface can dissolve native minerals to form colloidal-sized new mineral phases (feldspathoids and zeolites) (*23*, *24*). These new mineral phases can sorb and coprecipitate with Cs (*23*). If these minerals are mobile in the subsurface, there exists a risk for enhanced movement of Cs.

Colloid-facilitated transport of radionuclides has been reported from several field sites (*25*−*27*). In laboratory column studies, Cs transport in the presence and absence of mobile colloidal particles was investigated (*28*−*30*). Colloidal kaolinite was found to increase Cs migration velocity in a packed sand column by a factor of 2 when kaolinite concentration in the influent was increased from 0 to 200 mg/L (*30*). Noell et al. (*31*) studied the role of an amorphous silica colloid on facilitating Cs transport through glass bead columns. They found that when Cs was injected into columns with a constant flux of colloids, the retardation of Cs was reduced by 14−32% and 38−51% when the sizes of glass beads were 150−210 μm and 355−420 μm, respectively. Faure et al. (*32*) conducted packed-column experiments with sand mixed with 5% bentonite clay to study colloid and radionuclide transport induced by a salinity gradient. The results indicate that when the salt concentration decreased below a critical threshold of 0.16 M (NaCl), colloidal particles started to be mobilized and colloid-facilitated transport of ^{137}Cs was observed.

Chemical sorption experiments of Cs and other radionuclides have been performed using Hanford site materials (*2*, *12*, *22*, *33*). However, little is known about Cs transport in Hanford sediments characteristic of 2:1 clay minerals. Most of the previous studies have focused on Cs transport in silica-type sand and facilitated transport by colloids such as silica and kaolinite that have a lower sorption capacity for Cs than the 2:1 clays. Therefore, it is important to examine the role of micaeous colloids and their alteration products, which can form in situ under a Hanford Tank leak situation, in facilitating Cs transport through Hanford sediments.

The major objectives of this study were to investigate (i) Cs transport in two types of materials (Hanford sediment

* Corresponding author phone: (302)831-6962; fax: (302)831-0605; e-mail: yjin@udel.edu.
[†] University of Delaware.
[‡] Washington State University.

10.1021/es0264504 CCC: $25.00 © xxxx American Chemical Society
Published on Web 00/00/0000

TABLE 1: Selected Properties of the Hanford Sediment, Ottawa Sand, and Colloids

materials	CEC[a] ($cmol_c$/kg)	SA[b] (m^2/g)	Fe_0[c] (mg/kg)	Al_0[c] (mg/kg)	OM[d] (g/kg)	D_g[e] (mm)	mineralogy
Hanford sediment	6.6	12.22	6461	3220	1.0	0.52	mica, smectite, illite, vermiculite, kaolinite, quartz
Ottawa sand	0.6	0.070	28.7	18.4	0.4	0.44	quartz
Hanford colloid	6.7	39.43	56709	51722	na[f]	6.27×10^{-4}	mica, illite, smectite vermiculite, quartz, cancrinite, sodalite

[a] Cation exchange capacity. [b] Specific surface area (BET N_2 absorption measurements with ASAP2010, Micromeritics, Inc.). [c] 6 M HNO_3 dissolved Fe and Al, respectively. [d] Organic matter content. [e] Geometric diameter of sand grains or Z-averaged hydrodynamic diameter of colloidal particles, measured in 0.002 M $NaNO_3$ (pH 10 buffered with 2.4×10^{-5} M Na_2CO_3 and $NaHCO_3$) with a Zetasizer 3000HSA (Malvern Instruments, Ltd., England). [f] Not measured.

and Ottawa sand) and the facilitated migration by colloids formed by reacting Hanford sediment with simulated tank waste solutions and (ii) how Cs loading affects the facilitation efficiency of the colloids with respect to Cs transport. The conditions used in our study promoted colloid transport in porous media, i.e., we used low ionic strength pore water, saturated flow, and a colloid-free (prewashed) porous medium. While these conditions are not exactly transferable to the situation below Hanford waste tanks, they provide a worst-case scenario for colloid and colloid-facilitated cesium transport.

Materials and Methods

Porous Materials and Colloids. Two types of porous materials, Hanford sediment and Ottawa sand, were used in this study. Uncontaminated Hanford sediments, representative of the material underlying the Hanford waste tanks, were obtained from the Submarine Pit (218-E-12B) at the Hanford site. Detailed characterization data are given elsewhere (*34*). The sediment was dry-sieved through a 2-mm square grid and the material >2 mm was discarded. Ottawa sand, a typical silica sand, was obtained by mixing four sizes of the sands (C-190, C-109, 40/60, and 30/40), which were purchased from Unimin Corporation (Le Sueur, Minnesota, U.S.A.). Before the batch sorption and column experiments, both sediment and sand were washed in tap water until the rinse water was free of suspended impurities, followed by rinsing with deionized water and oven-drying at 105 °C. The rinsing of the Hanford sediment removed the fine fraction of sediments but was necessary to obtain a stable porous medium that does not contribute to in situ colloid mobilization during the transport experiments. Some properties of the materials are provided in Table 1.

The colloids used in this study (referred to as Hanford colloids) were synthesized under conditions similar to those of a leak of the waste tanks at the Hanford site, following the procedure described here. One liter of a simulated tank solution (2.8 M NaOH, 0.125 M $NaAlO_4$, and 3.7 M $NaNO_3$) was added to 1 kg of the <2 mm Hanford sediment. The mixture was kept at 50 °C and shaken periodically for 40 d. Then, the supernatant was decanted, and the sediment was washed with 1 M $NaNO_3$ by centrifugation. This process was repeated several times, and the suspension was dialyzed against deionized water until the electrical conductivity was smaller than 0.01 dS/m. Colloidal particles (<2 μm) were separated from the sediment by gravity settling, air-dried, and stored in a polyethylene bottle. X-ray diffraction (XRD) analyses, carried out using a Philips diffractometer with Cu−K radiation, showed that the colloids had similar mineralogical composition as the parent sediment material and contained newly formed mineral phases, cancrinite and sodalite (*23*). Colloidal suspensions were prepared by redispersing the air-dried colloids in artificial pore water and sonication for 20 min.

Artificial Pore Water. We used an artificial pore water consisting of 0.002 M $NaNO_3$, with its pH adjusted to 10 using 2.1×10^{-4} M $NaHCO_3$ and Na_2CO_3 at a CO_3^{2-} to HCO_3^- ratio of 0.562. This solution was chosen to maximize colloid stability and transport in the porous media. In addition, a chloride tracer (8.5×10^{-4} M NaCl) was used in the transport experiment. The high pH ensured that no carbonates were dissolved from the sediment during the experiments. The pore water composition at the Hanford site has higher ionic strength (*34*); consequently our experiments do not mimic Hanford conditions but rather are a worst-case scenario for colloid mobility.

Sorption of Cs on Colloids, Hanford Sediment, and Ottawa Sand. Sorption experiments were performed in duplicates at room temperature (22 ± 1 °C) in 50-mL Teflon centrifuge tubes using the artificial pore water as a background solution. The equilibrium suspension in the tubes consisted of 20-mL background solution, the synthesized colloids (0.1 g/L) or Na-saturated Hanford sediment, or Ottawa sand (40 g/L) and Cs with concentrations ranging from 2×10^{-10} to 2×10^{-4} M. In each tube a predetermined amount of ^{137}Cs was added for radioactive labeling and complemented with ^{133}Cs to achieve the desired Cs concentrations. The higher concentration generally matches the higher Cs concentrations reported in Hanford SX tank supernatant solutions (*19*). The samples were equilibrated by rotating the tubes end-over-end for 24 h. We chose the 24-h equilibration time based on preliminary kinetic studies, which showed that more than 95% of Cs sorption occurred in less than 4 h. After equilibration, the samples were centrifuged at 18 000 g for 15 min, and the activity of ^{137}Cs in the equilibrium aqueous phase was determined using a liquid scintillation analyzer Tri-Carb 2900TR (Packard Instrument Company, CT). ScintiSafe Econo 1 cocktail liquid (Fisher Scientific, NJ) was used as the scintillation solution for ^{137}Cs concentration measurements. Total cesium sorption was calculated assuming that stable ^{133}Cs and radioactive ^{137}Cs behaved identically in terms of sorption. UV/vis spectroscopic measurements of the supernatant after centrifugation showed no significant above-background turbidity, indicating that no colloids remained in suspension after centrifugation. The amount of Cs sorbed onto the solids was determined by the difference between the initial Cs concentration added and the equilibrium Cs concentration in the aqueous phase after centrifugation. Sorbent-free controls with initial ^{137}Cs concentration of 1×10^{-8} M showed that the loss of Cs to Teflon tubes was negligible. Values reported are means of the duplicates.

Column Transport Experiments. Nine breakthrough experiments of Cs in the presence and absence of Hanford colloids were performed under saturated flow conditions (Table 2) at room temperature (22 ± 1 °C). The column system used in the study was the same as that in Jin et al. (*35*). The column was made of acrylate, with an inside diameter of 5.1

TABLE 2. Conditions and Parameters of the Column Experiments

expt no.	matrix	colloid concn (mg/L)	Cs concn (mol/L)	ρ_b[a] (Mg/m^3)	ϕ[b]	V[c] (cm/h)	D[d] (cm^2/h)	Pe[e]
1	Hanford sediment	0	7.5×10^{-5}	1.45	0.45	10.0	0.86	116.3
2	Hanford sediment	50	7.5×10^{-5}	1.48	0.44	10.7	0.58	184.5
3	Hanford sediment	100	7.5×10^{-5}	1.47	0.45	9.9	0.85	116.5
4	Hanford sediment	37	1.4×10^{-8}	1.49	0.44	9.7	1.05	92.4
5	Hanford sediment	79	1.4×10^{-8}	1.47	0.45	8.7	1.23	70.7
6	Ottawa sand	0	7.5×10^{-5}	1.73	0.36	8.6	1.23	69.9
7	Ottawa sand	45	7.5×10^{-5}	1.78	0.34	8.8	0.96	91.7
8	Ottawa sand	0	1.3×10^{-8}	1.77	0.34	9.6	0.68	141.2
9	Ottawa sand	35	1.3×10^{-8}	1.73	0.36	9.9	0.64	154.7

[a] Bulk density. [b] Porosity. [c] Pore water velocity. [d] Hydrodynamic dispersion coefficient, determined from Cl data using CXTFIT. [e] Peclet number Pe = VL/D, where L is the column length.

cm and a length of 10.0 cm, and consisted of a top and a bottom plate and sealed by an O-ring on each end. The O-ring had no contact with the inside of the column. A stainless steel screen (0.3 mm pore size) was placed on the column end pieces for mechanical support. Teflon tubing was used throughout the system except for a portion of Tygon tubing in the peristaltic pump. When the column was packed, deaerated artificial pore water solution was preintroduced into the column from the bottom to a certain height, and then porous materials were slowly poured into the solution as 1-cm increments. During packing, the content in the column was continuously stirred with a plastic rod to ensure uniformity of packing and to avoid air entrapment in the column.

For each experiment, the column was flushed with the deaerated artificial pore water to establish a steady-state flow and to standardize the chemical conditions of the experimental system. Once the pH value of the effluent became the same as that of the influent (after roughly 15 pore volumes), the input solution containing either Cs or a preequilibrated Cs-colloid mixture was introduced into the column upward at a constant flow rate. The input solution was prepared in several steps. First, a mixture of ^{137}Cs and ^{133}Cs as well as chloride tracer (8.5×10^{-4} M NaCl) was added to a 1-L plastic bottle that contained artificial pore water. Cesium was added in two different concentrations: 7.5×10^{-5} M (2.19 MBq/mL) and 1.4×10^{-8} M (407 Bq/mL), which correspond to high and low concentrations used in the batch experiments. Then a predetermined amount of sonicated, concentrated Hanford colloidal suspension was added to the bottle while the solution was continuously stirred. The colloidal suspension was stirred slowly and equilibrated for 24 h. Before each experiment, three samples (15 mL for each) were taken from the prepared input solution to determine the total Cs concentration, amount of Cs sorbed on the colloids, and concentrations of colloids as well as chloride. Separation of colloids from solution and Cs quantification was done as described for the batch sorption experiments. Column experiments were not replicated. However, each column was packed carefully following the same procedure to ensure reproducibility between the columns.

During the transport experiments, a continuously stirred suspension of constant colloid concentration was fed to the column. The colloid concentration varied from 35 to 100 mg/L, a range frequently found in natural subsurface environments. Column outflow was collected into 15-mL polypropylene centrifuge tubes in regular time intervals using a fraction collector. Colloid concentrations in the inflow and outflow were measured with UV/vis spectrophotometry (DU Series 640, Beckman Instrument, Inc. MD) at 350 nm. A calibration curve was constructed by dilution of a 0.1 g/L colloid suspension. Colloid concentration versus spectrometer response was linear with a coefficient of determination of $R^2 = 0.9997$ ($n = 8$) between a concentration range of 0−100 mg/L. Wavelengths of 300−350 nm were found to be well suited for colloid quantification (*36*). After a stable colloid concentration in the effluent had been reached for a duration of 10 pore volumes, the input was switched to artificial pore water free of colloids and Cs. The Cs concentration was analyzed as described in the sorption experiments. The chloride tracer, which was used to test the hydrodynamic performance of the column, was analyzed using ion chromatography (Dionex Corporation, Sunnyvale, CA). Based on the tracer concentration data (C) and measured pore water velocity (V), the dispersion coefficient (D) of the porous media was determined by fitting the standard convection-dispersion equation for a conservative solute [$\partial C/\partial t = D(\partial^2 C/\partial x^2) - V(\partial C/\partial x)$] to the chloride breakthrough curves (*37*) using the CXTFIT program (*37*). Chloride, colloid, and cesium concentrations in the outflow were related to the concentrations in the inflow and represented as relative concentrations C/C_0.

Results and Discussion

Sorption Isotherms of Cs. Figure 1 illustrates the Cs sorption data on Hanford colloid, Hanford sediment, and Ottawa sand. The overall Cs sorption isotherms are nonlinear and fitted well by the Freundlich model. The fitted equations are $q = 90.5C^{0.71}$ ($R^2 = 0.994$) for Hanford colloid, $q = 58.3C^{0.84}$ ($R^2 = 0.996$) for Hanford sediment, and $q = 0.03C^{0.64}$ ($R^2 = 0.997$) for Ottawa sand, where q is the amount sorbed in mol/kg and C is the equilibrium concentration in mol/L. The observed nonlinear (Freundlich) sorption behavior indicates the presence of multiple types of Cs sorption sites on the colloids and matrices (*39*, *40*). The isotherms can also be approximated by three linear regions, each of them having a different slope (Figure 1). We speculate that three types of sorption sites exist on the heterogeneous surfaces. This concentration-dependent characteristic of Cs sorption agrees well with previous findings (*3*, *12*, *33*, *41*, *42*). Sorption sites may be broadly classified into three categories: sites with high affinity/low capacity, sites with intermediate affinity/low capacity, and sites with low affinity/high capacity. Each linear region of the isotherms is dominated by one type of sites, which possesses relatively uniform binding energy. The entire sorption process may be described as follows. The high affinity sites (frayed-edge sites) are responsible for the uptake of Cs at very low concentrations. As Cs concentration increases the frayed-edge sites are saturated because of their low sorption capacity. Then, the intermediate affinity sites become the major sites for Cs sorption. This type of sites also has a low capacity. Once they are completely occupied after the Cs concentration increases to a certain level, the third type of sites, which is referred to as the "planar sites" and has a lower affinity associated with the structural negative charge on the minerals arising from isomorphous substitution, starts to dominate Cs sorption.

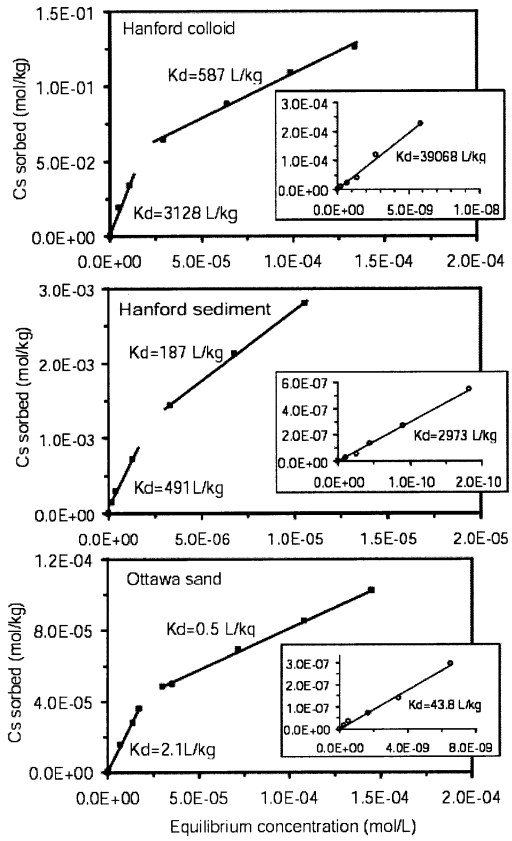

FIGURE 1. Sorption isotherms of Cs on Hanford colloids, Hanford sediment, and Ottawa sand. The inserts show a magnified view of the low concentrations, with the same units of the axes as in the larger plots.

TABLE 3. Single Point K_d Values for Sands and Colloids Measured at Different Cs Concentrations in 0.002 M $NaNO_3$[a] Background Solution

initial Cs concn (M)	K_d (L/kg) Hanford sediment	Ottawa sand	Hanford colloid
2×10^{-10}	2964	70.5	44057
2×10^{-9}	2295	53.0	43468
2×10^{-8}	1625	38.0	32399
2×10^{-7}	937	23.9	20484
2×10^{-6}	527	3.0	4609
2×10^{-5}	117	1.8	2549
2×10^{-4}	na[b]	0.5	490

[a] pH 10 buffered with 2.1×10^{-4} M Na_2CO_3 and $NaHCO_3$. [b] na = not available.

Nonlinear sorption leads to a dependence of the Cs distribution coefficient (K_d) on Cs concentration. Table 3 shows the single-point K_d values calculated for the three materials, which decrease with increasing Cs concentrations. Comparing the K_d values for each material at the same initial concentrations, we found that the values for Hanford colloids were over 10-fold higher than those for Hanford sediment and almost 1000-fold higher than those for Ottawa sand.

Cl Transport in Hanford Sediment and Ottawa Sand. Cl breakthrough curves in Hanford sediment and Ottawa sand were reproducible (see Figures 2 and 3). The analysis of the breakthrough curves showed that the column Peclet numbers were in the order of 70 or higher, indicating a convectively dominated flow regime (Table 2).

Cs and Colloid-Facilitated Cs Transport in Hanford Sediment. At the high Cs input concentration (7.5×10^{-5} M),

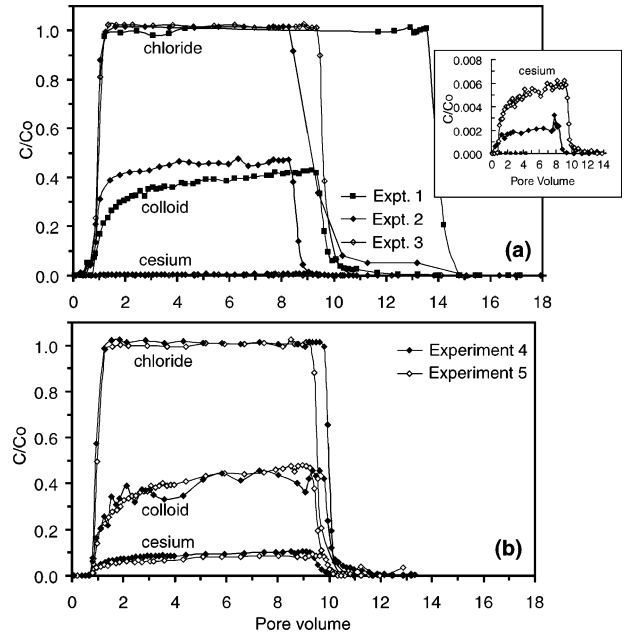

FIGURE 2. Breakthrough curves of Cs, Cl, and colloids in Hanford sediment at various colloid concentrations at (a) high Cs loading (7.5×10^{-5} M) and (b) low Cs loading (1.4×10^{-8} M). The insert shows a magnified view of the Cs breakthrough.

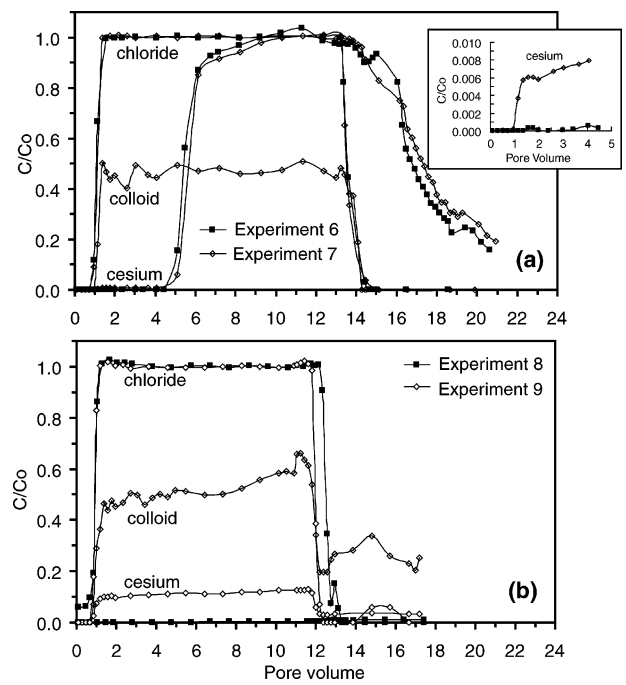

FIGURE 3. Breakthrough curves of Cs, Cl, and colloids in Ottawa sand at various colloid concentrations at (a) high Cs loading (7.5×10^{-5} M) and (b) low Cs loading (1.3×10^{-8} M). The insert shows a magnified view of the Cs breakthrough.

Figure 2a shows that in the absence of colloids (experiment 1), Cs in the aqueous phase was completely sorbed by the Hanford sediment in the column and no Cs breakthrough was observed. This result was expected because the retardation factor ($R = 1 + \rho_b K_d/\phi$) was calculated to be 243 based on the estimated K_d value of 75 L/kg at the Cs concentration of 7.5×10^{-5} M. However, in the presence of Hanford colloids, Cs was detected in the outflow, with relative Cs concentrations (C/C_0) of 0.2−0.3% (experiment 2) and 0.6% (experiment 3) at 50 and 100 mg/L colloid concentrations, respectively.

TABLE 4. Sorption and Desorption of Cs on Colloids in Inflow and Outflow Samples

				inflow			outflow	
				Cs sorbed on colloids				
expt. no.	matrix	colloid concn (mg/L)	Cs concn (mol/L)	(μg/g)[a]	(%)	Cs in solution (%)	Cs sorbed on colloids (μg/g)[a]	Cs desorbed from colloids[b] (%)
2	Hanford sediment	50	7.5×10^{-5}	12007	6.0	94.0	961	92.0
3	Hanford sediment	100	7.5×10^{-5}	12690	12.8	87.2	1269	90.0
4	Hanford sediment	37	1.4×10^{-8}	26	50.6	49.4	12	53.8
5	Hanford sediment	79	1.4×10^{-8}	17	68.2	31.8	5	70.8
7	Ottawa sand	45	7.5×10^{-5}	11569	5.3	94.7	3471	70.0
9	Ottawa sand	35	1.3×10^{-8}	29	53.4	46.6	12	58.6

[a] μg Cs/g colloid. [b] Amount of Cs desorbed from colloids in outflow compared to Cs on colloids in inflow.

Evidently, colloid-facilitated transport was solely responsible for the observed Cs movement.

At the low Cs input concentration (1.4×10^{-8} M), we did not run a Cs experiment in the absence of colloids. No Cs breakthrough was expected because the K_d measured in batch experiments at Cs concentration at 10^{-8} M was greater than that at 10^{-5} M (Table 3). Figure 2b shows that after adding colloids to the input solution at the low concentration of Cs, effluent concentrations of Cs reached ~12% C/C_0 (experiments 4 and 5), indicating a considerable migration of Cs via the colloids.

The efficiency of colloids in binding Cs, and thus facilitating Cs transport, varied with Cs concentration. Cesium association with the colloidal phase in the input solution of each experiment was calculated as percentages and on per gram colloids basis (Table 4). At the high Cs loading, sorption of Cs on unit mass of colloids was similar for both colloid concentrations (50 and 100 mg/L); therefore, the total amount of Cs sorbed in the inflow solutions was doubled when the amount of colloids was doubled. This resulted in an approximately 2-fold increase in outflow Cs concentration (Figure 2a, insert). In contrast, at the low Cs loading, there was minimal difference in Cs effluent concentrations when the colloid concentration increased from 37 to 79 mg/L (Figure 2b). Table 4 indicates that at low colloid concentration (37 mg/L), 26 μg Cs was sorbed on 1 g of the colloids, while at high colloid concentration (79 mg/L), only 17 μg Cs was sorbed on 1 g of colloid.

Cs and Colloid-Facilitated Cs Transport in Ottawa Sand. As shown in Figure 3a, at high Cs concentration (7.5×10^{-5} M) and in the absence of colloids (experiment 6), the initial breakthrough front of Cs occurred at ~5 pore volumes. Following the initial breakthrough front, relative concentrations of Cs in the effluent increased rapidly to 0.9 in one pore volume and then more slowly to reach unity. This different behavior from Hanford sediment was expected because Ottawa sand had considerably lower CEC (Table 1) and a much smaller sorption affinity for Cs (Table 3) as compared with Hanford sediment. In the presence of colloids (experiment 7), an almost identical main breakthrough curve of Cs was observed as in the absence of colloids. However, a small fraction of Cs was detected simultaneously with the detection of colloid breakthrough in the effluent (Figure 3a insert). This additional Cs peak was clearly due to colloid-facilitated transport, although the fraction of Cs transported via colloids was low (~0.8% C/C_0). The magnitude of the colloid-facilitated Cs transport was similar as in the Hanford sediment, corroborating the interpretation of colloid-assisted movement. It is, however, evident that dissolved Cs transport dominated the migration of Cs through Ottawa sand at the high Cs concentration.

At the low Cs concentration (1.3×10^{-8} M, equivalent to 344 Bq/mL), Cs was removed completely by Ottawa sand during transport without colloid involved (experiment 8, Figure 3b). This was expected based on batch sorption results. Addition of 35 mg/L Hanford colloids to the input solution caused 12% of Cs breakthrough (experiment 9). Obviously, at the low Cs concentration movement of the Cs-bearing colloids dominated Cs migration. This result agrees well with that of Saiers and Hornberger (*29*), where they used a similar Cs concentration (365 Bq/mL). They found that within 17 pore volumes Cs injected to the column was completely sorbed by the Ottawa sand, but addition of 50 mg/L kaolinite particles to the input solution caused breakthrough of Cs at about one pore volume.

Desorption of Cs from Colloids during Transport. For each experiment, we calculated the amount of Cs associated with each gram of colloids in the influent by taking the difference between the measured total Cs concentration and Cs concentration in solution after centrifugation. As we did not observe any dissolved Cs transport in the Hanford sediment and the Ottawa sand in the absence of colloids (except for experiment 7), we assume that all the cesium breaking through the columns in the presence of colloids was associated with the colloidal particles. We calculated the percentage of Cs desorption from colloids based on the difference in Cs concentrations sorbed on colloids between the inflow and outflow. Significantly less Cs was recovered on the colloids in the effluent compared with Cs sorption in the influent (Table 4). This suggests that during transport Cs was partially "stripped" off from the colloidal particles to equilibrate with the pore water solution and subsequently sorbed by the transport medium in the column. The results also suggest that the degree of stripping depends on both Cs concentration and the sorption capacity of the transport matrix. In both the Hanford sediment and Ottawa sand columns, the stripping was more pronounced at the higher Cs concentration. We attribute this to the nonlinearity of Cs sorption on the colloids. As discussed earlier, at high Cs loading, more Cs might have been sorbed on the relatively low affinity sites, while at low Cs loading most of the Cs might have been sorbed on high affinity sites. The weakly bound Cs at low affinity sites was more easily desorbed from the colloids than the strongly bound Cs at high affinity sites. Table 4 also indicates that at the same Cs concentration, more Cs was stripped off the colloids traveling through Hanford sediment than through Ottawa sand, likely because of the high sorption capacity of the Hanford sediment.

Effect of Nonlinear Cs Sorption and Sorption Reversibility on the Efficiency of Colloid-Facilitated Cs Transport. The nonlinear feature of Cs sorption resulted in the observation of a series of interesting scenarios of colloid-facilitated Cs transport. At the low Cs loading, a high percentage of Cs was retained on the colloids due to availability of adequate amount of high-affinity sorption sites on the particles. This resulted in relatively effective colloid-facilitated Cs transport (Figure 2b). When Cs concentration increased to a sufficiently high level at which the amount of high-affinity sorption sites on the colloidal particles could be saturated by Cs, colloid concentration became the limiting factor in affecting the

efficiency of colloid-facilitated Cs transport. This was the result we observed from the Hanford sediment column at the high Cs loading (Figure 2a). In this case, because the migration of Cs became more of a function of the behavior of the colloid than of the dissolved Cs, all factors (e.g., flow velocity, solution chemistry, medium and colloid properties) affecting colloid transport would govern the transport of Cs (*43*, *44*). Furthermore, if Cs concentration increased to a level high enough to saturate the high affinity sites of both the collector grains and the colloids, transport of Cs in the dissolved phase would dominate the breakthrough process. When our tests had > 10^{-5} M dissolved Cs, although the amount of Cs transport via colloids accounted for only a small fraction of the total amount of Cs in the effluent, rapid migration of the colloids considerably reduced the breakthrough time of Cs (Figure 3a). This phenomenon should be common for media with low CEC value (e.g., silica sand).

In a strongly sorbing sediment matrix, Cs transport via colloids will be limited due to desorption of Cs from colloids and sorption to the sediment matrix. Such desorption/sorption processes will also affect transport of other radionuclides that undergo reversible sorption on colloidal particles. Under constant geochemical conditions, the degree of desorption of radionuclides from colloids depends on type of radionuclide and colloidal material (*45*, *46*). For instance, sorption reversibility on hematite, montmorillonite, and silica colloids has been observed for ^{239}Pu and ^{243}Am but not for ^{237}Np and ^{238}U (*45*).

We found that the efficiency of colloid-facilitated Cs transport was controlled by the nonlinear nature of Cs sorption by both solid surfaces and colloids. Cesium sorbed onto the colloids was effectively stripped off from the colloids during transport. The extent of the stripping depends on Cs concentration and sediment matrix properties. The results show that colloid-facilitated Cs transport at the Hanford site is likely not an effective mechanism for Cs movement. At Hanford, it can be expected that Cs would be stripped from colloidal carriers as the colloids move through the 27−33 m thick uncontaminated vadose zone and only a very small fraction of initially sorbed Cs would move with mobile colloids. Furthermore, under the conditions at the Hanford site (pore water chemistry, degree of water saturation) colloids are less likely to be stable in suspension than under our experimental conditions, further limiting the possibility for colloid-facilitated transport. Our results can be interpreted as a worst-case scenario for colloid-facilitated Cs transport at the Hanford site, but even in this case, the quantitative amount of Cs that can be cotransported appears to be limited.

Acknowledgments

This work was supported by the Environmental Management Science Program, U.S. Department of Energy under Grant No. DE-FG07-99ER62882. We thank John Zachara and Jeff Serne (Pacific Northwest National Laboratory) for providing the Hanford sediments. We thank Jeff Serne, Wooyong Um, Eric Pierce, Chris Brown (Pacific Northwest National Laboratory), and an anonymous reviewer for constructive comments on the manuscript.

Literature Cited

(1) U.S. Department of Energy. *Groundwater/Vadose Zone Integration Project Specification, Report DOE/RL-98-48, Draft B, C and D*; 1998.
(2) McKinley, J. P.; Zeissler, C. J.; Zachara, J. M.; Serne, R. J.; Lindstrom, R. M.; Schaef, H. T.; Orr, R. D. *Environ. Sci. Technol.* **2001**, *35*, 3433−3441.
(3) Bradbury, M. H.; Baeyens, B. *J. Contam. Hydrol.* **2000**, *42*, 141−163.
(4) Staunton, S.; Roubaud, M. *Clays Clay Miner.* **1997**, *45*, 251−260.
(5) Anderson, K.; Allard, B. Report No. SKBF-KBS-TR-83-07; Svensk Kärnsbränsteförjning, Stockholm, 1983.
(6) Cremers, A.; Elsen, A.; De Preters, P.; Maes, A. *Nature* **1988**, *335*, 247−249.
(7) De Preter, P.; Van Loon, L.; Maes, A.; Cremers, A. *Radiochim. Acta* **1991**, *52/53*, 299−302.
(8) Adeleye, S. A.; Clay, P. G.; Oladipo, M. O. A. *J. Mater. Sci.* **1994**, *29*, 954−958.
(9) Ohnuki, T.; Kozai, N. *Radiochim Acta.* **1994**, *66/67*, 327−331.
(10) Wauters, J.; Elsen, A.; Cremers, A. *Appl. Geochem.* **1996**, *11*, 601−603.
(11) Bors, J.; Gorny, A.; Dultz, St. *Radiochim. Acta.* **1996**, *74*, 231−234.
(12) Zachara, J. M.; Smith, S. C.; Liu, C.; McKinley, J. P.; Serne, R. J.; Gassman, P. L. *Geochim. Cosmochim. Acta* **2002**, *66*, 193-211.
(13) Francis, C. W.; Brinkley, F. S. *Nature* **1976**, *260*, 511−513.
(14) Gutierrez, M.; Fuentes, H. R. *Appl. Clay Sci.* **1996**, *11*, 11−24.
(15) Krumhansl, J. L.; Brady, P. V.; Anderson, H. L. *J. Contam. Hydrol.* **2001**, *47*, 233−240.
(16) Sawhney, B. L. *Clays Clay Miner.* **1972**, *20*, 93−100.
(17) Cornell, R. M. J. Radioanal. *Nucl. Chem.* **1993**, *171*, 483−500.
(18) Kaplan, D. I.; Serne, R. J. *Radiochim. Acta* **1998**, *81*, 117−124.
(19) Serne, R. J.; Zachara, J. M.; Burke, D. S. *Chemical Information on Tank Supernatants, Cs Adsorption from Tank Liquids onto Hanford Sediments, and Field Observations of Cs Migration from Past Tank Leaks*; Project Report of Pacific Northwest National Laboratory, PNLL-11495; Richland, WA, 1998.
(20) Serne, R. J.; Last, G. V.; Schaef, H. T.; Lanigan, D. C.; Lindenmeier, C. W.; Ainsworth, C. C.; Clayton, R. E.; LeGore, V. L.; O'Hara, M. J.; Brown, C. F.; Orr, R. D.; Kutnyakov, I. V.; Wilson, T. C.; Wagnon, K. B.; Williams, B. A.; Burke, D. S. *Characterization of Vadose Zone Sediment: Borehole 41-09-39 in the S-SX Waste Management Area*; Project Report of Pacific Northwest National Laboratory, PNLL-13757-3; Richland, WA, 2002a.
(21) Serne, R. J.; Last, G. V.; Schaef, H. T.; Lanigan, D. C.; Lindenmeier, C. W.; Ainsworth, C. C.; Clayton, R. E.; LeGore, V. L.; O'Hara, M. J.; Brown, C. F.; Orr, R. D.; Kutnyakov, I. V.; Wilson, T. C.; Wagnon, K. B.; Williams, B. A.; Burke, D. S. *Characterization of Vadose Zone Sediment: Slant Borehole SX-108 in the S-SX Waste Management Area*; Project Report of Pacific Northwest National Laboratory, PNLL-13757-4; Richland, WA, 2002b.
(22) Knepp, A. J. *Field Investigation Report for Waste Management Area S-SX*; Project Report of Pacific Northwest National Laboratory, RPP-7884; Richland, WA, 2002.
(23) Zhao, H.; Harsh, J. B.; Flury, M.; Mashal, K. Abstracts, 222nd ACS National Meeting, August 26−30, 2002, Chicago, IL.
(24) Bickmore, B. R.; Nagy, K. L.; Young, J. S.; Drexler, J. W. *Environ. Sci. Technol.* **2001**, *35*, 4481−4486.
(25) Buddemeier, R. W.; Hunt, J. R. *Appl. Geochem.* **1998**, *3*, 535−548.
(26) Kaplan, D. I.; Bertsch, P. M.; Adriano, D. C.; Orlandini, K. A. *Radiochim. Acta* **1994**, *66/67*, 181−187.
(27) Kersting, A. B.; Efurd, D. W.; Finnegan, D. L.; Rokop, D. J.; Smith, D. K.; Thompson, J. L. *Nature* **1999**, *397*, 56−59.
(28) Sätmark, B.; Albinsson, Y.; Liang, L. *J. Contamin. Hydrol.* **1996**, *21*, 231−241.
(29) Grindrod, P. *J. Contamin. Hydrol.* **1993**, *13*, 167−181.
(30) Saiers, J. E.; Hornberger, G. M. *Water Resourc. Res.* **1996**, *32*, 33−41.
(31) Noell, A. L.; Thompson, J. L.; Corapcioglu, M. Y.; Triay, I. R. *J. Contamin. Hydrol.* **1998**, *31*, 23−56.
(32) Faure, M. H,; Sardin, M.; Vitorge, P. *J. Contamin. Hydrol.* **1996**, *21*, 255−267.
(33) Hakem, N. L.; Al Mahamid, I.; Apps, J. A.; Moridis, G. J. *J. Radioanal. Nucl. Chem.* **2000**, *246*, 275−278.
(34) Serne, R. J.; Bjornstad, B. N.; Schaef, H. T.; Williams, B. A.; Lanigan, D. C.; Horton, D. G.; Clayton, R. E.; Mitroshkov, A. V.; LeGore, V. L.; O'Hara, M. J.; Brown, C. F.; Parker, K. E.; Kutnyakov, I. V.; Serne, J. N.; Last, G. V.; Smith, S. C.; Lindenmeier, C. W.; Zachara, J. M.; Burke, D. S. *Characterization of Vadose Zone Sediment: Uncontaminated RCRA Borehole Core Samples and Composite Samples*; PNNL-13757-1; Pacific Northwest National Laboratory, U.S. Department of Energy, Richland, WA, 2002.
(35) Jin, Y.; Chu, Y.; Li, Y. *J. Contam. Hydrol.* **2000**, *43*, 111−128.
(36) Cherrey, K. D.; Flury, M.; Harsh, J. B. *Water Resourc. Res.* **2003**, 39, 1165, DOI: 10.1029/2002WR001944.
(37) van Genuchten, M. T.; Alves, W. J. Analytical Solutions of the One-Dimensional Convective-Dispersive Solute Transport Equation. *U.S. Dept. Agric. Tech. Bull.* **1982**, *1661*.
(38) Toride, N.; Leij, F. K.; van Genuchten, M. Th. The CXTFIT code for estimating transport parameters from laboratory or field tracer experiments, version 2.1, Research Report #137; U.S. Salinity Laboratory, U.S. Department of Agriculture, Riverside, CA, 1995.

(39) Atkins, P. W. *Physical Chemistry*, 4th ed.; Oxford University Press: Oxford, 1995; p 995.
(40) Sposito, G. *Soil Sci. Soc. Am. J.* **1980**, *44*, 652−654.
(41) Campbell, L. S.; Davies, B. E. *Appl. Geochem.* **1995**, *10*, 715−723.
(42) Comans, R. N. J.; Hallers, M.; De Preter, P. *Geochim. Cosmochim. Acta* **1991**, *55*, 433−440.
(43) Roy, S. B.; Dzombak, D. A. *Environ. Sci. Technol.* **1997**, *31*, 656−664.
(44) Um, W.; Papelis, C. *Environ. Geol.* **2002**, *43*, 209−218.
(45) Lu, L.; Conca, J.; Parker, G. R.; Leonard, P. A.; Moore, B.; Strietelmeier, B.; Triay, I. R. *Adsorption of Actinides onto Colloids as a Function of Time, Temperature, Ionic Strength, and Colloid Concentration*; Los Alamos National Laboratory Report LA-UR-00-51-21; 2000.
(46) Lu, N.; Cotter, C. R.; Kitten, H. D.; Bentley, J.; Triay, I. R. *Radiochim. Acta* **1998**, *83*, 167−173.

Received for review December 19, 2002. Revised manuscript received August 13, 2003. Accepted September 3, 2003.

ES0264504

Alteration of kaolinite to cancrinite and sodalite by simulated Hanford tank waste and its impact on cesium retention

Hongting Zhao, Youjun Deng, James B. Harsh, Markus Flury*, and Jeffrey S. Boyle

Department of Crop and Soil Sciences, Center for Multiphase Environmental Research, Washington State University, Pullman, WA 99164, USA

* Author to whom correspondence should be addressed. E-mail: flury@mail.wsu.edu

Telephone: (509)-335-1719

Fax: (509)-335-8674

Suggested running title:

Alteration of Kaolinite to Cancrinite and Sodalite

ABSTRACT

Caustic nuclear wastes have leaked from tanks at the U.S. Department of Energy's Hanford site in Washington State (USA) causing hundreds of thousands of gallons of waste fluids to migrate into the underlying sediments. In this study, four simulant tank waste (STW) solutions, which are high in NaOH (1.4 and 2.8 mol/kg), $NaNO_3$ (3.7 mol/kg) and $NaAlO_2$ (0.125 and 0.25 mol/kg), were prepared and reacted with reference kaolinite KGa-1 and KGa-2 at 50 and 80 °C for up to two months. The structure and morphology of the resulting products were characterized using X-ray diffraction (XRD), scanning electron microscopy (SEM), and Fourier transform infrared (FTIR) spectroscopy. The products were also examined for cation exchange and Cs^+ sorption as a function of ionic strength and types of cations in the background solutions. Cancrinite and sodalite were the only new minerals observed in all of the conditions tested in this experiment. Two major chemical processes were involved in the reactions: dissolution of kaolinite and precipitation of cancrinite and sodalite. Increasing NaOH concentration and temperature, and decreasing $NaAlO_2$ concentration increased the transformation rate. Both cancrinite and sodalite appeared stable thermodynamically under the experimental conditions. The newly formed feldspathoids were vulnerable to acid attack and pronounced dissolution occurred at pH below 5.5. Cancrinite and sodalite can incorporate $NaNO_3$ ion pairs in their cages or channels. Sodium in cancrinite and sodalite was readily exchangeable by K^+, but less easily by Cs^+ or Ca^{2+}. The feldspathoid products sorb nearly an order of magnitude more Cs^+ than the unaltered kaolinite. The cesium adsorption is reduced by competing cations in the background solutions. At low ionic strength (0.01 M $NaNO_3$ or 0.005 M $Ca(NO_3)_2$), Ca^{2+} was more competitive than Na^+. When the concentration of the background solution was increased 10 times, Na^+ was more competitive than Ca^{2+}.

Keywords: Cancrinite, Cation Exchange, Cesium Sorption, Feldspathoid, Hanford Waste Tanks, Kaolinite, Mineral Stability, Mineral Transformation, Sodalite.

INTRODUCTION

Many single-shell tanks of the 177 nuclear waste tanks located at the U.S. Department of Energy's Hanford Reservation near Richland, WA (USA) have leaked, allowing 0.6-1.4 million gallons of high level nuclear waste fluids to migrate into the underlying coarse-textured, relatively unweathered sediments (Hanlon, 1996; Gephart and Lundgren, 1998). Tank sludge, arising from the Pu production and extraction procedures at the Hanford Site, is chemically very complex and of extreme chemical conditions. In most cases, tank sludge has very high $NaNO_3$ (up to ~8 M), NaOH (pH > 13), and aluminate concentrations (> 0.1 M) (Serne *et al.*, 1998). The temperature in several tanks rose to above 100 °C during the storage time and was reported as high as 160 °C in one tank (Pruess *et al.*, 2002). The temperature in the immediate neighborhood sediments was estimated as high as 120 °C, and in the sediments 20 meters below the tanks could be as high as 70 °C (Pruess *et al.*, 2002).

Reaction of the leaked waste solution with the underlying soil and sedimentary matrix will potentially result in dissolution of native minerals and subsequent formation of new secondary mineral phases. These chemical reactions can alter mineral surface properties, as well as the porosity and flow paths of the surrounding porous media. The physicochemical and mineralogical alterations of the sediment matrix could cooperatively lead to significant changes in the fate and transport of tank contaminants. Recent studies have shown that cancrinite, a feldspathoid, was formed after reacting Hanford sediments or quartz with tank simulant solutions at 60-90 °C (Nyman *et al.*, 2000; Bickmore *et al.*, 2001). We have found another feldspathoid, sodalite, in

addition to cancrinite formed upon reacting the Hanford sediments with tank simulant for five weeks at 68 °C (our unpublished data). To the best of our knowledge, the retention properties of these materials for radionuclides have not yet been addressed. Quartz, feldspar, hornblende, mica, chlorite, illite, kaolinite, smectite, and calcite are the most common minerals in Hanford sediments (Serne *et al.*, 1998). We found that these minerals have different reactivities toward the simulant solutions. Even though kaolinite is not the most abundant clay mineral in Hanford sediments, here we report kaolinite alteration results because this mineral had shown the fastest alteration rate and the final precipitates are common products in the reactions with Hanford sediments. Kaolinite reactions give a high yield of the new mineral phases and the simplest mineral composition to study the retention behavior of radioactive nuclides on the new minerals.

It is known that kaolinite is not stable under highly alkaline conditions and various zeolite and feldspathoids can form (Breck, 1974). For instance, at high molarity of KOH (0.1 to 4.0 M) and temperatures of 35 and 80 °C, kaolinite transformed, in sequence, to illite, KI-zeolite, phillipsite, and finally, K-feldspar (Bauer *et al.*, 1998). Kaolinite has been used as the aluminum and silicon sources for zeolite synthesis. Linde Type A, X, and Y zeolites, cancrinite, sodalite, faujasite, and several other types of zeolites have been synthesized from kaolinite (Dudzik and Kowalak, 1974; Buhl, 1991; Alberti *et al.*, 1994; Gualtieri *et al.*, 1997). For zeolite synthesis, most of the experiments were carried out at high temperatures (e.g. 220 °C) and high pressures in autoclaves. These conditions are not likely to occur in the sediments underlying the tanks at the Hanford site. In addition, the presence of high concentrations of electrolytes such as $NaNO_3$ in the leaked waste solution may alter the reaction path.

The objectives of this study were to study (1) the mineral alteration of kaolinite after contacting simulant Hanford tank solutions, (2) the stability and ion exchange properties of

resulting precipitates, and (3) the sorption behavior of cesium, a common radioactive element of Hanford nuclear wastes, on the newly formed precipitates. We hypothesized that kaolinite, with a low Cs^+ sorption capacity, would be transformed to feldspathoids under conditions designed to mimic those under leaking high level waste tanks. Such a transformation should enhance the sorption of Cs^+.

MATERIAL AND METHODS

Kaolinite samples and their reaction with simulant solutions

Two kaolinite samples, a highly crystalline KGa-1 kaolinite and a poorly crystalline KGa-2 kaolinite, were used as received from the Clay Minerals Society (CMS) Source Clay Repository (Columbia, Missouri). Four simulant tank waste solutions (STWs) were prepared. The concentration of each component was within the range reported in Hanford waste process fluids (Serne *et al.*, 1998). Sodium hydroxide, sodium aluminate and sodium nitrate were divided into portions and added incrementally to make the four solutions (Table 1). Ten grams of KGa-1 or KGa-2 powder was mixed with STWs at a solid/solution ratio of 1/10 (w/v) in 250-ml Nalgene polypropylene centrifuge tubes. The tubes were capped and stored in an 80 °C oven for various time periods (1, 2, 4, and 8 weeks). The tubes were shaken 5 minutes each day on a reciprocal shaker. One set of parallel reactions between KGa-1 and STWs was performed at 50 °C for two months. After incubation for the designed time, the solids in the tubes were separated by centrifugation and dialyzed with 12,000-14,000 Dalton MWCO dialysis tubing against deionized water until the electrical conductivity was below 10 μS/cm. The untreated KGa-1 kaolinite was dialyzed for Cs adsorption experiment. The samples were dried at 40 °C and gently ground to break apart aggregates. The samples reacted at 80 °C were coded according to kaolinite sources, simulant

solutions and reaction time. For example, code "*KGa-1-STW1-4 weeks*" denotes the resulting solid sample of KGa-1 reacted with STW1 for four weeks at 80 °C. Sodium aluminate used in this experiment was of technical grade supplied by Strem Chemicals (Newburyport, MA). Other chemicals used were of analytical grade obtained from Fisher Scientific or Aldrich.

Characterization of new mineral phases

X-ray diffraction (XRD) analyses were performed on a Philips diffractometer with Cu-Kα radiation (Philips XRG 3100, Philips Analytical Inc., Mahwah NJ) operated at 35 kV and 30 mA. Step scan mode was used during the XRD analysis with a step size of 0.05 ° 2θ and a dwell time of 5 seconds at each step. The starting kaolinite samples were powder mounted on aluminum frames. The altered mineral suspensions were quickly dried on glass slides under a heating lamp. Infrared spectra were recorded with a Perkin Elmer Spectrum GX FTIR System spectrometer. Samples *KGa-1-STW1-8 weeks* and *KGa-1-STW3-8 weeks* were pressed into KBr pellets (<1% w/w) and heated at 150 °C or 350 °C overnight before IR analysis. The IR instrument was purged with dry and low-CO_2 air produced by a Whatman Lab Gas Generator (Haverhill, MA). Electron micrographs were obtained with a Hitachi S-570 scanning electron microscope (SEM) operated at 25 kV. Powder samples were directly mounted on carbon conductive tabs, and sputter-coated with gold before SEM analysis.

Stability of cancrinite and sodalite in acidic conditions

A series of 0.05 g samples of *KGa-1-STW3-8 weeks* were mixed with 20 ml solutions containing different amounts of HCl in 40-ml Nalgene centrifuge tubes. The tubes were shaken overnight at room temperature and centrifuged. The supernatants were collected for pH, Na^+ and

Al^{3+} analyses. The released Na^{+} and Al^{3+} were quantified with a Varian 220 Flame Atomic Absorption Spectrometer (Varian Ltd., Mulgrave, Australia) at 589 and 309 nm respectively. The remaining solids were washed with distilled water and oven dried at 50 °C before weighing and XRD analysis.

Cesium sorption isotherms

Cesium sorption isotherms were determined using the batch equilibration method. The samples of KGa-1 reacted with STW1 and STW3 at 80 °C were used. One hundred-twenty mg of powder sample was weighed into 40-mL polycarbonate Nalgene centrifuge tubes. Twenty-five mL of 0.01 or 0.1M $NaNO_3$, or 0.005 or 0.05 M $Ca(NO_3)_2$ background solution was added to each tube. An appropriate amount of $CsNO_3$ stock solution, prepared in the corresponding matrix solution, was spiked into the tubes. The initial Cs^{+} concentrations ranged from 0 to 0.4 mmol/L. The tubes were shaken on a reciprocal shaker at ambient condition (~23 °C) for 24 hours. Initial trials showed that the amount of Cs^{+} sorbed changed less than 1% after 2 hours of reaction. The tubes were centrifuged for 30 minutes at 12,062 g. An aliquot of the supernatant solution was sampled for cesium quantification with the atomic absorption spectrometer at a wavelength of 852.1 nm. To suppress ionization, both standards and samples were spiked with 2 M KCl solution to reach a final concentration of 1000 mg/L K in solution before analysis. The pH of the supernatants at the end of the sorption experiments were between 8.2 and 8.9. Sorption isotherms were constructed by plotting amounts sorbed, i.e., the difference between the quantity of Cs^{+} added and the quantity in the final solution, versus concentrations remaining in solution.

Accessibility of internal sites in cancrinite/sodalite

Sodalite and cancrinite are not considered as typical zeolite minerals because of the difficulty of molecular diffusion in their frameworks (Coombs *et al.*, 1997). To test if the internal sites of cancrinite and sodalite are accessible by inorganic ions, 0.05 g of sample *KGa-1–STW3-8 weeks* was mixed with 15 ml of 0.5 M KNO_3, $CsNO_3$, or 0.25 M $Ca(NO_3)_2$ solutions in a 40-ml Nalgene centrifuge tube. The tubes were kept in an oven at 80 °C for 24 hours. During the day time of the 24-hour storage, the tubes were shaken 20 minutes every 2 hours. At the end of the 24-hour treatment, the tubes were centrifuged, and about 15 ml of supernatant from each tube was collected for Na^+ quantification with the atomic absorption spectrometer. Additional 15 ml of corresponding KNO_3, $CsNO_3$, or $Ca(NO_3)_2$ solutions was added to the tubes. The tubes were stored, shaken, centrifuged as in the first washing. The washing process was repeated six times in total. After the sixth washing with the electrolyte solutions, the solids in the tubes were washed three times with deionized water, 15 ml of water was used in each washing. All these experiments were duplicated. The solids were mounted on glass slides for XRD analysis.

RESULTS

Mineralogy phase transformation in KGa-1 at 80 ℃

The major mineral in the KGa-1 sample is kaolinite as indicated by its characteristic X-ray diffraction peaks at 0.71 nm (001) and 0.356 nm(002) (Figure 1, bottom pattern). It also contains a minor amount of anatase (TiO_2) (101 diffraction at 0.351 nm) and mica. When KGa-1 reacted with the simulant solution STW1, the most distinct changes reflected on the XRD patterns are the intensity reduction of kaolinite peaks and the appearance of cancrinite and sodalite peaks. The intensity of kaolinite peaks reduced progressively with time during the 8 weeks of monitoring

period, whereas cancrinite and sodalite peaks enhanced accordingly (Figure 1). Kaolinite peaks are negligible after 8 weeks of reaction. Cancrinite and sodalite have several common peaks located at 0.632, 0.365, 0.259, and 0.211 nm on their XRD patterns, yet cancrinite can be identified by its characteristic diffraction peaks at 0.324 nm (121), 0.274 nm (400), 0.469 nm (101) and 0.415 nm (210). Sodalite has a unique peak at 0.284 nm (310) which can be used to differentiate it from other minerals. Other characteristic peaks of sodalite at 0.446 and 0.400 nm were too weak. The relative height of the (310) diffraction peak of sodalite at 0.284 nm to the nearby (400) peak of cancrinite at 0.274 nm appeared to be constant after one to eight weeks of reaction, indicating that both sodalite and cancrinite were thermodynamically stable under the experimental conditions.

The (101) peak of anatase at 0.351 nm remained on all of the XRD patterns during the eight-week monitoring period, indicating its stability in the caustic simulant solutions. Weak mica peaks (1.0 nm) were present in the one-week and two-week reaction patterns.

Morphology of the KGa-1 and new minerals under SEM

Kaolinite particles in KGa-1 showed platy structure with hexagonal outlines even though there were discontinuities observed on certain edges (Figure 2a). Some plates stack together forming a vermicular structure. All of these morphologies are typical for kaolinite. The new cancrinite/sodalite precipitates formed after contacting the simulant solutions showed very different morphology from kaolinite. The sizes of most of the individual new grains are a few tenths of a μm or even less (Figure 2b). Part of the grains developed along two dimensions forming platy structures with diameters of about 0.5 μm (Figure 2, c and d). The new type of plate does not have the abrupt edges or flat surfaces of the kaolinite plates. Moreover, one very common feature formed by the new plates is their intergrowth by which open spheres formed (Figure 2 c and d). This type

of morphology is termed *lepisphere* (a Greek word meaning sphere of blades). Another type of morphology, thin flake with a larger diameter, was occasionally observed in the reacted samples (e.g. a flake at the upper left corner of Figure 2c). The flakes were very often curled and they are believed to be mica.

Effect of aluminate concentration on mineral transformation rate

When aluminate concentration was doubled to 0.25 M as in the simulant solution STW3, similar mineral phase transformations occurred in the kaolinite samples. The small lepispheric morphology as in Figures 2 b and 2c was observed. The mineral transformation rate in STW3, however, appeared slower than that in STW1. More kaolinite remained in STW3 than in STW1 after same amount of time of reaction (Figure 3). Kaolinite peaks are still visible on the XRD pattern of the sample reacted 8-weeks with STW3. The slower transformation observed in STW3 compared to STW1 suggests that lower aluminate concentration in the simulant solution favors the dissolution of kaolinite and formation of cancrinite and sodalite. Similar to the nearly constant cancrinite/sodalite ratio during the eight weeks of reaction in STW1, the relative intensity of the 0.284 nm peak of sodalite to the 0.274 nm of cancrinite in STW3 did not show obvious changes during the eight weeks. Yet the 0.274, 0.324, and 0.469 nm peaks of cancrinite in the samples formed in STW3 are stronger than the corresponding peaks of cancrinite formed in STW1. This might be an indication of more cancrinite formed after reacting with STW3. We have also observed that the intensities of these peaks are strongly correlated to the crystallinity of cancrinite. The higher crystalline cancrinite produced stronger diffraction peaks at these three positions (Data not shown).

Incorporation of nitrate in cancrinite/sodalite

There were several distinct changes on the FTIR spectra (Figure 4) when KGa-1 reacted with the simulated solutions. The characteristic OH stretching vibrations of kaolinite at 3695, 3669, 3652, and 3620 cm^{-1} disappeared or weakened after reacting with the simulated solutions. Other kaolinite bands at 938 cm^{-1} (surface OH bending), and 914 cm^{-1}(inner OH bending) were weakened too. The reduction of the kaolinite bands in the solid phase formed in STW1 was more extensive than that in STW3. Weak kaolinite bands at 3695cm^{-1} (surface OH) and 3620 cm^{-1} were still visible in sample *KGa-1-STW3-8 weeks*. Coincident with the reduction or disappearance of kaolinite, cancrinite and sodalite bands appeared on the IR spectra, including the asymmetric Al-O stretch of cancrinite and sodalite located in the range of 980-1120 cm^{-1}, and the symmetric Al-O stretch of the minerals located in the range of 660-770 cm^{-1}. The bands in the range 560-630 cm^{-1} arose from the parallel 4- or 6-membered double rings of cancrinite and sodalite. The bands with wavenumbers less than 500 cm^{-1} arose from the bending vibrations of Si-O and Al-O of the tetrahedra of the feldspathoids. The detailed IR assignments for cancrinite and sodalite were summarized by Barnes et al. (1999b). Based on our pure mineral analyses (data not shown), the characteristic bands of cancrinite are located at 1113, 1032, 821, 618, 571, and 503 cm^{-1}. Sodalite can be distinguished by its bands at 733 and 707 cm^{-1}. The band positions shown in Figure 4 are slightly off from the bands observed in pure minerals, presumably due to crystallinity differences between the samples in this experiment and the synthetic pure minerals.

The FTIR spectra indicate that NO_3^- was incorporated in the precipitates. The 1422 and 1384 cm^{-1} bands are attributed to the NO_3^- group. Our IR analysis of pure minerals showed that nitrate-cancrinite has only one NO_3^- band at 1422 cm^{-1}. The 1384 cm^{-1} band arose from either

sodalite or $NaNO_3$ residue. Pure $NaNO_3$ salt alone has a band at 1384 cm^{-1}. It has been observed that pure nitrate-sodalite has a distinct NO_3^- band at 1380 cm^{-1}(Buhl and Loens, 1996). It is likely that the 1384 cm^{-1} band belonged to the nitrate group in sodalite, because free $NaNO_3$ should have been removed after extensive dialysis against deionized water. When the samples were heated at 350 °C overnight, an additional band appeared at 1351 cm^{-1} in both the *KGa-1-STW1-8 weeks* and *KGa-1-STW3-8 weeks* samples, and the 1422 cm^{-1} band was weakened. It is likely that the 1351 cm^{-1} band arose from the dehydrated nitrate group. The broad bands around 3500 cm^{-1} indicate that water remained in the feldspathoids even after heating overnight at 150 °C. Heating the samples at 350 °C reduced the moisture as reflected by the near disappearance of the broad band around 3500 cm^{-1}.

The FTIR spectra also indicate that NaOH was not incorporated to a significant extent in the cancrinite or sodalite lepispheres formed under the experimental conditions even though 1.4 M NaOH was used in the simulant solutions. There is no sharp NaOH band in the typical OH stretching band range (3000-4000 cm^{-1}) after the samples were heated at 350 °C. In a highly crystalline sodalite formed in 16 M NaOH, we have found a sharp band at 3640 cm^{-1} that was attributed to the incorporated NaOH (data not shown). The lack of NaOH bands in cancrinite/sodalite lepispheres in this experiment indicate that cancrinite and sodalite prefer nitrate groups to hydroxide groups in their cages or channels under the condition used.

Mineral transformation at lower temperature (50 °C)

When KGa-1 reacted with the simulant solutions at 50 °C, mineral transformation appeared similar to the transformation at 80 °C but with a slower reaction rate. Contrary to the near complete dissolution of kaolinite at 80 °C, kaolinite was still dominant after two months of reaction at 50 °C

(Figure 5). The area of the (001) peak of kaolinite at 0.71 nm and the common (110) peaks of cancrinite and sodalite at 0.632 nm were used to roughly estimate the quantity of undissolved kaolinite based on the percentage of each peak area. Calculation indicated 65-75 % of the solids was undissolved kaolinite. The total percentage of cancrinite and sodalite increased from 28 % to 34 % when NaOH concentration was raised from 1.4 to 2.8 mol/kg at 0.125 mol/kg $NaAlO_2$ level, and from 22% to 25% at 0.25 mol/kg $NaAlO_2$ level. These data also suggest that cancrinite and sodalite yield was reduced when aluminate concentration was doubled at the same NaOH concentration level. Cancrinite and sodalite formed at 50 °C also showed the lepispheric structure (Figure 2f). Combining the information from Figures 1, 3 and 5, we conclude that increasing temperature, increasing NaOH concentration, and decreasing aluminate concentration facilitate the transformation of kaolinite to cancrinite and sodalite.

Effect of kaolinite crystallinity on the transformation

The mineral transformation of the poorly crystalline KGa-2 in the simulant solutions was similar to that of KGa-1. The XRD patterns of the resulting solids of KGa-2 after reacting with the simulant solutions were very similar to those in Figures 1, 3, and 5, and therefore, were not shown here. No obvious morphology differences have been observed on the new mineral phases that formed from KGa-1 and KGa-2 kaolinites. The lack of a difference in the products formed from KGa-1 and KGa-2 kaolinites indicates that the reactant crystallinity is not an important factor in determining the mineral phases in alkaline solutions.

Stability of cancrinite and sodalite under acidic conditions

Cancrinite and sodalite were vulnerable to acid attack. When sample *KGa-1-STW3-8 weeks* was treated with HCl, the amount of Na^+ and Al^{3+} released to the solution increased with increasing HCl concentration (Figure 6a). When the pH of the suspension was dropped to 5.5 by adding 0.24 millimole of HCl, 0.25 millimole of Na^+, nearly 90% of the total Na^+ in the sample, and 0.09 millimole of Al^{3+} were released to the solution. The mass of solid was reduced by nearly 50%. The release of Na^+ and Al^{3+}, and the loss of the solid mass indicate pronounced dissolution of cancrinite and sodalite at pH 5.5. The released Al^{3+} concentration did not increase in synchrony with that of Na^+. The lag of Al^{3+} release to the solution indicates that there are other forms of Al-containing solids formed in weak acidic conditions. X-ray diffraction analysis indicates that only residual kaolinite, mica, and anatase remained as the crystalline phases in the solid after treating with a large amount of acid (Figure 6b). Between pH 5.5 and 3.65, the diffraction patterns were noisy and broad humps arose around 30 ° 2θ, indicating poorly crystalline materials in the samples. When pH was reduced from 3.65 to 1.4, the diffraction of residual kaolinite and mica enhanced progressively, indicating the loss of the amorphous phase. The XRD patterns also suggest that more anatase dissolved in the lower pH conditions as reflected by its reduced (101) diffraction at 0.351 nm relative to the kalinite peak.

Cesium adsorption

Most cesium isotherm curves showed L-type adsorption on samples *KGa-1-STW1* and *KGa-1-STW3* (Figures 8 and 9). The L-type isotherms were fitted with the Langmuir equation:

$$q = q_{max} K C/(1+KC) \quad (1)$$

Where q is the amount adsorbed, q_{max} is the maximum adsorption capacity of the solid phase, *K* is the Langmuir constant, and C is the final cesium aqueous concentration. The Langmuir parameters (Table 2) were determined by the normal nonlinear least square method as recommended by Schulthess and Dey (1996). The newly formed cancrinite and sodalite showed much higher adsorption for cesium than kaolinite given the same cesium solution concentration. Generally, there was a 4-6 times increase in Kq_{max} for cesium adsorption on the new minerals compared to KGa-1. Adsorption did not reach plateaus in the cesium solution concentration range tested. The ideal maximum adsorption should be equal to the CEC of each sample. Based on the formula $Na_6Al_6Si_6O_{24}\cdot 2NaX$ of cancrinite and sodalite, the theoretical CEC of the fully dehydrated minerals should be in the range of 704-879 cmol/kg depending on the incorporated anion X, assuming all of the Na^+ cations in the minerals are exchangeable. The maximum adsorption capacities estimated from the sorption isotherms (Table 2) were far below the theoretical CEC of the feldspathoids; this is likely the result of the strong competition from the cations in the background solutions. The calculated maximum adsorption q_{max} in 0.01 M $NaNO_3$ was nearly 9-12 times higher after reacting with the simulant solutions. The new solids formed in STW1 after 1, 2, 4, and 8 weeks displayed very similar adsorption isotherms indicating that mineral compositions of the solid phase was fairly constant over the eight week period. The precipitates formed in STW3 showed higher cesium adsorption than the corresponding precipitates formed in STW1, and the STW3 solids showed higher Cs^+ sorption with increasing reaction time (Figure 7). Since there is more kaolinite remaining after reacting with STW3, the difference observed on Cs^+ sorption is more likely caused by the relative amount of cancrinite to sodalite in the samples. It appears that cancrinite has a higher adsorption capacity for cesium adsorption than sodalite. The XRD peaks of cancrinite in *KGa1-STW3-8 weeks* were stronger than in *KGA1-STW1-8 weeks* as shown in Figures 1 and 3.

Cation competition in Cs^+ adsorption

Cations in the background electrolyte solutions compete for sorption sites on cancrinite and sodalite. Samples *KGa1-STW1-8 weeks* and *KGa1-STW3-8 weeks* had very similar response to the concentration change of the background electrolytes (Figure 8). When the background electrolyte concentration was increased, cesium adsorption decreased. Yet, the cations with different valence in the background electrolytes had different competition capacities. At low ionic strength, e.g. 0.01 M $NaNO_3$ or 0.005 M $Ca(NO_3)_2$, the cesium adsorption in the 0.005 M $Ca(NO_3)_2$ was much lower than that in 0.01 M $NaNO_3$, indicating stronger competition from Ca^{2+} than from Na^+. When the concentration of the two background electrolytes was increased 10 times, the reduction in $NaNO_3$ solution was more extensive than that in $Ca(NO_3)_2$ solution. Indeed, cesium adsorption in 0.05 M $Ca(NO_3)_2$ solution was higher than that in 0.1 M $NaNO_3$ solution even though the Ca^{2+} and Na^+ still had the same charge concentration. The lower adsorption of Cs^+ in the presence of high concentration of Na^+ compared to the same charge concentration of Ca^{2+} runs counter to what is expected for exchange between divalent and monovalent cations on phyllosilicate clay minerals and soils (McBride, 1994). The ability of 0.1 M Na^+ to compete more effectively with Cs^+ than the 0.05 M Ca^{2+} suggests that there are some sites that are accessible to Na^+ and Cs^+ but not to Ca^{2+}.

Accessibility of internal sites in cancrinite/sodalite

When the *KGa-1-STW3-8 weeks* sample was washed with pure $CsNO_3$, $Ca(NO_3)_2$, or KNO_3 solutions containing 0.5 M NO_3^-, a large amount of Na^+ was released in the first 24 hour washing at 80 °C (Figure 9), indicating that Na^+ in the cages of cancrinite and sodalite was exchangeable. Twice the amount of Na^+ was released by the first KNO_3 washing as that by $CsNO_3$ or $Ca(NO_3)_2$,

indicating K^+ is the most efficient cation in the ion exchange reaction. There are still substantial amounts of Na^+ released from the 3rd through the 6th washings with $CsNO_3$. The different amounts of Na^+ released from the sequential washings indicate that Na^+ ions can readily migrate out of or into the cages and channels of cancrinite and sodalite. Other cations, such as Cs^+, K^+, and Ca^{2+} can access the internal part of the minerals, yet they had different abilities to access those sites. Potassium ions can easily diffuse into the minerals, whereas Cs^+ ions take a longer time to reach the same sites, presumably due to slower diffusion of the large Cs^+ ion. Calcium cations appeared have the most difficulty in fully replacing the Na^+ even though the ionic radii of Ca^{2+} and Na^+ are about the same (0.099 and 0.097 nm respectively). That Cs^+ more easily accesses some sites occupied by Na^+ than does Ca^{2+} explains the lower adsorption of Cs^+ in the 0.1 M Na^+ system relative to 0.05 M Ca^{2+}. Na^+ displaces Cs^+ on internal sites of cancrinite and sodalite that Ca^{2+} cannot easily access.

The XRD patterns of the $CsNO_3$, $Ca(NO_3)_2$, and KNO_3 washed samples (Figure 10) indicate that KNO_3 washing expanded the minerals. For example, the common peaks of cancrinite and sodalite at 0.632 nm was expanded to 0.656 nm, the 0.365 nm peak was expanded to 0.379 nm after KNO_3 washing. Similarly, the d(101) of cancrinite was expanded from 0.469 nm to 0.486 nm, the d(400) of 0.274 nm was expanded to 0.284 nm, the d(310) of 0.284 nm of sodalite was expanded from 0.284 nm to 0.293 nm. There was little, if any, expansion or shrinkage caused by Ca exchange. The $CsNO_3$ washing did not shift the diffraction peak positions, but weakened the diffraction at 0.632, 0.365, 0.284 nm. The XRD diffraction intensity changes imply that the structure became more disordered when Cs^+ replaced the Na^+ in cancrinite and sodalite.

DISCUSSION

Thermodynamic stability of cancrinite and sodalite

The mineral phase transformation of kaolinite after contacting the simulated tank solutions indicates that there are two major processes involved in the reactions: dissolution of kaolinite releasing Si and Al (Equation 2), and precipitation of the feldspathoids cancrinite and sodalite (Equation 3).

$$Al_2Si_2O_5(OH)_4 + 6OH^- + H_2O = 2Al(OH)_4^- + 2H_2SiO_4^{2-} \quad (2)$$

$$6Al(OH)_4^- + 6H_2SiO_4^{2-} + 8\,Na^+ + 2X^- = Na_6Si_6Al_6O_{24}\cdot 2NaX + 12OH^- + 12\,H_2O \quad (3)$$

where X^- represents NO_3^-, OH^- or $0.5CO_3^{2-}$. Equation 2 suggests that the dissolution of kaolinite is favored at high NaOH concentration, which is likely the reason why more kaolinite converted to cancrinite and sodalite in the 2.8 mol/kg NaOH solutions than in 1.4 mol/kg NaOH. Theoretically, kaolinite [$Al_2Si_2O_5(OH)_4$] dissolution releases Si and Al at a 1:1 ratio, and the formation of ideal cancrinite and sodalite also requires a 1:1 of Si to Al ratio. The presence of excess aluminate or silicate in the starting solution will drive the reaction to the left side in Equation 2. This is likely why doubling aluminate concentration in the simulant solutions resulted in more unaltered kaolinite. Equation 3 implies that high silicate and aluminate concentration will favor the formation of cancrinite or sodalite thermodynamically, and increased NaOH will inhibit the formation of the feldspathoids. The kaolinite to cancrinite and sodalite ratios reflected in Figures 1, 3, and 5 imply that the dissolution of kaolinite (Equation 2) is the rate-determining step in the overall reaction.

The formation of cancrinite and sodalite has also been observed under similar experimental conditions. When synthetic Bayer liquors containing 3.9-5.4 M NaOH, 0.38 M Na_2CO_3,1.6-2.33 M $Al(OH)_3$ and 0.1 M SiO_2 were heated to 250 °C in an autoclave, Linde type A zeolite, sodalite and cancrinite formed, and cancrinite appeared more stable than sodalite (Barnes *et al.*, 1999a). It was proposed that the cancrinite would be the final product, whereas amorphous

material, Linde type A zeolite and sodalite would be the transition phases (Barnes *et al.*, 1999a). The presence of high concentration (e.g. 0.38 M) of sodium carbonate decreased the rate of cancrinite formation (Gerson and Zheng, 1997; Zheng *et al.*, 1997; Zheng *et al.*, 1998). Fetchtelkord et al. (2001) argued that sodalite is the thermodynamically more stable phase and cancrinite formation is kinetically favored at lower NaOH concentrations (< 5M) based on a series of tests in mixed solvents of butanediol and water. Combining these observations and our experimental results, it appears that the relative stability of sodalite and cancrinite depends on the initial chemical composition of the alkaline solutions. At high $NaNO_3$ concentration, such as the Hanford tank waste solutions, both cancrinite and sodalite are stable at NaOH concentration of 1.4 M. The consistent mineral phases observed at different temperatures, different NaOH or $NaAlO_2$ concentrations, and with different kaolinite sources are likely caused by the presence of high concentration of $NaNO_3$ in the experiment.

Incorporation of ion pairs in cancrinite and sodalite

The stoichiometry of cancrinite and sodalite has been reported as $Na_6Al_6Si_6O_{24}\cdot 2NaX$, where X is 1/2 CO_3^{2-}, 1/2 SO_4^{2-}, Cl^-, OH^- or NO_3^- (Barnes et al., 1999a;b). The crystal structure of cancrinite is similar to those of the zeolites, with a three-dimensional aluminosilicate host framework in which sodium and calcium cations, inorganic anions, and water molecules exist as the guest components (Gerson and Zheng, 1997). The hexagonal cancrinite framework contains two main structural features: the ε-cages and the large 12-membered ring channel along the crystallographic c-axis (Figure 11a), which can accommodate cations such as Na^+, K^+, and Ca^{2+}, as well as anions such as CO_3^{2-}, OH^-, and NO_3^- (Barrer, 1978; Hund, 1984). The cubic sodalite structure can be described by the space-filling array of a $[4^6 6^8]$-truncated octahedron known as the

sodalite- or β-cage (Figure 11b). Like cancrinite, each cage contains constituents of four water molecules or cation/anion pairs (Gerson and Zheng, 1997). The fundamental reason for the capability of cancrinite and sodalite to incorporate cation/anion pairs in their cages is their stability requirement. The Al/Si substitution in the sodalite framework requires three alkali metal cations within each β-cage to balance the charge of the AlO_4^- unit on the framework. This requirement will have the three alkali cations directly face to each other in each cage and their repulsion makes the arrangement unstable. Incorporating a cation/anion ion pair inside the cage will compensate the direct cation-cation repulsion. The incorporated anion will be in the center of the β-cage, and a monovalent anion will tetrahedrally coordinate to the four alkali cations (Rabo, 1976). It has also been suggested that the ion pairs serve as a template during the formation of cancrinite and can stabilize the one-dimensional channel as a "backbone" (Fechtelkord *et al.*, 2001).

Due to the high NO_3^- concentration and high pH of the STWs, and the possibility of sorbing CO_2 from the atmosphere, the potential anions for the cancrinite/sodalite in our experiments are NO_3^-, CO_3^{2-}, and OH^-. FTIR analysis indicate that NO_3^- is the major anion in the incorporated form. Carbonate or OH^- did not incorporate to a detectable extent. Incorporated CO_3^{2-} had two IR bands at 1410 and 1455 cm^{-1} (Hackbarth *et al.*, 1999). The IR band of incorporated CO_3^{2-} in sodalite synthesized in an autoclave has been reported at 1470 cm^{-1}(Barnes *et al.*, 1999c). No obvious bands near 1455 or 1470 cm^{-1} on the FTIR spectra of the precipitates formed in our experiment. The two NO_3^- bands at 1422 and 1384 cm^{-1} we observed suggested that both cancrinite and sodalite can incorporate NO_3^- in the structure. Since Na^+ was the only cation in the system, the $NaNO_3$ ion pairs are expected to occur in the cages and channels of the feldspathoids.

Accessibility of interior sites of cancrinite and sodalite

The accessibility of cations to the interior of cancrinite and sodalite is dependent on the feldspathoid structure, and the size and valence of the cations. The 12-membered channel in cancrinite might be easier to access than the ε-cage. Access to the cages of cancrinite and sodalite requires that the cations be smaller than aperture of the 6-member rings. The free aperture size of hydrated sodalite is estimated as 0.22 nm (Breck, 1974). The small size of the aperture requires that the cations must be dehydrated when they pass through the 6-member ring. The size limitation may explain why Cs^+ replaces Na^+ more slowly than does K^+. Divalent calcium has nearly the same ion radius as Na^+. It appears that Ca^{2+} can migrate into the channels of the cancrinite, but not into the cages. One possible reason is the difficulty of Ca^{2+} dehydration. The dehydration energy of Ca^{2+} is 1650 kJ/mol, which is nearly three times higher than that of Na^+. Another possible reason is that it would be less favorable electrostatically to distribute two Ca^{2+} cations as opposed to four Na^+ in the cages when the negative charges on the framework are strictly localized. It has been proposed that stacking faults in cancrinite could block channels and limit exchange and sorption (Bickmore *et al.*, 2001). The intergrowth of the plates observed in the cancrinite/sodalite lepispheres (Figure 2) implied that joint interface of the two plates may cause a discontinuity in cancrinite channels; yet, 5.3 mmol/g or 530 cmol/kg of Na^+ released by KNO_3 washing (Figure 9) indicates that the internal Na^+ of sodalite and cancrinite are readily exchangeable.

SUMMARY

There were two major chemical processes involved in the reaction when kaolinite contacted the caustic simulant tank solutions: dissolution of kaolinite and formation of the feldspathoids cancrinite and sodalite. Kaolinite dissolution appeared to be the controlling step in the transformation. At the NaOH concentrations tested, cancrinite and sodalite particles have diameters

of a few tenths of a μm or less. The new minerals form lepispheres by the intergrowth of their plates. Increasing NaOH concentration and temperature, and decreasing aluminate concentration in the initial solutions favor the dissolution of kaolinite and formation of cancrinite and sodalite. Both cancrinite and sodalite appeared stable under the experimental conditions presumably because of the presence of high concentration of $NaNO_3$ (3.7M). Cancrinite and sodalite can incorporate $NaNO_3$ in their cages or channels. No, or very little, NaOH or Na_2CO_3 was incorporated under the experimental condition. Cancrinite and sodalite are not stable under acidic conditions and pronounced dissolution occurred below pH 5.5. Cancrinite and sodalite have much higher cesium sorption capacities than kaolinite. This is because of the high degree of Al for Si substitution in the cancrinite and sodalite framework, whereas kaolinite has little or no Al for Si substitution. Cation exchange reactions indicate that Na^+ and K^+ can readily diffuse in cancrinite and sodalite, whereas cesium diffusion appeared relatively slow presumably due to its large ion radius. The frameworks of cancrinite and sodalite can be expanded by K^+ or become disordered by Cs^+. It is more difficult for Ca^{2+} to access the internal sites of the minerals. The difficulty of accessing the internal part of the minerals makes Ca^{2+} less competitive than Na^+ for Cs^+ sorption sites at high ionic strength.

ACKNOWLEDGMENTS

This work was supported by the Environmental Management Science Program, U.S. Department of Energy under contract DE-FG07-99ER62882. We thank the Electron Microscopy Center and the Department of Geology at Washington State University for the use of SEM and FTIR equipments. Dr. Daniel Strawn at the University of Idaho allowed us to use his FTIR spectrometer. We also thank three reviewers for their constructive comments.

REFERENCES

Alberti, A., Colella, C., Oggiano, G., Pansini, M., and Vezzalini, G. (1994) Zeolite production from waste kaolin-containing materials. *Materials Engineering (Modena, Italy)*, **5,** 145-158.

Barnes, M.C., Addai-Mensah, J., and Gerson, A.R. (1999a) The mechanism of the sodalite-to-cancrinite phase transformation in synthetic spent Bayer liquor. *Microporous Mesoporous Materials*, **31,** 287-302.

Barnes, M.C., Addai-Mensah, J., and Gerson, A.R. (1999b) A methodology for quantifying sodalite and cancrinite phase mixtures and the kinetics of the sodalite to cancrinite phase transformation. *Microporous Mesoporous Materials*, **31,** 303-319.

Barnes, M.C., Addai-Mensah, J., Gerson, A.R., and Smart, R.S.C. (1999c) The solubility of sodalite and cancrinite in synthetic spent liquor and the mechanism and kinetics of the sodalite to cancrinite phase transformation. *Light Metals (Warrendale, Pa.),***,** 131-140.

Barrer, R.M. (1978) *Zeolites and Clay Minerals as Sorbents and Molecular Sieves.* Academic Press, London.496 pp.

Bauer, A., Velde, B., and Berger, G. (1998) Kaolinite transformation in high molar KOH solutions. *Applied Geochemistry*, **13,** 619-629.

Bickmore, B.R., Nagy, K.L., Young, J.S., and Drexler, J.W. (2001) Nitrate-cancrinite precipitation on quartz sand in simulated Hanford tank solutions. *Environmental Science and Technology*, **35,** 4481-4486.

Breck, D.W. (1974) *Zeolite Molecular Sieves: Structure, Chemistry, and Use.* John Wiley, New York.752 pp.

Buhl, J.C. (1991) Synthesis and characterization of the basic and non-basic members of the cancrinite-natrodavyne family. *Thermochimica Acta*, **178,** 19-31.

Buhl, J.-C., and Loens, J. (1996) Synthesis and crystal structure of nitrate enclathrated sodalite $Na_8[AlSiO_4]_6(NO_3)_2$. *Journal of Alloys and Compounds*, **235,** 41-47.

Buhl, J.-C., Stief, F., Fechtelkord, M., Gesing, T.M., Taphorn, U., and Taake, C. (2000) Synthesis, X-ray diffraction and MAS NMR characteristics of nitrate cancrinite $Na_{7.6}[AlSiO_4]_6(NO_3)_{1.6}(H_2O)_2$. *Journal of Alloys and Compounds*, **305,** 93-102.

Coombs, D.S., Alberti, A., Armbruster, T., Artioli, G., Colella, C., and Galli, E. et al. (1997) Recommended nomenclature for zeolite minerals: report of the sbucommittee on zeolites for the Internaltional Mineralogist Association, Commission on New Minerals and Mineral Names. *Canadian Mineralogist*, **35,** 1571-1606.

Dudzik, Z., and Kowalak, S. (1974) Preparation of zeolites of faujasite type from kaolinite. *Przemysl Chemiczny*, **53,** 616-618.

Fechtelkord, M., Posnatzki, B., and Buhl, J.-C. (2001) Synthesis of basic cancrinite in a butanediol-water system. *Chemistry of Materials*, **13,** 1967-1975.

Gephart, R.E., and Lundgren, R.E. (1998) *Hanford Tank Cleanup: A Guide to Understanding the Technical Issues.* 4th ed. Battelle Press, Columbus.

Gerson, A.R., and Zheng, K. (1997) Bayer process plant scale: transformation of sodalite to cancrinite. *Journal of Crystal Growth*, **171,** 209-218.

Gualtieri, A., Norby, P., Artioli, G., and Hanson, J. (1997) Kinetic study of hydroxysodalite formation from natural kaolinites by time-resolved synchrotron powder diffraction. *Microporous Materials*, **9,** 189-201.

Hackbarth, K., Gesing, T.M., Fechtelkord, M., Stief, F., and Buhl, J.C. (1999) Synthesis and crystal structure of carbonate cancrinite $Na_8[AlSiO_4]_6CO_3(H_2O)_{3.4}$, grown under low-temperature hydrothermal conditions. *Microporous Mesoporous Materials*, **30,** 347-358.

Hanlon, B.M. (1996) Waste tank summary report for month ending January 31, 1996 WHC-EP-0182-94. Westinghouse Hanford Company, Richland, WA.

Hund, F. (1984) Nitrate-, thiosulfate-, sulfate-, and sulfide cancrinite. *Zeitschrift für Anorganische und Allgemeine Chemie*, **509,** 153-160.

Nyman, M., Krumhansl, J.L., Zhang, P., Anderson, H., and Nenoff, T.M. (2000) Chemical evolution of leaked high-level liquid wastes in Hanford soils. *Materials Research Society Symposium Proceedings*, **608,** 225-230.

Pruess, K., Yabusaki, S., Steefel, C., and Lichtner, P. (2002) Fluid flow, heat transfer, and solute transport at nuclear waste storage tanks in the Hanford vadose zone. *Vadose Zone Journal*, **1,** 68-88.

Rabo, J.A. (1976) Salt occlusion in zeolite crystals. In *Zeolite Chemistry and Catalysis*, J.A. Rabo, ed. Zeolite Chemistry and Catalysis, ACS monograph 171. American Chemical Society, Washington, D.C., 332-349.

Schulthess, C.P., and Dey, D.K. (1996) Estimation of Langmuir constants using linear and nonlinear least squares regression analyses. *Soil Science Society of America Journal*, **60,** 433-442.

Serne, R.J., Zachara, J.M., and Burke, D.S. (1998) Chemical Information on tank supernatants, Cs adsorption from tank liquids onto Hanford sediments, and field observations of Cs migration from past tank leaks PNNL-11498/UC-510. Pacific Northwest National Laboratory, Richland, WA.

Sieger, P., Wiebcke, M., Felsche, J., and Buhl, J.C. (1991) Orientational disorder of the nitrite anion in the sodalite sodium aluminum silicate nitrite ($Na_8[AlSiO_4]_6(NO_2)_2$). *Acta Crystallographica, Section C: Crystal Structure Communications*, **C47,** 498-501.

Zheng, K., Gerson, A.R., Addai-Mensah, J., and Smart, R.S.C. (1997) The influence of sodium carbonate on sodium aluminosilicate crystallization and solubility in sodium aluminate solutions. *Journal of Crystal Growth*, **171,** 197-208.

Zheng, K., Smart, R.S.C., Addai-Mensah, J., and Gerson, A. (1998) Solubility of sodium aluminosilicates in synthetic Bayer liquor. *Journal of Chemical and Engineering Data*, **43,** 312-317.

Table 1. Chemical compositions of simulated tank waste (STW) solutions

Simulant Solutions	NaOH (mol/kg)	$NaAlO_2$ (mol/kg)	$NaNO_3$ (mol/kg)
STW1	1.4	0.125	3.7
STW2	2.8	0.125	3.7
STW3	1.4	0.250	3.7
STW4	2.8	0.250	3.7

Table 2. Langmuir parameters for Cs^+ sorption calculated with nonlinear regression analysis.

Sample	Background Electrolyte	q_{max} (cmol/kg)	*K* (L/mmol)	Initial Slope (L/kg)	Correlation Coefficient† n^{*2}
KGa-1-STW1, 1week	0.01M $NaNO_3$	6.70	2.94	197.3	0.997
KGa-1-STW1, 2weeks	0.01M $NaNO_3$	5.31	4.53	241.1	0.997
KGa-1-STW1, 4weeks	0.01M $NaNO_3$	5.61	4.05	226.7	0.999
KGa-1-STW1, 8weeks	0.01M $NaNO_3$	4.65	6.23	289.8	0.999
KGa-1-STW3, 1week	0.01M $NaNO_3$	5.39	5.38	289.9	0.999
KGa-1-STW3, 2weeks	0.01M $NaNO_3$	5.83	5.22	304.6	0.999
KGa-1-STW3, 4weeks	0.01M $NaNO_3$	5.73	5.58	319.5	0.999
KGa-1-STW3, 8weeks	0.01M $NaNO_3$	6.14	6.40	393.1	0.999
KGa-1-STW1, 8weeks	0.1M $NaNO_3$	0.93	2.85	26.5	0.932
KGa-1-STW3, 8weeks	0.1M $NaNO_3$	5.79	0.59	34.3	0.995
KGa-1-STW1, 8weeks	0.005M $Ca(NO_3)_2$	4.12	2.83	116.8	0.990
KGa-1-STW3, 8weeks	0.005M $Ca(NO_3)_2$	6.54	2.65	173.4	0.996
KGa-1-STW1, 8weeks	0.05M $Ca(NO_3)_2$	2.04	3.46	70.6	0.988
KGa-1-STW3, 8weeks	0.05M $Ca(NO_3)_2$	4.41	2.33	102.7	0.996
KGa-1	0.01M $NaNO_3$	0.54	11.41	61.8	0.995
KGa-1	0.1M $NaNO_3$	0.92	1.01	9.3	0.948

† n^{*2} assumes that a normal minimum correlates best (Schulthess and Dey, 1996).

FIGURE LIST

Figure 1. Normalized X-ray diffraction patterns of KGa-1 kaolinite and the solid phases formed at different times following reaction with STW1 at 80 °C. The vertical solid lines indicate the peak positions of cancrinite as published by Buhl et al. (2000). The vertical dotted lines indicate sodalite as published by Sieger et al. (1991). The dashed line is for anatase.

Figure 2. Mineral morphology change of KGa-1-kaolinite after reacting with STW1 for different times. (a). starting KGa-1 kaolinite with vermiform structure; (b to e). after 1, 2, 4, 8 weeks of reaction at 80 °C, respectively; (f). after 2 months of reaction at 50 °C.

Figure 3. Normalized X-ray diffraction patterns of KGa-1-kaolin and the solid phases reacted for different time with STW3 at 80 °C.

Figure 4. FTIR spectra of KGa-1 and samples *KGa-1-STW1-8 weeks* and *KGa-1-STW3-8-weeks*. The pellets were heated overnight at 150 °C and 350 °C respectively. The asterisk marked spectra were recorded with less concentrated unheated samples.

Figure 5. Normalized X-ray diffraction patterns of KGa-1 reacted with four simulant solutions for two months at 50 °C.

Figure 6. Acid attack on sample *KGa-1-STW3-8 weeks*, (a) remaining solid mass, released Na^+ and Al^{3+}, and suspension pH, and (b) XRD patterns of residue.

Figure 7. Cesium adsorption isotherms and fitted Langmuir curves of KGa-1 and the solid phases after reacting with (a) STW1 and (b) STW3 for 1, 2, 4 and 8 weeks at 80 °C. Background electrolyte was 0.01 M $NaNO_3$, and pH of final solutions was in the range of 8.2 to 8.9.

Figure 8. Cesium adsorption isotherms and fitted Langmuir curves of samples (a) *KGa-1-STW1-8 weeks* and (b) *KGa-1-STW3-8 weeks*. Background electrolytes are marked on the curves, and pH of final solutions was in the range of 8.2 to 8.9.

Figure 9. Released Na^+ from sample *KGa-1-STW3-8 weeks*. The sample was washed at 80 °C with 0.5 M $CsNO_3$, 0.25 M $Ca(NO_3)_2$ or 0.5 M KNO_3, respectively.

Figure 10. X-ray diffraction patterns of sample *KGa-1-STW3-8 weeks* before and after six washing with $CsNO_3$, $Ca(NO_3)_2$ or KNO_3 solutions at 80 °C.

Figure 11. The 12-membered channel, ε-cage in cancrinite and the β-cage in sodalite frameworks. Images were generated with WebLab ViewerLite software (Accelrys, San Diego, CA, USA) according to structural data published by the International Zeolite Association (www.iza-structure.org, accessed March 2003).

Cesium Migration in Saturated Silica Sand and Hanford Sediments as Impacted by Ionic Strength

Markus Flury*, Szabolcs Czigány, Gang Chen, and James B. Harsh

Department of Crop and Soil Sciences, Center for Multiphase Environmental Research, Washington State University, Pullman, WA 99164, USA

Abstract

Large amounts of ^{137}Cs have been accidentally released to the subsurface from the Hanford nuclear site in the state of Washington, USA. The cesium-containing liquids varied in ionic strengths, and often had high electrolyte contents, mainly in form of $NaNO_3$ and NaOH, reaching concentrations up to several moles per liter. In this study, we investigated the effect of ionic strengths on Cs migration through two types of porous media: silica sand and Hanford sediments. Cesium sorption and transport was studied in 1, 10, 100, and 1000 mM NaCl electrolyte solutions at pH 10. Sorption isotherms were constructed from batch equilibrium experiments and the batch-derived sorption parameters were compared with column breakthrough curves. Column transport experiments were analyzed with a two-site equilibrium-nonequilibrium model. Cesium sorption to the silica sand in batch experiments showed a linear sorption isotherm for all ionic strengths, which matched well with the results from the column experiments at 100 and 1000 mM ionic strength; however, the column experiments at 1 and 10 mM ionic strength indicated a nonlinear sorption behavior of Cs to the silica sand. Transport through silica sand occurred under one-site sorption and equilibrium conditions. Cesium sorption to Hanford sediments in both batch and column experiments was best described with a nonlinear Freundlich

*corresponding author, FAX: (509) 335-8674, e-mail: flury@mail.wsu.edu

isotherm. The column experiments indicated that Cs transport in Hanford sediments occurred under two-site equilibrium and nonequilibrium sorption. The effect of ionic strength on Cs transport was much more pronounced in Hanford sediments than in silica sands. Effective retardation factors of Cs during transport through Hanford sediments were reduced by a factor of 10 when the ionic strength increased from 100 to 1000 mM; for silica sand, the effective retardation was reduced by a factor of 10 when ionic strength increased from 1 to 1000 mM. A two order of magnitude change in ionic strength was needed in the silica sand to observe the same change in Cs retardation as in Hanford sediments.

Key words: cesium migration; equilibrium; kinetic; sorption; ionic strength; silica sand; Hanford sediments

---

1 Introduction

The Hanford Reservation in southcentral Washington State, USA, has been the major production facility of weapons-grade plutonium in the United States. Radioactive byproducts from the Pu production process have been disposed of directly to the subsurface or, in the case of high-level waste, stored in underground tanks. Over the last 40 years, it was suspected that as many as 67 tanks of the 149 single-shell tanks at Hanford had leaked into the subsurface (Gephart and Lundgren, 1998). A major radioactive element in these tanks is ^{137}Cs, which, decay-corrected as of 1996, contributes 24% of the total radioactivity of the waste (Gephart and Lundgren, 1998). It is estimated that more than 1 million curies of radioactivity may have been released into the subsurface due to the leaking of ^{137}Cs (U.S. DOE, 1998; McKinley et al., 2001).

It is difficult to assess the spatial distribution of ^{137}Cs below the tanks, but core sampling has indicated that ^{137}Cs has moved considerable distances through the subsurface (Serne

et al., 2002a; McKinley et al., 2001). Peak concentrations of ^{137}Cs below the 241 SX-tank farm have been found at 25 to 26-m depth, with traces of ^{137}Cs up to 38 m (Serne et al., 2002a; Serne et al., 2002b). The waste tanks contain solutions of high ionic strength (> 1 mol/L), consisting, in part, of large amounts of NaOH and $NaNO_3$ (Serne et al., 1998). These high ionic strength solutions, in particular the high Na concentrations, have been shown to reduce Cs sorption to Hanford sediments (Zachara et al., 2002). Hanford sediments contain both nonexpandable (biotite, muscovite) and expandable (vermiculite, smectite) phyllosilicates. Under normal (low ionic strength) environmental conditions, phyllosilicates sorb Cs strongly and selectively (Tamura and Jacobs, 1960; Sawhney, 1970; Sawhney, 1972; Cornell, 1993). Two major types of Cs sorption have been proposed: (1) ion-exchange with hydrated cations on planar sites of expandable phyllosilicates, and (2) selective sorption to the frayed edge sites of nonexpandable phyllosilicates (micas) and interlayer sites of vermiculites (Francis and Brinkley, 1976; Cornell, 1993). Sodium at high concentrations has been found to effectively compete with Cs for planar as well as frayed edge sites (Zachara et al., 2002) and, consequently, Cs migration in sediments below the Hanford tanks has likely occurred with little retardation, at least initially, when ionic strengths of the leaking solutions were high and not yet diluted by dispersion and mixing with soil water.

The distinct sorption properties of Cs on phyllosilicates has been represented mathematically by using multiple sorption sites with different sorption characteristics. Most commonly, a two-site sorption model, one site with high affinity and one site with low affinity, for Cs sorption was used. On an empirical basis, the two sorption sites were modeled as equilibrium and kinetically-controlled reaction sites (Fukui, 1978; Fujikawa and Fukui, 1991; Comans and Hockley, 1992). This two-site equilibrium-nonequilibrium approach, in combination with a

Freundlich isotherm representing the sorption equilibrium has been applied to silica sands (Fukui, 1978), illite (Comans and Hockley, 1992), and different types of rock materials (Fujikawa and Fukui, 1991). A similar two-site (equilibrium and non-equilibrium) kinetic sorption model, but using a Langmuir instead of a Freudlich-type isotherm, was used to describe Cs sorption to silica sands in transport experiments under ionic strengths varying from 0.002 to 0.1 M (Saiers and Hornberger, 1996).

Cesium transport in natural porous media has not been studied extensively. Most transport experiments were conducted in silica sands (Fukui, 1978; Saiers and Hornberger, 1996; Sätmark et al., 1996) or glass beads (Noell et al., 1998). While these studies have shown that Cs sorption and transport can be simulated with model calculations, little effort has been devoted to the comparison of batch sorption and column transport data.

Given that large amounts of Cs, dissolved in high ionic strength solutions, have leaked from underground Hanford waste tanks, there is a need to understand Cs fate and transport in natural sediments under conditions of varying ionic strengths ranging from millimolar to molar concentrations. It was clearly demonstrated that high electrolyte concentrations reduce Cs sorption to Hanford sediments, and the competitive sorption process in electrolyte solutions varying from 0.01 to 5 mol/L $NaNO_3$, was best described with a two-site (high- and low-affinity) equilibrium ion-exchange model (Zachara et al., 2002). Based on these results it is anticipated that Cs migration in Hanford sediments has been significantly affected by the high ionic strength solutions of the Hanford waste tanks. Indeed, depth profiles of Cs obtained from cores drilled beneath the Hanford tanks have provided evidence for reduced Cs sorption (McKinley et al., 2001; Serne et al., 2002a).

The goal of this study was to investigate the influence of solution ionic strengths, i.e., Na

concentrations, on cesium migration through subsurface sediments. Our specific objectives were (1) to compare Cs sorption to the silica sand and Hanford sediments in batch and column transport experiments, and (2) to elucidate the impact of ionic strengths, i.e., Na concentrations, on Cs migration through silica sand and Hanford sediments. A non-linear two-site (equilibrium and nonequilibrium) model was used to analyze the experimental data.

2 Materials and Methods

2.1 Artificial Pore Water and Cs Analysis

To mimic the conditions under leaking Hanford tanks, artificial pore water used in our experiments was adjusted to concentrations of 1, 10, 100, and 1000 mM NaCl. The pH of the solution was buffered at pH 10 with equimolar 0.1 mM $NaHCO_3/Na_2CO_3$. The solutions were filtered through a 0.1 μm Millipore filter and degassed before use.

Cesium-133 solutions were made from $CsNO_3$ (VWR, West Chester, PA) at a concentration of 0.1 mM for the column experiments, and at various concentrations up to 0.5 mM for the batch sorption experiments. Concentrations of about 0.1 mM Cs are representative for ^{137}Cs in Hanford waste tank solutions (Serne et al., 1998). Cesium concentrations were determined with atomic emission spectrometry (AES) at a wavelength of 852.1 nm using a Varian 220 Flame Atomic Absorption Spectrometer (AAS) (Varian Ltd., Mulgrave, Australia). The detection limit for Cs was 0.38 μmol/L. To suppress ionization, both standards and samples were spiked with 2 M KCl solution to reach a final concentration of 1000 mg/L K in solution before analysis.

2.2 Silica Sand and Hanford Sediments

Two types of materials were used for the experiments: a commercially available silica sand and Hanford sediments. The silica sand (Lot Nr. L11623, J.T. Baker, Phillipsburg, NJ) was first rinsed with deionized water 12 times and decanted through a 53 μm sieve. An aliquot of the sand was further treated to remove carbonates by using 0.5 M Na-acetate and "free" iron oxides following the citrate-bicarbonate-dithionite method (Loeppert and Inskeep, 1996). The two different treatments of the silica sand are denoted as "water-washed" and "iron-removed".

Hanford sediments were obtained from the U.S. Department of Energy's Hanford Reservation (Submarine Site, 218-E-12B). The material stems from the cataclysmic events of the Missoula floods and belongs to the Hanford Formation. The sediments were taken from a trench wall in January 2000, air-dried, dry-sieved through a 2-mm square screen, and stored in five-gallon plastic buckets. The pH, measured in a 1:1 w/w water extract, was 8.0. After sieving, the particles had the following size distribution: 89% of the mass was larger than 0.5 mm and only 1% smaller than 2 μm. The sand and silt fractions were dominated by quartz, amphibole, plagioclase, K-feldspar, mica, and magnetite. Among the micas, both muscovite and biotite were common. The clay-size fraction consisted mainly of chlorite, smectite, vermiculite, kaolinite, illite, and quartz (Flury et al., 2002). Carbonate and Fe removal with the citrate-bicarbonate-dithionite method was attempted, but was not successful due to the large Fe content of the sediments.

Total content of "free" iron oxides in the "water-washed", "iron-removed" silica sand, and the Hanford sediments was determined using the citrate-bicarbonate-dithionite method (Loeppert and Inskeep, 1996) with Fe measured by atomic absorption spectrometry. The

dithionite treatment resulted in a complete removal of Fe from the silica sand. Cation exchange capacity was determined with the compulsive exchange method using Ba and Mg (Sumner and Miller, 1996). Selected properties of the porous materials used are listed in Table 1.

2.3 Batch Sorption Experiments

Batch sorption experiments were carried out in 50 ml polypropylene centrifuge tubes (Nalgene tubes, Nalge Company, Rochester, NY) containing $CsNO_3$ at concentrations ranging from 0.025 to 0.2 mM for the silica sand and from 0.025 to 0.5 mM for the Hanford sediments. The solid-to-liquid mass ratios were 1:1.7 to 1:5 for silica sand and 1:8.3 for Hanford sediments. Soild-to-liquid mass ratios were varied for the silica sand to improve analytical accuracy, and initial tests showed that the solid-to-liquid ratio did not affect the isotherm determinations. Batch experiments were carried out in 1, 10, 100, and 1000 mM NaCl background electrolyte buffered at pH 10 with equimolar 0.1 mM $NaHCO_3/Na_2CO_3$. Centrifuge tubes were sealed with Teflon-lined screw caps and agitated on a reciprocal shaker for 24 hours. Initial tests showed that sorption equilibrium was reached within much less than 24 hours. The solution was then centrifuged at 48,800 g for 20 minutes, and cesium concentrations in the supernatant were analyzed with AAS. Batch experiments were performed in triplicate and included two blank treatments, one without solids and one without Cs. Amount of Cs sorbed was calculated based on mass balance considerations. Experiments were carried out at room temperature (20 to 22°C).

2.4 Column Transport Experiments

The columns used for the transport experiments consisted of glass cylinders with 1.0-cm i.d. and 7.2-cm length, equipped with Teflon end pieces and 25 μm frits (Omnifit, Cambridge, UK). All tubing at in- and outflow was of Teflon. Flow was controlled with a peristaltic pump (Ismatec, Glattbrugg, Switzerland). Outflow was collected with a fraction collector. The media used for the column experiments, the silica sands and Hanford sediments, were filled into the columns by incrementally packing 1 cm sediment under a CO_2 atmosphere and saturating with a 1 M NaCl electrolyte solution to prevent dispersion of fine particles from the Hanford sediments. The columns were then preconditioned with 30 pore volumes of 1 M NaCl followed by 30 pore volumes of the artificial pore water with the appropriate ionic strength. By the end of the preconditioning, the pH of the effluent was consistent with the influent pH. A pulse of a conservative tracer (nitrate in form of 0.1 mM $NaNO_3$) was introduced to determine the hydrodynamics of the column system. Nitrate was analyzed using a UV/VIS Spectrophotometer (HP 8452A, Hewlett Packard) at a wavelength of 202 nm. After the NO_3^- had eluted from the columns, we introduced a pulse of Cs. In total, ten different Cs transport experiments were conducted: four in each "water-washed" and "iron-removed" silica sand (1, 10, 100, 1000 mM NaCl), and two in Hanford sediments (100 and 1000 mM NaCl); only the higher ionic strength solutions were run for the Hanford sediments because colloidal material dispersed in the pore water and eluted from the column in the 1 and 10 mM NaCl electrolyte solutions, and consequently the matrix was not stable at these ionic strengths. Experiments were carried out in duplicate at room temperature (20 to 22°C). Operating conditions and column parameters are summarized in Table 2.

3 Theory

We represent the migration of Cs through the homogeneously packed columns by the one-dimensional advection-dispersion equation (ADE)

$$\theta \frac{\partial C}{\partial t} + \rho \frac{\partial S}{\partial t} = \theta D \frac{\partial^2 C}{\partial z^2} - \theta V \frac{\partial C}{\partial z} \tag{1}$$

where C is the solution-phase concentration (flux concentration), S is the sorbed-phase concentration, t is time, z is distance, θ is the volumetric water content, ρ is the bulk density, D is the dispersion coefficient, and V is the pore water velocity. The sorption reactions of Cs can be described by a two-site (equilibrium and nonequilibrium) model, combined with an appropriate sorption isotherm model. This approach has been successfully used to describe Cs transport through silica sands using a Langmuir isotherm (Saiers and Hornberger, 1996). Based on the batch sorption data, we found a linear and non-linear Freundlich isotherm to be best suited for the concentration range in our experiments. The two-site model can then be written as (Selim et al., 1976; Rao et al., 1979)

$$S = S_1 + S_2 \tag{2}$$

$$S_1 = f K C^n \tag{3}$$

$$\frac{\partial S_2}{\partial t} = \alpha \left[(1-f) K C^n - S_2 \right] \tag{4}$$

where S_1 and S_2 are the sorbed-phase concentrations for equilibrium and non-equilibrium sorption sites, K is the sorption coefficient, n is the Freundlich exponent, f is the fraction of equilibrium sorption sites, and α is the sorption rate coefficient. Equations 1 and 2 in combination with a Dirichlet boundary condition at the top and a Neumann condition at the bottom were solved numerically with the Hydrus code (Šimůnek et al., 1998). Model parameters were either measured or obtained by non-linear least-square optimization using

the Levenberg-Marquardt algorithm. The pore water velocity V was calculated from the measured water flux as J_w/θ and the dispersion coefficient D was obtained by fitting the ADE to the conservative nitrate tracer breakthrough. We estimated the sorption parameters by least-square optimization from batch and column experiments.

The two-site model was fitted to the breakthrough data in an incremental fashion, i.e., by sequentially increasing the complexity of the model from one-site linear equilibrium sorption to two-site nonequilibrium sorption. The model performance was compared with an extra sum of squares analysis to test whether the inclusion of new model parameters led to a significant improvement of the model fit (Bates and Watts, 1988).

4 Results

4.1 Batch Sorption Experiments

Batch sorption data indicated that Cs sorption to the silica sand could be described with a linear isotherm, whereas the sorption to Hanford sediments was best described with a non-linear Freundlich isotherm (Figure 1, Table 3). The Fe-removal on the silica sand reduced the Cs sorption only slightly but significantly. Cesium sorption to the silica sand is usually weak, whereby cesium exchanges with the protons of the Si-OH groups of SiO_2. At alkaline pH, hydrous Fe-oxides have a higher Cs sorption capacity than quartz (Cornell, 1993; Ferris et al., 2000), and it consequently can be expected that Fe-coated silica sand retards the movement of Cs more as compared with Fe-removed silica sand. Cesium sorption to the silica sands was reduced by one order of magnitude when ionic strengths increased from 1 to 1000 mM.

There was considerable sorption of Cs to the Hanford sediments, and for all ionic strengths tested, the sorption isotherm was non-linear. No clear trend of the degree of

nonlinearity with regard to ionic strength was observed. The pronounced non-linearity of Cs sorption to similar Hanford sediments has also been reported by others (Zachara et al., 2002).

4.2 Column Transport Experiments

In silica sand, little or no tailing was observed at high ionic strengths (100 and 1000 mM NaCl), but pronounced tailing occurred at low ionic strength (1 and 10 mM NaCl) (Figure 2). We used the batch-derived sorption parameters in combination with a one-site equilibrium model to predict the Cs migration through the silica sands, and the results are shown as dashed lines in Figure 2. Close agreement between experimental observations and independent model predictions was obtained at 100 and 1000 mM, but not at 1 and 10 mM ionic strengths. Best model fits to the experimental data are shown as solid lines in Figure 2, and model parameters are listed in Table 4. While the one-site linear, equilibrium assumption was appropriate for 100 and 1000 mM ionic strengths, a one-site non-linear, equilibrium model was best suited for the 1 and 10 mM ionic strengths. The pronounced tailing of the experimental data at low ionic strengths, however, could not fully be reproduced by the model.

Cesium transport through Hanford sediments could only be measured at 100 and 1000 mM ionic strengths; at 1 and 10 mM NaCl artificial pore water, colloidal material was mobilized and eluted from the columns, and no stable column system could be achieved. The one-site equilibrium model predictions using the sorption parameters from the batch experiments failed to reproduce the experimental Cs breakthrough curves, at both the breakthrough and the elution portions (dashed lines in Figure 3). The least-square model optimization indicated

that the two-site, non-equilibrium model, including a non-linear sorption isotherm, was best for describing Cs breakthrough in the Hanford sediments (solid lines in Figure 3). The experimental breakthrough curves were well represented by the model. The model parameters showed that the equilibrium sorption sites comprised an equilibrium fraction f of about 0.3 at the two ionic strengths (Table 4). The sorption rate coefficient α, however, was affected by the ionic strength, with α being smaller at 1000 mM than at 100 mM ionic strength. The slower sorption rate at high ionic strength could be related to the stronger competition of Na with Cs for the non-equilibrium sorption sites. The optimized Freundlich parameters showed a one order of magnitude difference of the K-value between the two ionic strengths. Consequently, the equilibrium sorption of Cs at the maximum fluid concentration of 0.1 mM on Hanford sediments decreased by a factor of 10 with the increase of ionic strength from 100 to 1000 mM. Compared to the Hanford sediments, the impact of ionic strength on Cs sorption was less significant for both water-washed and Fe-removed silica sands, which experienced a 5- and 7-fold decrease, respectively. Another comparison can be made using the retardation of cesium relative to the speed of water. We can define an effective retardation factor using the first temporal moment of the cesium breakthrough curves (e.g., Dohse and Lion, 1994)

$$R = \frac{\int_0^\infty C(\vartheta)\vartheta \, \mathrm{d}\vartheta}{\int_0^\infty C(\vartheta) \, \mathrm{d}\vartheta} - \frac{\vartheta_p}{2} \tag{5}$$

where ϑ is the pore volume and ϑ_p is the pulse length of the cesium input. The calculated retardation at 1000 mM ($R = 31$) is about ten times less than at 100 mM ($R = 289$) (Table 3). A similar reduction in retardation was observed for the silica sand.

4.3 Comparison between Batch and Column Experiments

The batch and column derived sorption parameters for silica sand displayed fairly good agreement at high ionic strengths when the sorption isotherm was linear (Table 3, Figure 4). At high ionic strengths, batch sorption data could well predict cesium breakthrough through the silica sand. Less agreement was observed at low ionic strengths where batch data indicated a linear isotherm, but column data indicated a non-linear isotherm. The approximate shape of the cesium breakthrough curves could be predicted from the batch experiments, but the steepening of the breakthrough front and the tailing of the elution part, caused by the non-linear sorption isotherm, are not reproduced.

In contrast to the silica sand, transport of cesium in the Hanford sediments occurred under non-equilibrium conditions, so that the batch sorption data, which were obtained under equilibrium conditions, were not sufficient to predict cesium breakthroughs in the columns. While the approximate shape of the breakthrough curves could be reproduced, the early breakthrough and pronounced tailing, caused by the sorption non-equilibrium, could not be captured by the batch predictions (Figure 3).

5 Discussion

Our results indicate that Cs sorption was at equilibrium during transport through the silica sand, but not during transport through the Hanford sediments. Hanford sediments consist of various minerals, including micas and their weathering products, both of which are known to consist of high and low affinity sorption sites for Cs. These two types of sorption sites are also known to sorb Cs at different rates (Comans and Hockley, 1992). Silica sands have also been reported to possess both equilibrium and non-equilibrium sorption sites during transport

of Cs (Fukui, 1978; Saiers and Hornberger, 1996); however, the mechanistic interpretation of the non-equilibrium sorption in silica sand is less straightforward than for phyllosilicates. Variations in surface composition and differences between smooth and rough surfaces on silica grains have been considered to cause different sorption rates (Saiers and Hornberger, 1996). There are, however, large differences in Cs sorption properties between different silica sands, and for the cases reported by Fukui (1978) and Saiers and Hornberger (1996), Cs sorbed much stronger to their sands compared to ours. The lack of non-equilibrium found in our experiments is likely due to the small Cs sorption affinity of our silica sand. The maximal amount of Cs sorbed to the silica sand in the column experiments was about two orders of magnitude smaller than the CEC of the sand.

In our experiments, we used a higher flow rate for the Cs transport in the Hanford sediments than in the silica sand, which could induce the observed non-equilibrium in the Hanford sediments. We repeated some of the silica sand experiments with the same flow rates as used in the Hanford sediments and did not see a difference in the Cs breakthrough curves (data not shown). Even at the higher flow rates, Cs transport through the silica sand remained at equilibrium. In contrast, Cs transport in the Hanford sediments was strongly affected by sorption non-equilibria. Consequently, batch sorption parameters determined under equilibrium conditions could not accurately reproduce Cs breakthrough curves in the column experiments. Effective retardation of Cs transport in Hanford sediments was reduced by a factor of 10 when the ionic strength increased from 100 to 1000 mM, clearly demonstrating the important effect of Na competition for Cs transport under Hanford tank leaking conditions.

Acknowledgements

This work was supported by the Environmental Management Science Program, U.S. Department of Energy under contract DE-FG07-99ER62882, Project Officers Drs. Frank Wobber and Chester Miller. We thank Jeff Boyle and Jon Mathison (Washington State University, WSU) for their help with cesium measurements, the Electron Microscopy Center at WSU for use of their facility, John Zachara and Jeff Serne (Pacific Northwest National Laboratory) for providing us with the Hanford sediments.

References

Bates, D. M. and Watts, D. G., 1988. Nonlinear Regression Analysis and its Applications. John Wiley & Sons, New York.

Comans, R. N. J. and Hockley, D. E., 1992. Kinetics of cesium sorption on illite. Geochim. Cosmochim. Acta, 56: 1157–1164.

Cornell, R. M., 1993. Adsorption of cesium on minerals: a review. J. Radioanal. Nuclear Chem., 171: 483–500.

Dohse, D. M. and Lion, L. W., 1994. Effect of microbial polymers on the sorption and transport of phenanthrene in a low-carbon sand. Environ. Sci. Technol., 28: 541–548.

Ferris, F. G., Hallberg, R. O., Lyvén, B. and Pedersen, K., 2000. Retention of strontium, cesium, lead, and uranium by bacterial iron oxides from a subterranean environment. Appl. Geochem., 15: 1035–1042.

Flury, M., Mathison, J. B. and Harsh, J. B., 2002. *In situ* mobilization of colloids and transport of cesium in Hanford sediments. Environ. Sci. Technol., p. (submitted).

Francis, C. W. and Brinkley, F. S., 1976. Preferential adsorption of ^{137}Cs to micaceous minerals in contaminated freshwater sediments. Nature, 260: 511–513.

Fujikawa, Y. and Fukui, M., 1991. Analysis of radioactive cesium and cobalt adsorption to rocks using the two-site kinetic model equations. J. Contam. Hydrol., 8: 43–69.

Fukui, M., 1978. Evaluation of a combined sorption model for describing cesium transport in a soil. Health Phys., 35: 555–562.

Gephart, R. E. and Lundgren, R. E., 1998. Hanford Tank Cleanup: A Guide to Understanding the Technical Issues. 4th edn. Battelle Press, Columbus.

Loeppert, R. H. and Inskeep, W. P., 1996. Iron. In: D. L. Sparks (Editor), Methods of Soil Analysis. Part 3. Chemical Methods. American Society of Agronomy, Madison, Wisconsin, pp. 639–664.

McKinley, J. P., Zeissler, C. J., Zachara, J. M., Serne, R. J., Lindstrom, R. M., Schaef, H. T. and Orr, R. D., 2001. Distribution and retention of Cs-137 in sediments at the Hanford Site, Washington. Environ. Sci. Technol., 35: 3433–3441.

Noell, A. L., Thompson, J. L., Corapgioglu, M. Y. and Triay, I. R., 1998. Evaluation of a combined sorption model for describing cesium transport in a soil. J. Contam. Hydrol., 31: 23–56.

Rao, P. S. C., Davidson, J. M., Jessup, R. E. and Selim, H. M., 1979. Evaluation of conceptual models for describing nonequilibrium adsorption-desorption of pesticides during steady-flow in soils. Soil Sci. Soc. Am. J., 43: 22–28.

Saiers, J. E. and Hornberger, G. M., 1996. Migration of ^{137}Cs quartz sand: experimental results and modeling approaches. J. Contam. Hydrol., 22: 255–270.

Sätmark, B., Albinsson, Y. and Liang, L., 1996. Chemical effects of goethite colloid on the transport of radionuclides through a quartz-packed column. J. Contam. Hydrol., 21: 231–241.

Sawhney, B. L., 1970. Potassium and cesium ion selectivity in relation to clay mineral structure. Clays Clay Miner., 18: 47–52.

Sawhney, B. L., 1972. Selective sorption and fixation of cations by clay minerals. Clays Clay Miner., 20: 93–100.

Selim, H. M., Davidson, J. M. and Mansell, R. S., 1976. Evaluation of a two-site adsorption-desorption model for describing solute transport in soils. Summer Computer Simulation Conference, Washington DC. Simulation Councils, Inc., La Jolla, CA, pp. 444–448.

Serne, R. J., Clayton, R. E., Kutnyakov, I. V., Last, G. V., LeGore, V. L., Wilson, T. C., Schaef, H. T., O'Hara, M. J., Wagnon, K. B., Lanigan, D. C., Brown, C. F., Williams, B. A., Lindenmeier, C. W., Orr, R. D., Burke, D. S. and Ainsworth, C. C., 2002a. Characterization of Vadose Zone Sediment: Borehole 41-09-39 in the S-SX Waste Management Area. Pacific Northwest National Laboratory, US Department of Energy, PNNL-13757-3, Richland, Washington.

Serne, R. J., Clayton, R. E., Kutnyakov, I. V., Last, G. V., LeGore, V. L., Wilson, T. C., Schaef, H. T., O'Hara, M. J., Wagnon, K. B., Lanigan, D. C., Brown, C. F., Williams, B. A., Lindenmeier, C. W., Orr, R. D., Burke, D. S. and Ainsworth, C. C., 2002b. Characterization of Vadose Zone Sediment: Slant Borehole SX-108 in the S-SX Waste Management Area. Pacific Northwest National Laboratory, US Department of Energy, PNNL-13757-4, Richland, Washington.

Serne, R. J., Zachara, J. M. and Burke, D. S., 1998. Chemical Information on Tank Supernatants, Cs Adsorption from Tank Liquids onto Hanford Sediments, and Field Observations of Cs Migration from Past Tank Leaks. Pacific Northwest National Laboratory, PNNL-11495/UC-510, Richland, WA.

Sumner, M. E. and Miller, W. P., 1996. Cation exchange capacity and exchange coeffi-

cients. In: D. L. Sparks (Editor), Methods of Soil Analysis. Part 3. Chemical Methods. American Society of Agronomy, Madison, Wisconsin, pp. 1201–1229.

Tamura, T. and Jacobs, D. G., 1960. Structural implication in cesium sorption. Health Phys., 2: 391–398.

U.S. DOE, 1998. Groundwater/Vadose Zone Integration Project Specification. DOE/RL-98-48, Draft C, United States Department of Energy, Richland, WA.

Šimůnek, J., Šejna, M. and van Genuchten, M. T., 1998. The HYDRUS-1D Software Package for Simulating the One-Dimensional Movement of Water, Heat and Multiple Solutes in Variably-Saturated Media. U.S. Salinity Laboratory, Agricultural Research Service, U.S. Department of Agriculture, Riverside, CA.

Zachara, J., Smith, S. C., Liu, C., McKinley, J. P., Serne, R. J. and Gassman, P. L., 2002. Sorption of Cs^+ to micaceous subsurface sediments from the Hanford Site, USA. Geochim. Cosmochim. Acta, 66: 193–211.

Table 1. Selected Properties of Porous Materials.

Material	Particle Size Distribution (% mass)			Median Diameter	"Free" Fe	CEC
	$< 2\mu$m	$2 - 50\mu$m	$50 - 2000\mu$m	(μm)	(mg/kg)	(mmol$_c$/kg)
Water-washed silica sand	0	0	100	704	27.3	12.38
Fe-removed silica sand	0	0	100	704	0	11.88
Hanford sediments	1	3.8	95.2	1369	2307.6	21.58

Table 2. Column Parameters and Operating Conditions.

Parameters	Silica sand[a]	Hanford sediment
Length and diameter (cm)	$L = 7.2$, i.d. $= 1.0$	L = 7.2, i.d. = 1.0
Bulk density (g/cm^3)	1.70	1.54
Saturated water content (cm^3/ cm^3)	0.37	0.45
Pore volume (cm^3)	2.09	2.54
Flow rate Q (cm^3/hr)	11.8	22.74
Water flux J (cm/hr)	15.02	28.95
Pore water velocity V (cm/hr)	40.6	64.33
Temperature (°C)	20–22	20–22
Eluent Solutions		
- pH buffer	0.1 mM $NaHCO_3/Na_2CO_3$, pH 10	0.1 mM $NaHCO_3/Na_2CO_3$, pH 10
- Ionic strength	1, 10, 100 and 1000 mM NaCl	100 and 1000 mM NaCl
Column Peclet numbers[b] ($Pe = VL/D$)	30.3 (water-washed)	12.63
	21.2 (iron-removed)	

[a] Operating conditions were the same for "water-washed" and "iron-removed" silica sand, except when noted.

[b] Peclet numbers determined from nitrate breakthrough curves (V: pore water velocity, L: column length, D: hydrodynamic dispersion coefficient).

Table 3. Comparison between batch and column sorption parameters and effective retardation factors.

Ionic Strength	Batch		Column		Retardation Factor[a]
	K (mL/g)	n	K (mL/g)	n	R (–)
Water-Washed Silica Sand					
1 mM	0.951±016[b]	1.0	0.359±0.012	0.69±0.02	5.0
10 mM	0.550±0.014	1.0	0.260±0.010	0.71±0.01	2.9
100 mM	0.274±0.020	1.0	0.308±0.018	1.0	1.7
1000 mM	0.098±0.004	1.0	0.061±0.010	1.0	0.6
Fe-Removed Silica Sand					
1 mM	0.798±0.014	1.0	0.440±0.018	0.72±0.02	5.0
10 mM	0.400±0.009	1.0	0.368±0.014	0.95±0.01	2.2
100 mM	0.175±0.014	1.0	0.201±0.086	1.0	0.8
1000 mM	0.070±0.002	1.0	0.028±0.031	1.0	0.6
Hanford Sediments					
1 mM	18.04±1.47	0.418±0.025	na[c]	na	na
10 mM	26.30±1.85	0.714±0.035	na	na	na
100 mM	11.07±0.31	0.693±0.019	31.71±1.02	0.81±0.015	289
1000 mM	3.093±0.341	0.759±0.047	3.14±0.042	0.76±0.001	31

[a] Retardation factors calculated from experimental breakthrough curves with equation 5.

[b] Values after the ±-signs represent one standard error. Values without standard errors were not fitted.

[c] na: not applicable.

Table 4. Parameters of linear equilibrium and non-linear equilibrium transport models.

Ionic Strength	K (mL/g)	n	f	α (1/hr)	SSQ[a] ($\times 10^{-1}$)
		Water-Washed Silica Sand			
1 mM	0.359±0.012[b]	0.69±0.02	na[c]	na	0.23
10 mM	0.260±0.010	0.71±0.01	na	na	0.19
100 mM	0.308±0.018	na	na	na	0.51
1000 mM	0.061±0.010	na	na	na	0.24
		Fe-Removed Silica Sand			
1 mM	0.440±0.018	0.72±0.02	na	na	0.19
10 mM	0.368±0.014	0.95±0.01	na	na	0.25
100 mM	0.201±0.086	na	na	na	0.12
1000 mM	0.028±0.031	na	na	na	0.27
		Hanford Sediments			
100 mM	31.71±1.02	0.81±0.015	0.339±0.023	0.163±0.011	0.02
1000 mM	3.14±0.042	0.76±0.001	0.324±0.001	0.115±0.001	0.43

[a] SSQ: sum of squares.

[b] Values after the ±-signs represent one standard error.

[c] na: not applicable.

Figures

Figure 1. Cesium sorption isotherms obtained from batch experiments for water-washed silica sand, Fe-removed silica sand, and Hanford sediments. Vertical bars represent ± one standard deviation. Solid lines are fitted linear (silica sand) and non-linear (Hanford sediments) isotherms.

Figure 2. Cesium breakthrough curves in (a) water-washed and (b) Fe-removed silica sand for different ionic strength NaCl solutions. Lines represent model calculations: dashed line is model prediction based on batch isotherm data, solid line is best model fit.

Figure 3. Cesium breakthrough curves in Hanford sediments for different ionic strength NaCl solutions. Lines represent model calculations: dashed line is model prediction based on batch isotherm data, solid line is best model fit.

Figure 4. Comparison of sorption coefficients in silica sand determined from batch sorption and column transport experiments at 100 and 1000 mM ionic strength. Vertical bars represent ± one standard error.

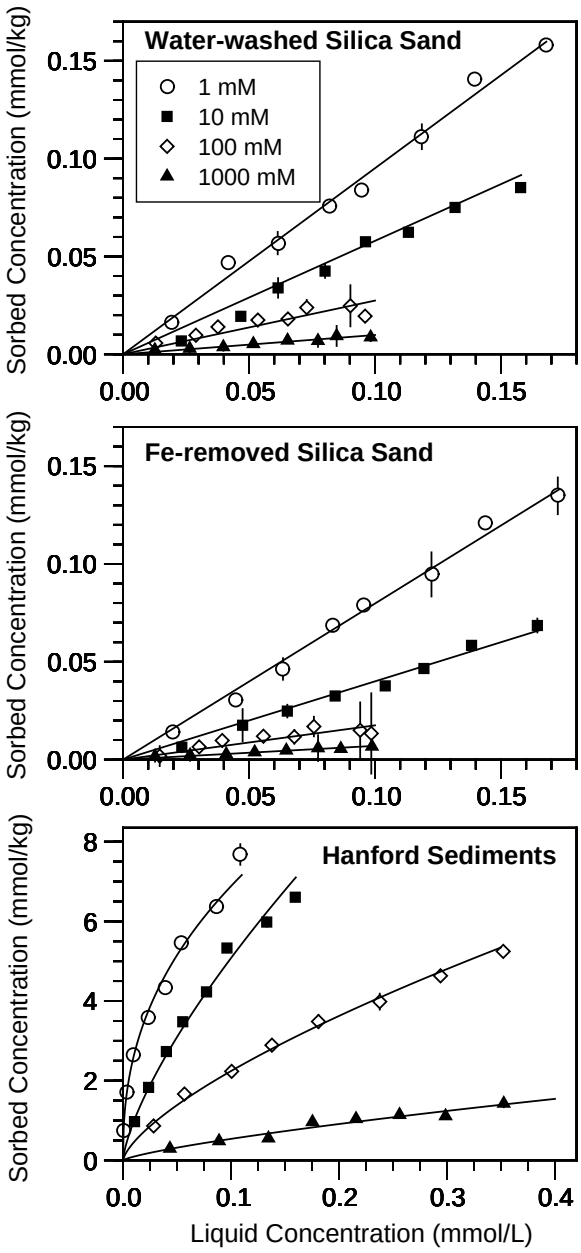

Fig. 1. Cesium sorption isotherms obtained from batch experiments for water-washed silica sand, Fe-removed silica sand, and Hanford sediments. Vertical bars represent ± one standard deviation. Solid lines are fitted linear (silica sand) and non-linear (Hanford sediments) isotherms.

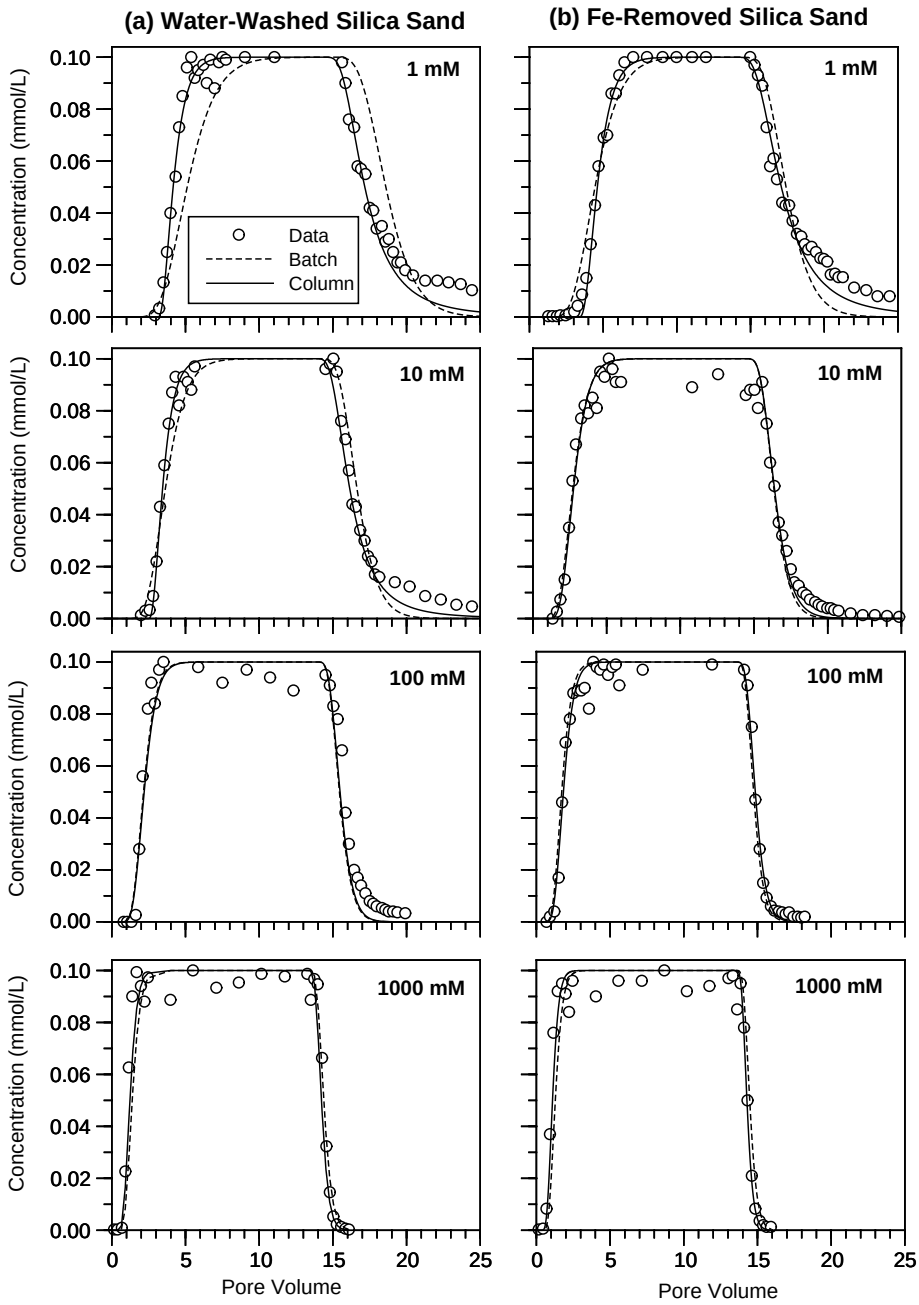

Fig. 2. Cesium breakthrough curves in (a) water-washed and (b) Fe-removed silica sand for different ionic strength NaCl solutions. Lines represent model calculations: dashed line is model prediction based on batch isotherm data, solid line is best model fit.

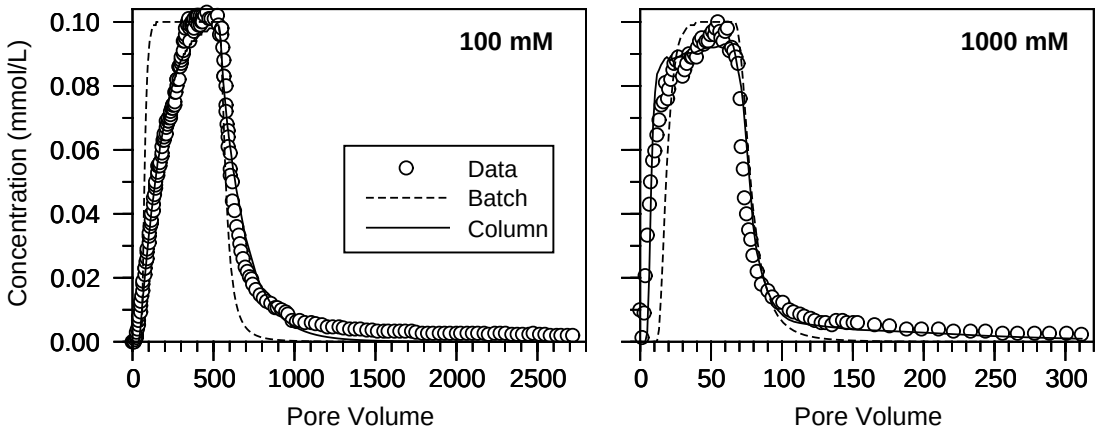

Fig. 3. Cesium breakthrough curves in Hanford sediments for different ionic strength NaCl solutions. Lines represent model calculations: dashed line is model prediction based on batch isotherm data, solid line is best model fit.

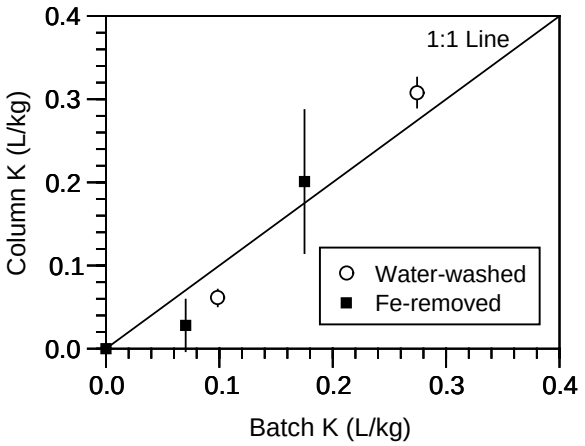

Fig. 4. Comparison of sorption coefficients in silica sand determined from batch sorption and column transport experiments at 100 and 1000 mM ionic strength. Vertical bars represent ± one standard error.

Colloid Formation in Hanford Sediments Reacted with Simulated Tank Waste

Kholoud Mashal[1], James B. Harsh[1], Markus Flury[1] and Andrew R. Felmy[2]

[1]*Department of Crop and Soil Sciences, Center for Multiphase Environmental Research, Washington State University, Pullman, WA 99164-6420*

[2]*Pacific Northwest National Laboratory, Richland, WA 99352*

*Corresponding author:

Markus Flury

Department of Crop and Soil Sciences

Washington State University

Pullman, WA 99164-6420

Phone: 1-509-335-1719

Fax: 1-509-335-8674

E-mail: flury@mail.wsu.edu

Solutions of high pH, ionic strength, and aluminum concentration have leaked into the subsurface from underground waste storage tanks at the Hanford Reservation in Washington State. Here, we test the hypothesis that these waste solutions alter and dissolve the native minerals present in the sediments, and that colloidal (diameter < 2 μm) feldspathoids form. We reacted Hanford sediments with solutions representative of Hanford waste tanks. The solutions consisted of 1.4 or 2.8 mol/kg NaOH, 0.125 or 0.25 mol/kg $NaAlO_4$ and 3.7 mol/kg $NaNO_3$ and were contacted with the sediments for a period of 25 or 40 days at 50°C. The colloidal size fraction was separated from the sediments and characterized in terms of mineralogy, morphology, chemical composition, and electrophoretic mobility. Upon reaction with tank waste solutions, native minerals released Si and other elements into the solution phase. This Si precipitated with the Al present in the waste solutions to form secondary minerals, identified as the feldspathoids cancrinite and sodalite. The solution phase was modeled with GMIN for solution speciation and saturation indices with respect to sodalite and cancrinite. The amount of colloidal material in the sediments increased upon reaction with waste solutions. At the natural pH found in Hanford sediments (pH 8) the newly-formed minerals are negatively charged, similar to the unreacted colloidal material present in the sediments. The formation of colloidal material in Hanford sediments upon reaction with tank waste solutions is an important aspect to consider in the characterization of Hanford tank leaks, and may affect fate and transport of hazardous radionuclides present in the tank waste.

Introduction

Hazardous waste containing radionuclides, such as ^{137}Cs and ^{90}Sr, stored in the underground tanks at the Hanford site (Washington State, USA) has leaked into the vadose zone. Hanford

tank waste consists of supernatant liquids, slurries, sludges, and salt cakes (*1*). It is estimated that more than a million gallons of supernatant fluids have leaked into the subsurface, containing, at the time when the leaks occurred, 3.7×10^{16} to 7.4×10^{16} Bq (1 to 2 million Ci) of radiation, mainly from ^{137}Cs (*1*). The radioactive cesium is currently located in the vadose zone below the tanks with the majority of the activity concentrated between 20.1 and 25.6 m below ground surface with a leading edge perhaps reaching 40 m (*2, 3*). It is likely that Cs has moved to the observed depths by chromatographic transport within a high ionic strength liquor (*4, 5, 6*).

The composition of the tank waste at Hanford varies considerably, and there is large uncertainty about concentrations and composition, but in general the supernatants show high pH, high aluminate concentrations, and high ionic strength, mainly contributed by NaOH, $NaNO_3$, and $NaNO_2$ (*7*). In some of the tanks, like the SX-108 and SX-109 tanks, it is estimated that concentrations of NaOH, $NaNO_3$, and $NaNO_2$ can reach 5 molar or higher (*7, 8*). When such concentrated liquors contact subsurface sediments, natural minerals are partially dissolved by the high alkaline waste solutions. Most Al and Si oxides show elevated solubility under high pH conditions; for instance, the solubility of silica compounds above pH 12.8 is greater than 0.1 mol/L (*9*). Dissolution rates of many aluminosilicates above pH 12 are similar to those below pH 3 (*9*).

At Hanford, leaking waste solutions are released to the sediments of the Hanford formation. These sediments are cataclysmic flood deposits, and contain various mineral phases, including unstable primary minerals (e.g., feldspars and micas), and stable minerals (e.g., quartz, aluminosilicate clays, and sesquioxides) (*2*). Preliminary studies showed that considerable amounts of Si and Al are released from mineral phases when Hanford sediments were

contacted with high pH solutions consisting of 1 M NaOH (*10*). As concentrations of Si and Al in the solution phase increase, secondary mineral phases can precipitate.

Different types of minerals may form under the conditions of extreme pH, ionic strength, and aluminum concentration as found at a Hanford leak situation. It is likely that amorphous and poorly-crystalline aluminosilicates will form rapidly. As pH increases beyond mildly alkaline conditions, certain minerals, such as montmorillonite, are no longer stable and are transformed to tectosilicates, such as zeolites (*11*). Other minerals, such as kaolinite, have been found to transform to feldspathoids, i.e., sodalite and cancrinite, when reacted with NaOH at temperatures of 80 to 140°C (*11*). From studies involving the Bayer process, where liquors of high NaOH concentration are reacted with bauxite ores, it has been reported that at high aqueous SiO_2 concentrations the mineral transformations follow a specific sequence, ie., amorphous aluminosilicates $\rightarrow$ zeolite (Linde A) $\rightarrow$ sodalite $\rightarrow$ cancrinite (*12*). In experiments representing Hanford site conditions, where quartz was reacted with caustic $NaNO_3$ solutions containing dissolved Al, nitrate cancrinite precipitated on the quartz surface (*13*), and in an experiment with kaolinite, neo-formation of the zeolite chabazite and the feldspathoids cancrinite and sodalite was observed (*14*).

Based on these studies of mineral transformations, we expect that, under conditions of a Hanford tank leak, native primary and secondary minerals will dissolve and transform to feldspathoid- and zeolite-type minerals. These newly formed minerals have a negative charge under alkaline conditions, and contain both cations and anions in their framework. Consequently, contaminant cations present in the tank supernatants, such as ^{137}Cs can adsorb to or co-precipitate with them. If the new minerals occur in the colloidal size fraction, then there exists the possibility for colloid-facilitated transport of ^{137}Cs in the Hanford vadose

zone.

We hypothesize that the elevated hydroxide concentrations of leaking Hanford tank waste cause native minerals to dissolve, thereby releasing Si from the mineral lattices. The increased Si concentrations, together with high Al concentrations originating from the tank waste itself, will lead to the precipitation of feldspathoid- and zeolite-type minerals, which are in the colloidal size fraction (operationally defined in this work as < 2 μm in diameter). Based on this hypothesis, the objectives of this work were to (1) determine the chemical, physical, and mineralogical characteristics of colloids formed by reacting Hanford sediments with simulated tank waste, and (2) determine how colloid formation changes with tank waste composition.

Materials and Methods

Sediments and Sediment Characterization. Sediments used in this study were collected from the submarine pit (218-E-12B) at the Hanford site in January 2000. These sediments are representative, both in texture and mineralogy, of the material underlying the immediate vicinity of the S-SX (single-shell) tank farm at Hanford (personal communication, Bruce N. Bjornstad, September 2001, Pacific Northwest National Laboratories, Richland, WA). Detailed characterization data are given elsewhere (*15*). The sediments collected were uncontaminated and consisted of pebbly coarse sand belonging to the Hanford Formation. The sediments were air dried and sieved through a 2 mm square screen. The sieved sediments were characterized in terms of pH (in 1:1 w/w water extract), organic carbon, EC, "free" Fe, cation exchange capacity, and particle size distribution. Particle size distribution was analyzed by wet sieving and static light-scattering with a Helium-Neon laser of 633 nm wavelength and reverse Fourier optics (MasterSizer S, Malvern Instruments Ltd., Malvern,

UK). For particle size analysis, organic matter and calcium carbonate were removed with 30% w/w H_2O_2 and 0.5 M Na-acetate. The mineralogy of the sand and silt fraction of the sediments was determined by preparing thin-sections and examination with a petrographic microscope (*16*). The colloidal fraction (diameter $< 2\ \mu$m) of the sediments was characterized for a series of properties as described below.

Simulated Tank Waste Solutions. As there exists considerable uncertainty about, and variability in, the composition of Hanford tank waste (*7, 10*), we used four different simulated tank waste (STW) solutions (Table 1). The solutions were prepared by incrementally dissolving various salts in deionized water, and the final solutions differed in NaOH and Al concentrations while NO_3 concentration was kept constant (Table 1). The composition of the STW solutions was chosen to represent conditions found in the Hanford waste tanks (*7*). The waste solutions were always freshly prepared for each batch reaction experiment. Table 1

Batch Reaction Experiments. We reacted the Hanford sediments with the STW solutions in a series of batch experiments. One kilogram of sediment ($<$ 2 mm) and 1 L of STW (STW1, STW2, STW3, STW4) were placed into air-tight capped 2 L polyethylene bottles. Temperature was controlled at 50°C by an electric oven and the reaction times were 25 and 40 days. Bottles were shaken by hand in an orbital motion once a day. The control treatment consisted of sediments with distilled water only.

A temperature of 50°C was chosen based on ambient temperatures measured below Hanford waste tanks (*17*). Model simulations indicate that temperatures below SX-108 waste tanks at the time of leaks ranged from 30 up to 100°C (*18*). Measured temperatures below the SX-108 waste tank in August 2000 were reported to be up to 55°C and possibly even higher (*17*). The reaction times of 25 and 40 days were chosen based on the results of a

preliminary study (data not shown), which showed that Si dissolution increased for the first 25 days of reaction time, and then decreased, indicating both dissolution and precipitation processes.

After the specified time periods, sediments and liquids were transferred to polyethylene centrifuge bottles and centrifuged at 27,140 rgf for 60 minutes. The supernatant solution was decanted and stored at room temperature in polypropylene bottles sealed with a screw cap. The solid materials were washed with deionized water and centrifuged as specified above. This washing procedure was repeated four times. Solids were then transferred into a polyethylene graduated cylinder, dispersed in deionized water by sonication, and the fraction with diameter < 2 μm was separated by gravity sedimentation. The fraction < 2 μm was dialyzed with deionized water until the electrical conductivity of the dialysate fell below 0.01 dS/m. The dialyzed colloidal material, suspended in the dialysis solution, was stored in polyethylene bottles. An aliquot of the suspension was air-dried to determine colloid yield.

Solution Characterization. We measured Al, Si, Fe, K, Ca, Mg in the supernatant solution by ICP-AES (Thermo Jarrell Ash IRIS ICP-AES), and Na by atomic absorption spectroscopy (Varian 220 Flame Atomic Absorption Spectrometer, Varian Ltd., Mulgrave, Australia). The pH and CO_3 were determined by titration. Nitrate was measured with an ion-selective electrode. An aliquot of the supernatant was titrated with 0.53 M HCl to pH 8 and aged for one week. The precipiated solids were dried at 105°C for 24 hrs and weighed to measure solid yield.

Colloid Characterization. The colloidal fraction (diameter < 2 μm) was characterized in terms of mineralogy, morphology, and surface characteristics. Mineralogy was determined by X-ray diffraction (XRD) with Cu-Kα radiation (Philips XRG 3100, Philips Analytical

Inc., Mahwah NJ) with scanning rates of 0.02 degrees 2-θ/sec. The scans were collected using Datascan and processed with Jade (Materials Data, Inc.). The samples for XRD analysis were prepared by placing a small amount of colloidal material, suspended in deionized water, on a glass XRD slide, and letting the water evaporate at room temperature. We obtained FTIR spectra using KBr pellets (1% w/w) and a Perkin Elmer 2000 IR spectrometer. The analyses were carried out in transmission mode between 400 and 4000 cm^{-1}. The resolution was 1.0 cm^{-1} with 64 scans. We measured ^{29}Si and ^{27}Al-NMR at 119.217 and 156.375 MHz, respectively, with an Avance 600 spectrometer at 14.09 Tesla. For ^{29}Si-NMR measurements, pulse duration was 5.8 μs, pulse delay was 10.0 s and spinning rate was 15 kHz. For ^{27}Al-NMR pulse duration was 0.75 μs, pulse delay was 6.0 s and spinning rate was 35 kHz. Chemical shifts of ^{29}Si and ^{27}Al nuclei were measured relative to the standard samples of tetramethylsilane and $Al(NO_3)_3$, respectively. For scanning electron microscopy (SEM), the samples were diluted with deionized water, sonicated for one hour, and a drop of suspension was placed on aluminum or carbon stubs. After air-drying, the samples were sputter-coated with gold or carbon and examined with an SEM Hitachi S-570. Carbon-coated samples were used for energy dispersive X-ray analysis (EDAX) with a Kevex Micro-X7000 unit coupled with SEM. Electrophoretic mobilities were determined by dynamic light scattering using a ZetaSizer 3000 HSA with a Helium-Neon laser of 633-nm wavelength (Malvern Instruments Ltd., Malvern, UK) in a background electrolyte concentration of 1 mM $NaNO_3$ and a particle concentrations of about 50 mg/L. The pH of the suspensions was adjusted between pH 4 and 11 with HNO_3 or NaOH. After pH adjustment, the solutions were gently agitated on a reciprocal shaker overnight. A final pH reading was taken immediately prior to the electrophoretic mobility measurement.

Thermodynamic Modeling. The GMIN chemical equilibrium model (*19*) was used in this study to predict the aqueous species and solid phases of Al and Si in equilibrium with the supernatant solutions after reactions with the sediments. GMIN is based upon the aqueous thermodynamic model of Pitzer and coworkers and is valid to high ionic strength. The Pitzer ion-interaction parameters in the GMIN data base for aluminate ($Al(OH)_4^-$) are from Wesolowski (*20*) and for monomeric and polymeric silica species from Felmy et al. (*21*). The equilibrium constants for dissolution of sodalite (*22*) and two different crystalline phases of nitrate-cancrinite (*13*) were added to the thermodynamic database. The equilibrium constants calculated for the nitrate-cancrinite phases were determined only at one temperature (i.e. 89°C) and since no information was available to correct these results to other temperatures, the 89°C values were used for all temperatures.

Results and Discussion

Sediment and Supernatant Characterization. Unreacted sieved sediments were very coarse, consisting mainly of material between 50 and 2000 μm. Selected properties of the sediments are shown in Table 2. Table 2

After 40 days reaction time with STW1, STW2, STW3, and STW4, the Al concentration in the supernatant solution was lower than its initial concentration in the simulated tank solution (Figure 1). Only a small fraction (up to 2%) of the Al added to the solution remained in the supernatant. The fraction of Al remaining in solution was higher for the low initial Al concentrations (STW1 and STW2) than for the high initial Al concentrations (STW3 and STW4). A considerable amount of Si was released from the sediments (Figure 1). High NaOH concentrations produced higher Si concentrations after 40 days. The pH dropped

consistently relative to the initial pH, indicating the consumption of OH during dissolution of the minerals. The high pH treatments (STW2, STW4) resulted in a greater pH decrease, corresponding to the high dissolved Si concentration in the solution. The control solution (Hanford sediments reacted with deionized water, pH 7.1) had insignificant amounts of soluble Si in solution (0.001 mol/kg) and Al (0 mol/kg). The pH of the solution increased from pH 7.1 to 7.85 after 40 days, indicating a small amount H^+ consumption in these samples. Figure 1

The composition of the solution after 40 days reflects the initial composition, OH attack of the sediment minerals, and precipitation of secondary phases (Table 3). Sodium and NO_3 concentrations have been reduced as a result of the formation of cancrinite and sodalite, each of which contain these ions in their framework. Potassium and Fe are released from dissolution of native mineral sediments, including feldspars, micas, and magnetite (Table 2). Table 3

Colloid Formation and Characterization. After treatment of the sediments with simulated tank wastes, the mass of colloidal particles in the sediments increased considerably (Figure 2a), indicating formation of secondary solids in the colloidal size range. In addition, the supernatant solution contained high amounts of dissolved silica, which upon titration to pH 8, precipitated as colloidal silica gel (Figure 2b), as confirmed by EDAX. The high amount of Si remaining in solution while most Al was precipitated (Figure 1a,b) indicates that Al was limiting colloid formation. Colloid yield from precipitating soluble material (mostly Si) from the supernatant solution at pH 8, was consistent with an Al limiting reaction. More Si was available for precipitation as gel at the higher NaOH concentrations (STW2 vs STW1 and STW4 vs STW3), but was lowered by increasing Al concentration (STW3 vs STW1 and STW4 vs STW2) (Figure 2b). Figure 2

The X-ray diffraction pattern of the untreated Hanford sediments indicates that the < 2

μm fraction consisted of four major layered aluminosilicates, chlorite, smectite, kaolinite and illite, and primary minerals, including quartz, christobalite, albite, and microcline (Figure 3). Upon reaction with STW, the diffraction peaks of the aluminosilicate clays became less pronounced, indicating alteration or dissolution of the clays. Under the high pH treatments (STW 2 and 4), chlorite, smectite, and kaolinite peaks almost disappeared. Illite appeared to be more resistant against STW treatment than the other aluminosilicate clays. The illite peak is stronger than the kaolinite, smectite and chlorite peaks at the higher NaOH and Al concentrations. The quartz peak declined relative to the illite peak, indicating that colloidal quartz along with the aluminosilicate clays, was a significant source of Si in the sediments. It is also apparent that the high NaOH and low Al treatment of STW2 led to a large poorly crystalline component. Secondary minerals were formed upon reaction with STW, and were identified as nitrate-cancrinite and sodalite, both feldspathoids. Nitrate-cancrinite dominated the diffraction patterns for all STW treatments, indicating an abundance of this mineral. Sodalite was present, but less abundant than cancrinite, as evidenced by the small peak at 20° 2θ, which is representative of sodalite alone. Figure 3

The FTIR spectra corroborate the results from the XRD patterns. The unreacted sediments exhibit vibrational spectra typical of the same aluminosilicate and primary minerals indicated by XRD, namely kaolinite, smectite, chlorite, illite, quartz, and feldspars (Figure 4). We recognize the sharp OH doublet of kaolinite at 3696 and 3620 cm^{-1}. The absorption bands at 829 and 758 cm^{-1} and the slight broadening under the 3620 cm^{-1} band are indicative of illite, kaolinite, and smectite. The OH-stretching at 3425 cm^{-1} and the absorbance at 758 cm^{-1} are indicative of chlorite. The Al-OH stretching frequency band at 3620 cm^{-1} and the deformation band at 914 cm^{-1} are characteristic of dioctahedral smectites (*23*). The

1163, 1081, 798, 779, and 695 cm^{-1} bands indicate the presence of quartz. Albite can be identified at 531 and 470 cm^{-1} and microcline at 583 and 431 cm^{-1}. Figure 4

The spectra of the reacted sediments provide evidence for the alteration of pre-existing clay minerals and the formation of new minerals. The characteristic peaks for the pre-existing aluminosilicates became less pronounced in some regions. The disappearance of the band at 914 cm^{-1} indicates that significant aluminum has been removed from octahedral environments. We also notice a decrease in intensity of the quartz bands and the appearance of new absorption bands. Strong peaks occurred at 682, 620, 573, 501, 463, and 430 cm^{-1}, which are characteristic for nitrate-cancrinite (*24, 25, 26*). There is evidence for the enclathration of nitrate groups in the cancrinite regardless of the STW composition. The peak at 1421 cm^{-1} is interpreted as NO_3^- inside the cancrinite structure, while the peak at 1382 cm^{-1} is attributed to small amounts of precipitated $NaNO_3$ on the outer surface of the crystal (*26*). These two peaks became sharper going from STW 1 to 4. The broad asymmetric Al-O-Si stretch at 1081 and 1011 cm^{-1} for the unreacted sediments shifted to 1032 and 993 cm^{-1}, consistent with the formation of feldspathoids (*27, 28*), at the expense of quartz (1081 cm^{-1}) and layer aluminosilicate clays (1011 cm^{-1}).

The ^{29}Si NMR-spectra of unreacted Hanford sediments show a main resonance at -91.8 ppm corresponding to the signal of Si nuclei in the Q^3 polymerization state (*29*). The Q^n notation represents the number of bridging oxygen per Si tetrahedron. This chemical shift is close to what is found in kaolinite and illite (*30*). The ^{29}Si NMR-spectra of the reacted Hanford sediments show a single resonance line at -87.29 ppm, which can be assigned to the Q^4 Si(4Al) of nitrate cancrinite (*26*) and nitrate sodalite (*31*). The ^{27}Al NMR-spectra of untreated Hanford sediments consisted of two intense peaks having chemical shifts of 59.68

and 4.1 ppm and a minor peak at 70.61 ppm, representing four- and six-coordinated Al, respectively (*29*). The ^{27}Al NMR-spectra of the treated Hanford sediments show that most of the Al is in tetrahedral coordination with oxygen, corroborating the structural information from ^{29}Si spectra. There was only a weak peak at 4.1 ppm, which was probably due to the remaining illite seen in the XRD patterns.

The electron micrograph of the untreated sample (colloid 0) shows the distinct morphology of the clay minerals present (Figure 5). Kaolinite, illite, and chlorite are platy in morphology, and the hexagonal structures are likely kaolinites, whereas the veil-like structures are smectites (*32*). After reaction with STW, we still see distinct plate-like features of the original clay minerals, but, in addition, there occur spherical and rod-shaped structures (Figure 5). These new morphologies are typical for sodalite (ball-shaped) and cancrinite (rod-shaped) minerals (*12, 13*). These new minerals seem to nucleate and grow out of the platy structures of the original clay minerals, although it is also likely that particles have aggregated when colloidal suspensions dried on the electron microscopy stubs. There appears to be no significant morphological differences among the different tank waste compositions. Figure 5

Electron micrographs of colloids formed from sediment after 25 days of reaction time with STW1 illustrate how the secondary minerals are formed (Figure 6). The spherical structures, associated with sodalite, clearly grow out of the plate-like structures of the original clay minerals (Figure 6b). This indicates that sodalite and cancrinite are the product of secondary nucleation and not the result of a direct solid state transformation (*12*). A similar observation has been reported from reactions of simulated tank liquors with pure quartz (*13*). The new ball-shaped structures contain mainly Si and Al, with smaller amounts of K, Ca, Fe, and Na, as identified by EDAX. Figure 6

The electrophoretic mobility of the colloidal particles changed considerably after reaction with STW (Figure 7). The unreacted colloids have a negative electrophoretic mobility for pH values ranging from 2.5 to 11, typical for aluminosilicate clays, like kaolinite, smectite, illite, and chlorite (*33*). The mobility becomes less negative at low pH due to protonation of edge sites or dissolution-exchange reactions with Al (*34*). The charge reversal observed between pH 6 and 8 is probably due to an artifact resulting from dissolution of the feldspathoids and formation of poorly crystalline aluminosilicates (allophane) and/or aluminum hydroxide at lower pH values.

At higher pH, the particles remain negatively charged and have a similar electrophoretic mobility to the unreacted colloids, although slightly more negative. Based on the results from XRD, FTIR, and electron microscopy, we know that the reacted colloids are a composite of unreacted, native minerals, altered native minerals, and secondary mineral phases. The electrophoretic mobility measured is an average of these composite samples, and does not represent the mobility of any individual mineral phase.

The negative charge on the colloids at pH values typical for the vadose zone at Hanford (pH $>$ 7.5) suggests that the colloids (1) are likely to form relatively stable suspensions, (2) are not electrostatically attracted to the predominantly negatively charged surfaces of Hanford sediments, and (3) cations such as Cs^+ and Sr^{2+} will be electrostatically attracted to the colloids.

Thermodynamic Modeling. The results of the thermodynamic modeling showed that, despite the very high dissolved silica concentrations after reactions of simulated tank solutions with sediments, the dominant aqueous species in solution were monomeric (i.e., the $H_2SiO_4^{2-}$ species). Monomeric species accounted for 75 to 85% of the total silica species

in solution. The most important polysilicate species were the linear and cyclic trimers (*21*). The high base concentration (0.3 to 0.8 M) enhanced the formation of $H_2SiO_4{}^{2-}$ from the polysilicates via reactions such as,

$$Si_3O_6(OH)_3^{3-}(\text{cyclic}) + 3OH^- = 3H_2SiO_4^{2-}.$$

The calculations also indicated that both forms of nitrate-cancrinite and sodalite were close to equilibrium, but all of the solutions were slightly oversaturated with respect to these minerals (Table 4). In the case of nitrate-cancrinite the calculated oversaturation could result from the use of a solubility product for these phases determined at 89°C rather than the experimental temperature of 50°C. It could also result from differences in the nature of the solids in this study. In any event, the thermodynamic modeling results indicate that precipitation of sodium aluminum silicate phases is indicated for these solutions, in agreement with the experimental observations. Table 4

Implications for Hanford Tank Leaks

When solutions leak from Hanford waste tanks, native minerals are partially dissolved, releasing Si into the solution phase, and secondary mineral phases—cancrinite and sodalite—are formed. In addition, upon titration of the high pH solutions to pH 8, silica gel precipitates. The newly formed minerals are in the colloidal size range and carry a negative net charge within the pH range found in natural Hanford sediments. Contaminant cations, such as ^{137}Cs are likely to sorb to the newly formed minerals. If these colloids can move through the sediments, there exists the potential for colloid-assisted radionuclide transport at Hanford. Dissolution and precipitation of minerals due to the extreme chemical nature of the waste

tank solutions needs to be considered in the characterization and interpretation of Hanford tank leaks.

Acknowledgments

This work was supported by the Environmental Management Science Program, U.S. Department of Energy under contract DE-FG07-99ER62882. We thank Jeff Boyle (Washington State University, WSU) for his help with XRD and cesium measurements, the Electron Microscopy Center at WSU for use of their facility, Dan Mitchell for the NMR work, Dan Strawn for the use of FTIR, and John Zachara and Jeff Serne (Pacific Northwest National Laboratory) for providing us with the Hanford sediments.

Literature Cited

(1) Gephart, R. E.; Lundgren, R. E. *Hanford Tank Cleanup: A Guide to Understanding the Technical Issues*, 4th ed.; Battelle Press: Columbus, 1998.

(2) Serne, R. J.; Clayton, R. E.; Kutnyakov, I. V.; Last, G. V.; LeGore, V. L.; Wilson, T. C.; Schaef, H. T.; O'Hara, M. J.; Wagnon, K. B.; Lanigan, D. C.; Brown, C. F.; Williams, B. A.; Lindenmeier, C. W.; Orr, R. D.; Burke, D. S.; Ainsworth, C. C. *Characterization of Vadose Zone Sediment: Borehole 41-09-39 in the S-SX Waste Management Area*; Pacific Northwest National Laboratory, US Department of Energy, PNNL-13757-3: Richland, Washington, 2002.

(3) Serne, R. J.; Clayton, R. E.; Kutnyakov, I. V.; Last, G. V.; LeGore, V. L.; Wilson, T. C.; Schaef, H. T.; O'Hara, M. J.; Wagnon, K. B.; Lanigan, D. C.; Brown, C. F.; Williams, B. A.; Lindenmeier, C. W.; Orr, R. D.; Burke, D. S.; Ainsworth, C. C. *Characterization of Vadose Zone Sediment: Slant Borehole SX-108 in the S-SX Waste Management Area*; Pacific Northwest National Laboratory, US Department of Energy, PNNL-13757-4: Richland, Washington, 2002.

(4) Zachara, J. M.; Smith, S. C.; Liu, C.; McKinley, J. P.; Serne, R. J.; Gassman, P. L. *Geochim. Cosmochim. Acta* **2002**, *66*, 193–211.

(5) Knepp, A. J. *Field Investigation Report for Waste Management Area S-SX*; RPP-7884, Rev. 0, CH2M HILL Hanford Group, Inc.: Richland, Washington, 2002.

(6) Steefel, C. I.; Carroll, S.; Zhao, P.; Roberts, S. *J. Contam. Hydrol.* **2003**, *65*, in press.

(7) Serne, R. J.; Zachara, J. M.; Burke, D. S. *Chemical Information on Tank Supernatants, Cs Adsorption from Tank Liquids onto Hanford Sediments, and Field Observations of*

Cs Migration from Past Tank Leaks; Pacific Northwest National Laboratory, PNNL-11495/UC-510: Richland, WA, 1998.

(8) Lichtner, P.; Felmy, A. *Computers Geosci.* **2003**, *29*, 371–383.

(9) Brady, P. V.; Walter, J. V. *Geochim. Cosmochim. Acta* **1989**, *53*, 2823–2830.

(10) Kaplan, D. I.; Parker, K. E.; Ritter, J. C. *Effects of Aging Quartz Sand and Hanford Sediment with Sodium Hydroxide on Radionuclide Sorption Coefficients and Sediment Physical and Hydrologic Properties: Final Report for Subtask 2a.*; Pacific Northwest National Laboratory, US Department of Energy, PNNL-11965: Richland, Washington, 1998.

(11) Barrer, R. M. *Hydrothermal Chemistry of Zeolites*; Academic Press: London, 1982.

(12) Barnes, M. C.; Addai-Mensah, J.; Gerson, A. R. *Microporous Mesoporous Mat.* **1999**, *31*, 287–302.

(13) Bickmore, B. R.; Nagy, K. L.; Young, J. S.; Drexler, J. W. *Environ. Sci. Technol.* **2001**, *35*, 4481–4486.

(14) Chorover, J.; Choi, S.; Amistadi, M. K.; Karthikeyan, K. G.; Crosson, G.; Mueller, K. T. *Environ. Sci. Technol.* **2003**, *37*, 2200–2208.

(15) Serne, R. J.; Bjornstad, B. N.; Schaef, H. T.; Williams, B. A.; Lanigan, D. C.; Horton, D. G.; Clayton, R. E.; Mitroshkov, A. V.; LeGore, V. L.; O'Hara, M. J.; Brown, C. F.; Parker, K. E.; Kutnyakov, I. V.; Serne, J. N.; Last, G. V.; Smith, S. C.; Lindenmeier, C. W.; Zachara, J. M.; Burke, D. S. *Characterization of Vadose Zone Sediment: Uncontaminated RCRA Borehole Core Samples and Composite Samples*; Pacific Northwest

National Laboratory, US Department of Energy, PNNL-13757-1: Richland, Washington, 2002.

(16) Cady, J. G.; Wilding, L. P.; Drees, L. R. In *Methods of Soil Analysis. Part 1. Physical and Mineralogical Methods*; Klute, A., Ed.; American Society of Agronomy: Madison, Wisconsin, 1986; 2nd ed., pp 185–218.

(17) Gardner, M. G.; Reynolds, K. D. *SX-108 Slant Borehole Completion Report*; prepared for CH2M HILL Hanford Group, Inc., Single Shell Tank Farms Vadose Zone Program by Waste Management Technical Services, Report No. RPP-6917, Rev. 0: Richland, WA, 2000.

(18) Pruess, K.; Yabusaki, S.; Steefel, C. I.; Lichtner, P. C. *Vadose Zone J.* **2002**, *1*, 68-88.

(19) Felmy, A. R. In *Chemical Equilibrium and Reaction Models*; Soil Science Society of America, Special Publication 42: Madison, WI, 1995; pp 377–407.

(20) Wesolowski, D. J. *Geochim. Cosmochim. Acta* **1992**, *56*, 1065–1091.

(21) Felmy, A. R.; Cho, H. M.; Rustad, J. R.; Mason, M. J. *J. Solution Chem.* **2001**, *30*, 509–525.

(22) Park, H.; Englezos, P. *Industrial Eng. Chemical Resourc.* **1999**, *38*, 4959–4965.

(23) Borchardt, G. In *Minerals in the Soil Environment*; Dixon, J. B.; Weed, S. B., Eds.; Soil Science Society of America: Madison, WI, 1989; pp 675–727.

(24) Barrer, R. M.; Cole, J. F.; Villiger, H. *J. Chem. Soc. A* **1970**, 1523–1531.

(25) Moenke, H. H. In *The Infrared Spectra of Minerals*; Farmer, V. C., Ed.; Mineralogical Society: London, 1974; pp 365–382.

(26) Buhl, J. C.; Stief, F.; Fechtelkord, M.; Gesing, T. M.; Taphorn, U.; Taake, C. *J. Alloys Compounds* **2000**, *305*, 93–102.

(27) Farmer, V. C.; McHardy, W. J.; Palmieri, F.; Violante, A.; Violante, P. *Soil Sci. Soc. Am. J.* **1991**, *55*, 1162–1166.

(28) Whittington, B. I.; Fletcher, B. L.; Talbot, C. *Hydrometallurgy* **1998**, *49*, 1–22.

(29) Wilson, M. A. *NMR Techniques and Applications in Geochemistry and Soil Chemistry*; Pergamon Press: Oxford, 1987.

(30) Kinsey, R. A.; Kirkpatrick, R. J.; Hower, J.; Smith, K. A.; Oldfield, E. *Am. Mineral.* **1985**, *70*, 537–548.

(31) Buhl, J.-C.; Löns, J. *J. Alloys Compounds* **1996**, *235*, 41–47.

(32) McHardy, W. J.; Birnie, A. C. In *A Handbook of Determinative Methods in Clay Mineralogy*; Wilson, M. J., Ed.; Chapman and Hall: New York, 1987; pp 174–208.

(33) McBride, M. B. In *Minerals in the Soil Environment*; Dixon, J. B.; Weed, S. B., Eds.; Soil Science Society of America: Madison, WI, 1989; pp 35–88.

(34) Swartzen-Allen, S. L.; Matijevic, E. *Chem. Rev.* **1974**, *74*, 385–400.

(35) Loeppert, R. H.; Inskeep, W. P. In *Methods of Soil Analysis. Part 3. Chemical Methods*; Sparks, D. L., Ed.; American Society of Agronomy: Madison, Wisconsin, 1996; pp 639–664.

Table 1. Composition of simulated tank waste (STW), prepared at room temperature (20 to 22°C), and experimental conditions of batch experiments.

Designation of solution	NaOH	$NaAlO_4$ (mol/kg)	$NaNO_3$	pH	Density (20°C) (kg/L)	Temperature[a] (°C)	Time[a] (days)	Designation of colloids formed
Control[b]	0	0	0	7.1[b]	0.99	50	40	colloid 0
STW1	1.4	0.125	3.7	14.2[c]	1.20	50	25, 40	colloid 1
STW2	2.8	0.125	3.7	14.5[c]	1.40	50	40	colloid 2
STW3	1.4	0.25	3.7	14.2[c]	1.30	50	40	colloid 3
STW4	2.8	0.25	3.7	14.5[c]	1.40	50	40	colloid 4

[a]Temperature and duration of batch reactions with sediments.

[b]Distilled water.

[c]Determined by titration which measures non-carbonate alkalinity (NCA), values reported are $14 + \log_{10}(\text{NCA})$.

Table 2. Selected properties of Hanford sediments (diameter < 2 mm).

Attribute	Value
Particle Diameter (% weight)	
$< 2\ \mu$m	1
$2 - 50\ \mu$m	3.8
$50 - 2000\ \mu$m	95.2
Median Diameter[a] (μm)	1369
"Free" Fe[b] (mg/kg)	2307.6
Organic Carbon[c] (g/kg)	2.19
pH (1:1 w/w H_2O)	7.8
EC (dS/m)	0.24
Clay Mineralogy	kaolinite, illite, chlorite, smectite
Primary Minerals	quartz, christobalite, amphibole, plagioclase, feldspar, mica, magnetite, microcline, albite

[a]By weight.

[b]Citrate-bicarbonate-dithionite method (*35*).

[c]Dry combustion using a LECO CNS 2000 Analyzer, St. Joseph, MI.

Table 3. Measured chemical composition of the solution following reaction of simulated tank wastes (STWs) with Hanford sediments at 50°C for 40 days.

Designation	Al	Ca	Fe	K	Mg	Si	Na	NO_3	CO_3	NCA[a]
	mol/kg									
Control	0	3.9×10^{-4}	0	7×10^{-5}	1.3×10^{-4}	0.0010	4.2×10^{-4}	0	0	7.1×10^{-7}
STW 1	0.0015	5.3×10^{-5}	0.0035	0.030	8.4×10^{-6}	0.2516	2.542	2.0642	0.0274	0.6254
STW 2	0.0008	1.1×10^{-5}	0.0021	0.031	8.1×10^{-5}	0.3129	2.669	1.6276	0.0427	1.1682
STW 3	0.0006	2.3×10^{-5}	0.0018	0.027	3.6×10^{-5}	0.1948	2.326	2.0096	0.0299	0.6026
STW 4	0.0008	2.1×10^{-5}	0.0018	0.033	6.0×10^{-5}	0.2704	2.691	1.8323	0.0320	1.0871

[a]NCA: non-carbonate alkalinity

Table 4. Calculated saturation indices[a] for sodium aluminosilicates. Solution compositions are given in Table 3.

Solution	Saturation Index		
	Low OH Cancrinite[a]	High OH Cancrinite[a]	Sodalite
STW 1	0.26	0.43	0.79
STW 2	0.12	0.29	0.65
STW 3	0.15	0.32	0.65
STW 4	0.14	0.29	0.65

[a] The saturation index is defined as (Log IAP/K)/N. Where IAP is the ion activity product, K is the thermodynamic equilibrium constant, and N is the number of ions in the dissolution reaction.

[b] Based on equilibrium constants from Bickmore et al. (*13*) for solutions of 0.1 m OH^- (log K_{eq} = 30.4) and 1.0 m OH^- (log K_{eq} = 36.2).

Figures

Figure 1. Measured concentrations of (a) Al and (b) Si and (c) non-carbonate alkalinity in solutions from batch reactions of Hanford sediments with simulated tank waste after 40-days reaction time at 50°C. The percentages shown for Al are percentages of Al remaining from the initial solutions; the inner bars for the alkalinity show the initial alkalinity of the solutions.

Figure 2. Amount of colloids (diameter $< 2\ \mu$m) present after 40-days reaction time at 50°C in (a) reacted Hanford sediments and (b) from solution after titration to pH 8.

Figure 3. XRD patterns of unreacted and reacted Hanford sediments at 50°C after 40-days reaction time. Vertical lines are characteristic spacings for nitrate-cancrinite and sodalite.

Figure 4. FTIR spectra of unreacted and reacted Hanford sediments at 50°C after 40-days reaction time.

Figure 5. Scanning electron images of colloidal material in unreacted and reacted Hanford sediments following 40-days reaction time at 50°C. Images were taken at 20 kV.

Figure 6. Scanning electron images of colloidal material in reacted Hanford sediments with STW1 following 25-days reaction time at 50°C. Images were taken at 20 kV.

Figure 7. Electrophoretic mobility of colloidal material in unreacted and reacted Hanford sediments following 40-days reaction time at 50°C. Measurements were made in 0.001 M $NaNO_3$ electrolyte.

—Figures—

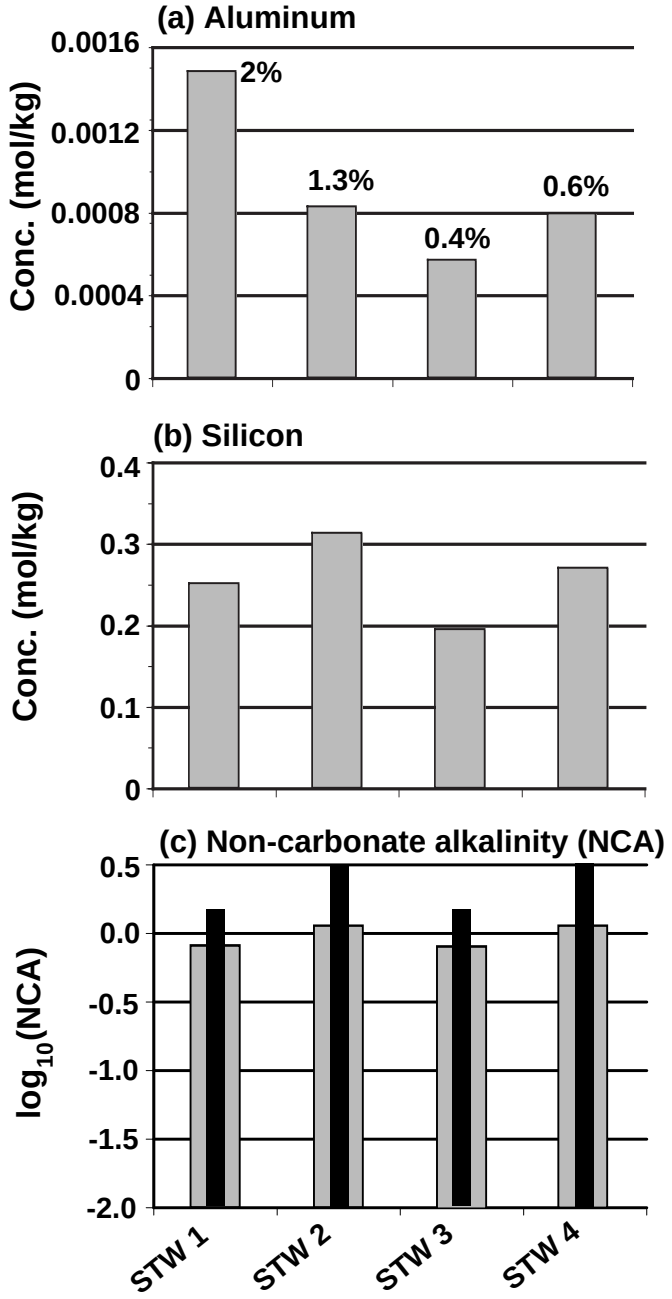

Figure 1. Measured concentrations of (a) Al and (b) Si and (c) non-carbonate alkalinity in solutions from batch reactions of Hanford sediments with simulated tank waste after 40-days reaction time at 50°C. The percentages shown for Al are percentages of Al remaining from the initial solutions; the inner bars for the alkalinity show the initial alkalinity of the solutions.

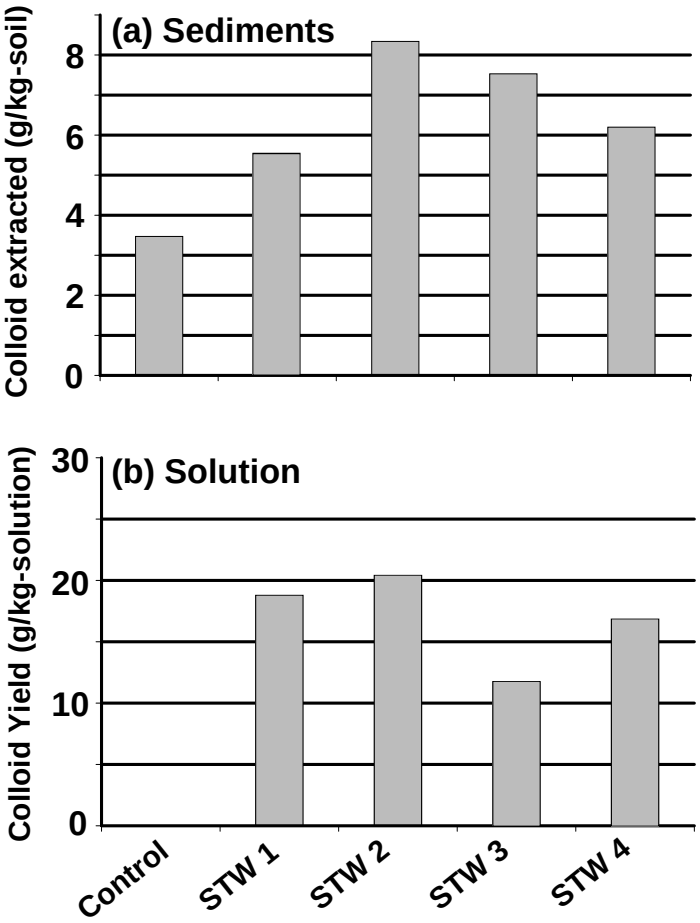

Figure 2. Amount of colloids (diameter $< 2\ \mu$m) present after 40-days reaction time at 50°C in (a) reacted Hanford sediments and (b) from solution after titration to pH 8.

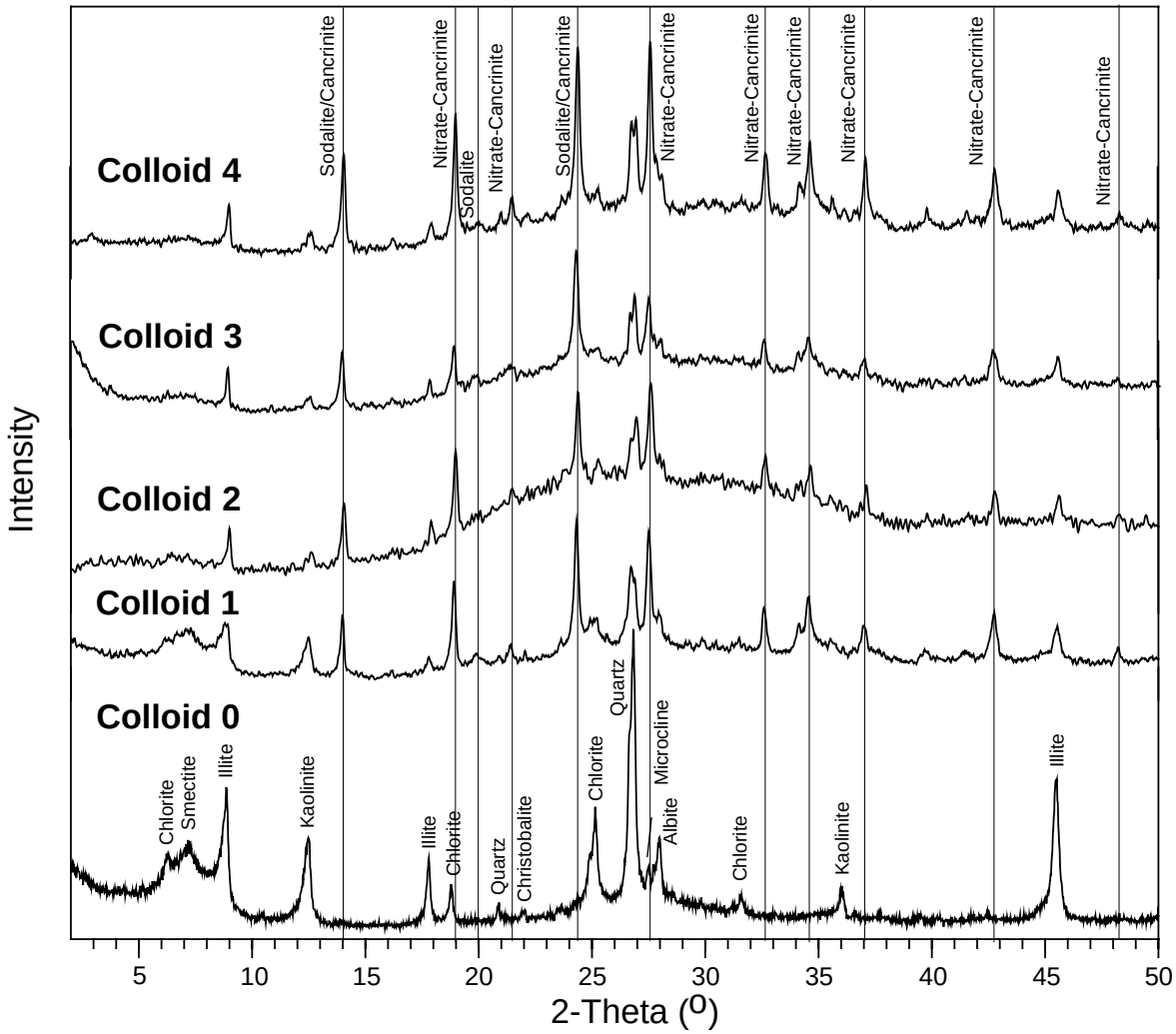

Figure 3. XRD patterns of unreacted and reacted Hanford sediments at 50°C after 40-days reaction time. Vertical lines are characteristic spacings for nitrate-cancrinite and sodalite.

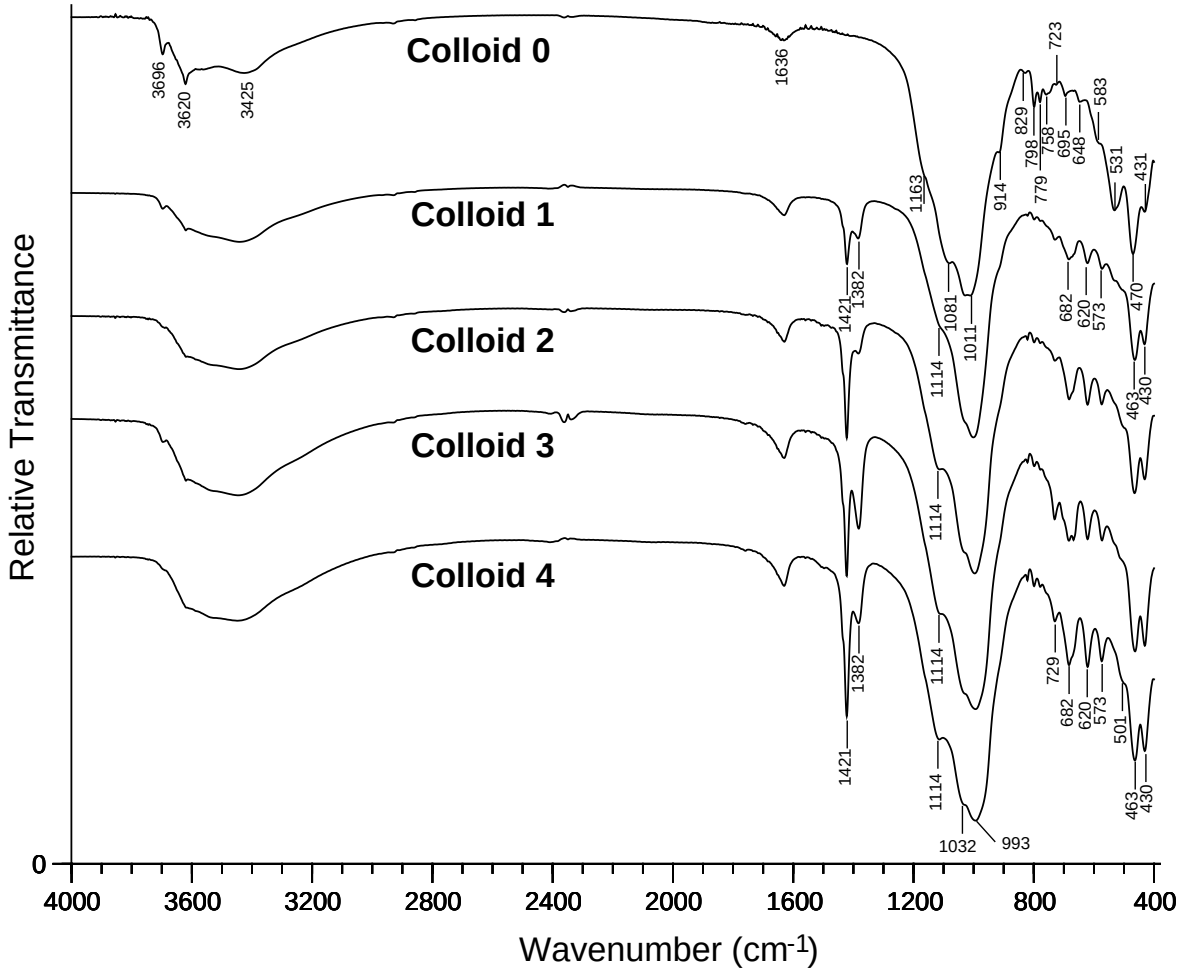

Figure 4. FTIR spectra of unreacted and reacted Hanford sediments at 50°C after 40-days reaction time.

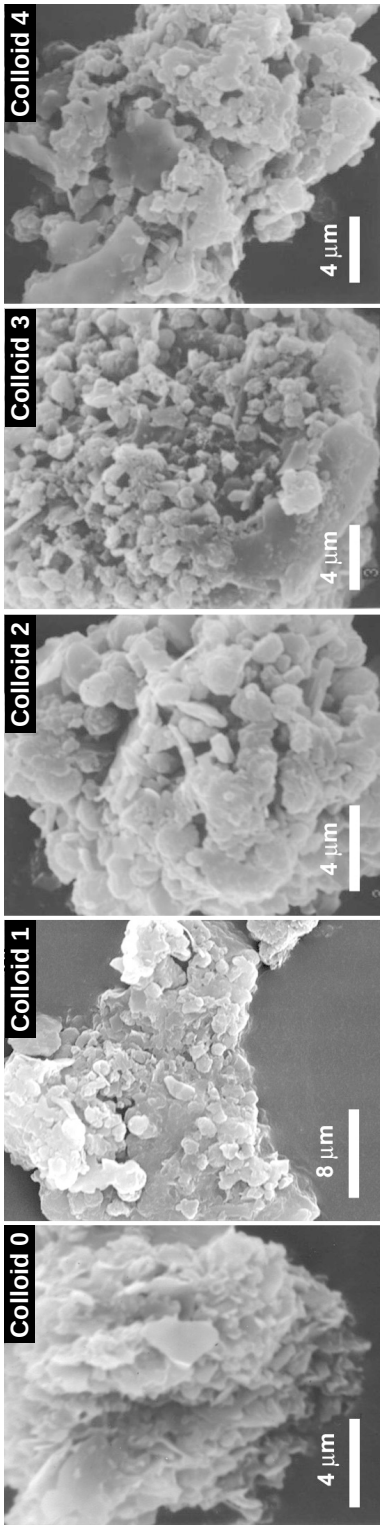

Figure 5. Scanning electron images of colloidal material in unreacted and reacted Hanford sediments following 40-days reaction time at 50°C. Images were taken at 20 kV.

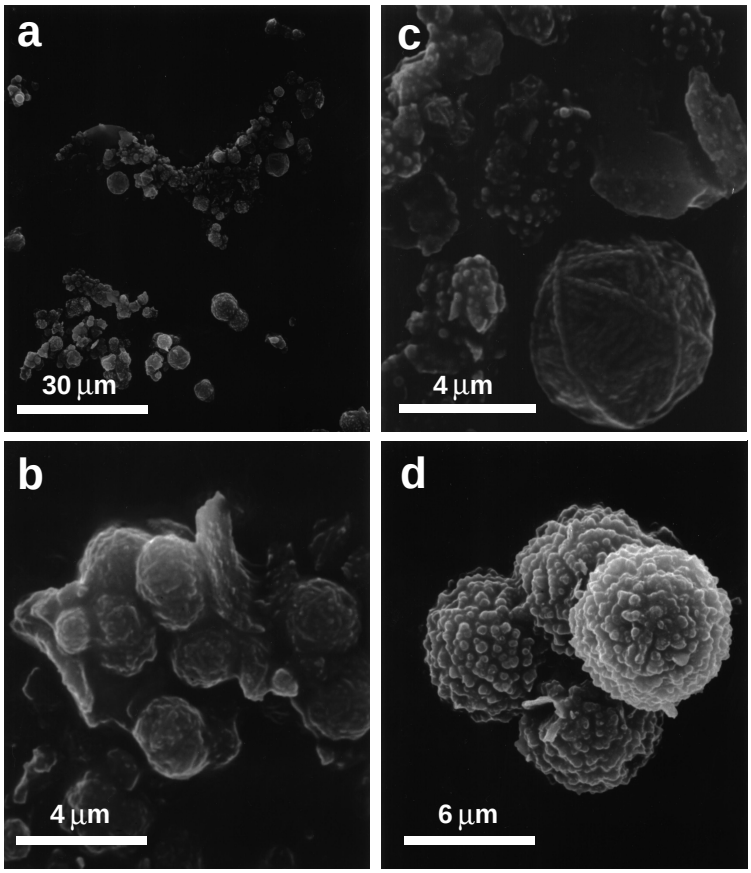

Figure 6. Scanning electron images of colloidal material in reacted Hanford sediments with STW1 following 25-days reaction time at 50°C. Images were taken at 20 kV.

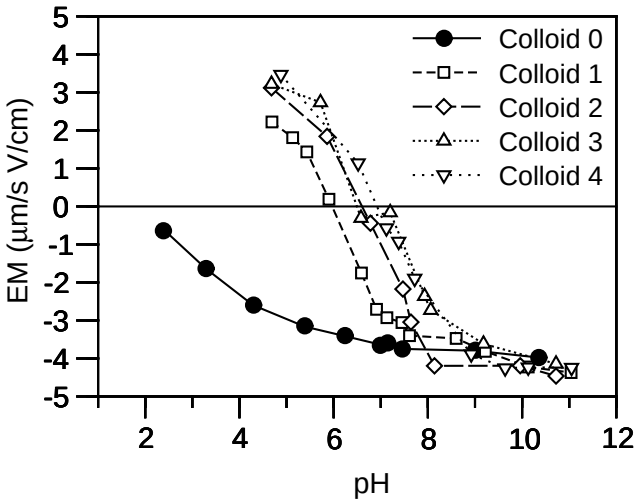

Figure 7. Electrophoretic mobility of colloidal material in unreacted and reacted Hanford sediments following 40-days reaction time at 50°C. Measurements were made in 0.001 M $NaNO_3$ electrolyte.

Comparison of Hanford Colloids and Kaolinite Transport in Porous Media

Jie Zhuang[1], Yan Jin[1*], and Markus Flury[2]

[1]*Department of Plant and Soil Sciences, University of Delaware, Newark, Delaware 19717*

[2]*Department of Crop and Soil Sciences, Center of Multiphase Environmental Research, Washington State University, Pullman, Washington 99164*

ABSTRACT

Understanding colloid transport at the Hanford site in Washington State is critical in assessing migration of radionuclides because colloid transport is a potential means for facilitated off-site migration of radioactive wastes. In this study, eight saturated column experiments were conducted to investigate transport of Hanford colloids and a model colloid (kaolinite) through two types of porous media (Hanford sediments characteristic of 2:1 clay minerals and silica Accusand). Experiments were conducted at a pH value of 10 to mimic the conditions at the Hanford site. The Hanford colloids used were obtained by reacting Hanford sediments with simulated tank waste solutions. The results show that factors influencing transport of Hanford colloids and kaolinite include flow velocity, solution ionic strength, medium type, and colloid properties. Hanford colloids exhibited higher deposition rates than kaolinite in both Hanford sediments and Accusand. Likewise, Hanford sediments retained more colloids than did the silica Accusand. Comparison of transport behaviors of the two colloids through two sands supports the assumption that

chemical heterogeneity is important in controlling particle-particle and particle-collector interactions in colloid retention and transport.

INTRODUCTION

Colloids are ubiquitously present in subsurface formations and are formed in situ through geochemical alterations of primary minerals (McCarthy and Zachara, 1989). Colloid transport and its potential to enhance subsurface contaminant transport have been well-documented (Mills et al., 1991; Ryan and Elimelech, 1996; Kretzschmar et al., 1999; Ryan et al., 2000; McGechan and Lewis, 2002). Colloid-facilitated transport has been recognized to be an important mechanism controlling migration of strongly sorbing contaminants in subsurface environments (Ramsay, 1988; Grolimund et al., 1996; Saiers and Hornberger, 1996; Zhuang et al., 2003).

Colloid deposition kinetics in natural and model porous media has been studied as a function of colloid size, colloid type, surface properties, flow velocity, water content, pore size, and solution chemistry (Goldenberg et al., 1989; Elimelech and O'Melia, 1990a,b; McDowell-Boyer, 1992; Wan and Tokunaga, 1997; James and Chrysikopoulos, 2000; Gamerdinger and Kaplan, 2001; Lenhart and Saiers, 2002). Although great advancements have been made on colloid reaction and transport in porous media, both theoretically and experimentally, our understanding of colloid-soil interactions and our ability to predict transport of colloids in natural subsurface media are limited. In many of the studies conducted to date, model colloids (latex microspheres, silica and pure mineral colloids) and model porous media have been used to study colloid or colloid-facilitated contaminant transport (Kretzschmar et al., 1999). These colloids, however, are not

necessarily good surrogates for colloids that are found in the natural environment (Grolimund et al., 1998) because surface properties of model colloids are different from those colloids that are heterogeneous in composition and properties.

The objective of this study was to examine how transport of Hanford colloids, which are heterogeneous in nature, is influenced by flow velocity, solution ionic strength, and matrix properties. We also included kaolinite in the study to provide a systematic comparison on transport behavior between chemically heterogeneous Hanford colloids and a relatively homogenous mineral colloid kaolinite.

THEORY

Calculation of Colloid Attachment Efficiency (α) and Travel Distance (L_T)

Colloid deposition in porous media can be described by the following equation (Yao et al. 1971; O'Melia, 1990):

$$\frac{dC}{dx} = -\frac{3}{2}\alpha\eta\frac{(1-\varepsilon)}{d_g}C \tag{1}$$

where C is colloid concentration (mg/L), d_g the diameter of collectors (sand grains) (m), ε the porosity of porous medium (m^3/m^3), η the collector efficiency, and α the attachment efficiency, both of which are dimensionless.

The collector efficiency (η) describes the approach of colloids to the collector surface. It can be determined from (Rajagopalan and Tien, 1976; Logan et al., 1995):

$$\eta = 4A_s^{1/3}N_{Pe}^{-2/3} + A_s N_{Lo}^{1/8} N_R^{15/8} + 0.00338 A_s N_G^{1.2} N_R^{-0.4} \tag{2}$$

where A_s is Happel's porosity-dependent parameter, accounting for the influence of neighboring collectors on the flow, and N_{Pe}, N_{Lo}, N_R, and N_G are dimensionless parameters

accounting for colloid-collector collisions due to diffusion, London-van der Waals interactions, interception, and sedimentation, respectively. A_s can be calculated by $A_s = 2(1 - \gamma^5)/(2 - 3\gamma + 3\gamma^5 - 2\gamma^6)$, where $\gamma = (1 - \varepsilon)^{3}$. The diffusion term is given by the Peclet number, $N_{pe} = qd_g/D_p$, where q is the water flux (m/s) defined as $q = v\varepsilon$ with v being the pore water velocity, and D_p is the aqueous diffusion coefficient of colloidal particles. The diffusion coefficient D_p can be calculated from the Stokes-Einstein equation $D_p = B_zT/(3\pi\mu d_c)$, where B_z is the Boltzmann constant ($1.38\text{x}10^{-23}$ J/K), T is the absolute temperature (K), d_c is the diameter (m) of colloidal particles, and μ is the dynamic viscosity ($1.025 \text{ x } 10^{-3}$ kg/(m s) at 20°C) The interception and sedimentation terms are defined as $N_R = d_c/d_g$, and $N_G = g(\rho_c\text{-}\rho_f)/(18\mu d_c^2 q)$, respectively, where ρ_c is the colloid density (kg/m^3), ρ_f is the fluid density (kg/m^3), and g is acceleration due to gravity. The term accounting for London-van der Waals interactions is given as $N_{Lo} = 4H/(9\pi\mu q d_c^2)$, where H is the Hamaker constant. For both Hanford sand and Accusand, we used the same Hamaker constant of $1.6\text{x}10^{-21}$ J, which is the measured Hamaker constant (in water) for quartz (Ackler et al. 1996), because H does not vary very much for different materials and we do not know the value for Hanford sand.

The attachment efficiency (α) describes the attachment of colloids to collector surfaces by accounting for electrostatic interactions between colloids and the porous medium. It is the ratio of the number of colloids approaching the collector surface to the number of colloids attached on that surface, and can be calculated by (Yao et al, 1971):

$$\alpha = \frac{2}{3}\frac{d_g}{(1-\varepsilon)}\frac{K_a}{v\eta} \tag{3}$$

where K_a is the deposition rate, defined as $K_a = -(v/L)\ln(C_e/C_0)$, where C_e represents the stable effluent concentration of the colloid (g/m^3), C_0 the influent colloid concentration (g/m^3), and L the column length (m).

Integrating Eq. (1) with the boundary conditions of $C = C_0$ at $x = 0$ and $C = C_L$ at $x = L$ yields (Yao et al., 1971):

$$\ln\left(\frac{C_L}{C_0}\right) = -\left(\frac{3(1-\varepsilon)\alpha\eta L}{2d_g}\right) \tag{4}$$

This equation can be rearranged in terms of column length L and can be used to calculate how far a certain fraction of colloids will move in a porous medium. For this study, we define the distance (L_T) at which 99.9% of colloids (C_L/C_0=0.001) are removed as the maximum travel distance for the colloids.

Calculation of Fractional Surface Coverage (θ)

The dynamics of colloid deposition in porous media can be illustrated by the temporal change of fractional surface coverage of sediment grains. For irreversible colloid deposition on spherical collectors, the dimensionless collector surface coverage (θ) can be estimated as a function of time from experimental results of colloid breakthrough from the porous media according to (Song and Elimelech, 1993a):

$$\theta = \frac{q d_g C_0 \int_0^t (1 - C/C_0)\,dt}{4\rho d_c L(1-\varepsilon)} \tag{5}$$

where ρ is the specific density of the colloids (taken as 2650 kg/m^3), t is time, and we have assumed that the colloidal particles in our experiments are spherical.

It should be noted that filtration theory in its present form is only applicable to ideal systems where colloids are spherical and monodisperse, which is not the case in our

experimental systems, especially with the Hanford colloids. Therefore, the calculated parameters presented in this paper allow only qualitative comparisons between the experiments and should not be used for prediction. Absolute values calculated in this study should be considered with caution.

MATERIALS AND METHODS

Porous Materials and Colloids

Two types of porous materials, Hanford sediments and Accusand, were used in this study. Coarse Hanford sediments, representative of the material underlying the Hanford waste tanks, were obtained from the Submarine Pit (218-E-12B) at the Hanford site, Washington State, USA. The sediments came from the same site as the ones used by Zhuang et al (2003), but from a different layer of the Hanford formation. The sediments had the same mineralogical composition, but a different particle size distribution, as the ones used by Zhuang et al (2003) (Table 1). Detailed characterization of the sediments is given in Serne et al. (2002). The sediments were dry-sieved and the fraction between 0.053 and 2 mm grains (particle size distribution by weight: 0.65% of 0.053-0.3 mm, 4.58% of 0.3-0.5 mm, and 94.77% of 0.5-2.0 mm) was used in the experiments. Accusand, a typical silica sand, was purchased from Unimin Corporation (Le Sueur, MN, USA). Its particle size distribution was 9% of 0.1-0.25 mm, 69.8% of 0.25-0.5 mm, and 21.2% of 0.5-1.0 mm. The two sands were rinsed with deionized water until no particles suspended in the liquid phase as verified by turbidity measurement, and dried at 60°C.

The Hanford colloids used in this study were specially prepared to mimic vadose zone conditions after a waste tank leak. These colloids are considered to represent

colloidal material in Hanford sediments after a tank leak occurred (Zhao et al., 2002; 2004). Hanford colloids were obtained by reacting Hanford sediments with a simulated solution in the waste storage tanks at the Hanford site (Zhao et al., 2002). The procedure is briefly described as follows. First, one liter of the simulated tank solution (2.8 mol/kg NaOH, 0.125 mol/kg $NaAlO_4$, and 3.7 mol/kg $NaNO_3$) was added to 1 kg of the Hanford sediment of sizes smaller than 2 mm. The mixture was kept at 50°C and shaken periodically for 40 d. Then, colloidal particles (diameter <2 μm) were separated by gravity sedimentation. The colloidal particles were equilibrated with 1 M $NaNO_3$ for 24 h, centrifuged, washed and dialyzed against deionized water until the conductivity was less than 0.01 dS/m. By tank solution treatment, some of the native colloidal particles, quartz and kaolinite, partially dissolved and new minerals, cancrinite and sodalite, formed. About 20 g of colloidal material was obtained from 1 kg of Hanford sediment.

The kaolinite particles (diameter <2 μm) were extracted by gravity sedimentation in deionized water from well-crystalline kaolin (KGa-1, Source Clay Minerals Repository, University of Missouri, Columbia MO). Some basic properties of the materials are provided in Table 1.

Transport Experiments

A series of saturated column experiments were performed to investigate effects of flow velocity, solution ionic strength, properties of matrix, and colloid types on colloid deposition and transport (Table 2). The column system used in the study is similar to that illustrated in Jin et al. (2000). The column was made of acrylate, with an inner diameter of 5.1 cm and height of 10.0 cm. In the experiments, a stainless steel screen (0.3 mm mesh size) was placed on the bottom plate for mechanical support. Teflon tubing was used

throughout the system except for a portion of tygon tubing used in the peristaltic pump. When the column was packed, a deaerated $NaNO_3$ background solution (pH 10, either 1 mM, buffered with 0.024 mM mixture of Na_2CO_3 and $NaHCO_3$ or 10 mM, buffered with 0.24 mM mixture of Na_2CO_3 and $NaHCO_3$) was pre-introduced into the column from its bottom to a certain height. Then, the sand was slowly poured into the column as 1-cm increments while stirred with a plastic rod to ensure packing uniformity and to avoid air entrapment in the column.

Before each experiment was run, the deaerated $NaNO_3$ background solution was flushed through the column overnight (at least 15 pore volumes) to precondition the columns for the transport experiments. The flushing removed residual colloids present in the columns, established a steady-state flow, and standardized background ionic strength and pH. The background solution was adjusted to pH 10 to mimic the high pH condition in the pore water at the Hanford site and to avoid dissolution of carbonates from the sediments during the experiments. The input solution, composed of the $NaNO_3$ background solution along with the experimental colloid (50 mg/L) and a chloride tracer (0.68 mM in NaCl), was then pumped into the column at a constant flow rate. For experiments that involved different ionic strengths, we adjusted the concentrations of $NaNO_3$ and the carbonate buffer. The influent reservoir was stirred during the entire experiment. Colloids were infused for 6 to 10 pore volumes, and followed by application of a colloid-free $NaNO_3$ buffer solution until effluent colloid returned to a baseline level that was determined at the beginning of each experiment. During the course of the experiments, effluent samples were collected from the top of the column into 15 mL polypropylene centrifuge tubes in regular time intervals using a fraction collector. The

chloride tracer was analyzed using ion chromatography (Dionex Corporation, Sunnyvale CA). We determined the colloid concentration from predetermined calibration curves by turbidity measurements at 350 nm (Zhuang et al., 2003) using a UV-VIS spectrophotometer (DU Series 640, Beckman Instruments, Inc., Fullerton CA). During the experiments room temperature was 22±1°C.

RESULTS AND DISCUSSION

Effect of Flow Velocity

Fig. 1 illustrates the effect of flow velocity on the transport of both Hanford colloids and kaolinite through Hanford sediments. Colloid breakthrough occurred at about one pore volume, and reached a plateau at 1.4 to 2 pore volumes (Figs. 1a, b). The shape of the breakthrough curves indicates that the initial attachment of colloidal particles on the sand and elution process by colloid-free background solution were insensitive to the change of flow velocity. However, the steady-state breakthrough concentrations (C/C_0) of the two colloids at high velocity were higher than at low velocity, suggesting that a hydrodynamic effect occurred for the colloid attachment. This result agrees with previous studies performed with various colloids and porous media (Goldenberg et al., 1989; Kretzschmar et al., 1997; Compere et al., 2001). A possible mechanism is that high velocity decreased thickness of shear interface of immobile/mobile phase on the sand, and helped the colloids remain in streamlines because of fluid-particle phase stresses, hydrodynamic drag and lift forces. Consequently, high-velocity decreased colloid deposition on the sediment surfaces. The absence of tailing of the breakthrough curves indicates an irreversible sorption of the particles on the sand.

The dynamics of surface coverage (θ) (calculated using Eq. 5) and the relationship between θ and attachment efficiency (α) (calculated using Eq. 3) is determined for the breakthrough experiments. Figs. 1c and d show that the values of θ of both Hanford colloids and kaolinite in the early stage of transport were not affected by flow velocity, indicating that chemical interactions likely dominated the initial sorption process. As shown in Table 2, the colloid Peclet number ($N_{pe} = qd_g/D_p$), which represents influence of hydrodynamic interaction, is about three times larger for the larger kaolinite particles than for Hanford colloids. This suggests that influence of the hydrodynamic interactions is more pronounced for larger particles (Ko et al., 2000).

The θ-α relationship shows how retained particles affect the retention of the subsequent particles approaching the collector surface. Figs. 1e and f indicate that the retained particles blocked attachment of the subsequent particles. For Hanford colloids, at the same fractional surface coverage, their attachment efficiency of colloids was higher at higher flow velocity. This effect of flow velocity agrees with the experimental results of Kretzschmar et al. (1997) with latex colloids and theoretical predictions by Song and Elimelech (1993b) of colloid deposition rate under unfavorable particle-surface interaction conditions. At higher flow velocity, more colloids can stay in the streamlines of flow, and consequently the number of colloids approaching the collector surface was reduced as indicated by the calculated collector efficiency (η) (Table 2). In contrast, kaolinite, with larger sizes than the Hanford colloids, behaved differently. The attachment efficiency (α) of kaolinite decreased as the flow velocity increased during the early stage of transport but was not affected by flow velocity at the plateau stage (Table 2, Fig. 1f). The deposition rate (K_a) increased for both Hanford and kaolinite colloids as the flow rate increased

(Table 2). Song and Elimelech (1993b) concluded that at low to moderate flow velocities (10^{-6} to 10 m/s) the deposition rate of colloids is controlled by both flow intensity and particle-surface interaction and the effects of fluid convection and colloidal interaction cannot be separated.

Effect of Solution Ionic Strength

Solution ionic strength influences electrostatic interactions of particle-surface and particle-particle through charge screening effect. Transport of Hanford colloids and kaolinite through Hanford sediments at two ionic strengths (1 and 10 mM) is compared in Figs. 2a and b. No Hanford colloids broke through the Hanford sand column in 10 mM solution, whereas kaolinite particles exhibited a steady-state breakthrough rate of 0.2 C/C_0 under the same experimental conditions. In 1 mM solution, the maximum effluent concentrations reached ~0.6 C/C_0 for kaolinite particles and ~0.45 C/C_0 for Hanford colloids. Evidently, kaolinite was less filtered than Hanford colloids during the transport, regardless of the larger size of the kaolinite particles. This effect of ionic strength on the transport of both colloids is expected (Elimelich and O'Melia, 1990a). The dynamics of θ (Figs. 2c, d) indicates that increasing ionic strength did not cause a significant change in colloid deposition in the early transport stage. However, in the plateau stage, high ionic strength increased surface coverage by Hanford colloids, but had a minimum effect on kaolinite coverage on the sand. This implies that electrostatic interactions were more dominant for the attachment of Hanford colloids than kaolinite particles. Fig. 2f shows that the attachment efficiency of kaolinite increased as solution ionic strength rose. For Hanford colloids at 10 mM ionic strength, the value of α was equal to one, since screening of surface charge resulted in attachment for every collision. The strong non-linear

relationship of θ-α suggests the involvement of different retention mechanisms at different transport stages.

The influence of ionic strength on colloid mobility can be further illustrated by calculating colloid travel distances using Eq. 4. Table 2 shows that Hanford colloids can travel two meters in 1 mM $NaNO_3$ in Hanford sediments, while kaolinite particles move about three meters before 99.9% of the colloids are captured by the porous media.

Effect of Medium Surface Properties

Breakthrough results of kaolinite and Hanford colloids in two types of sands are plotted in Figs. 3a and b. Different column packing and the use of a peristaltic pump that only could be adjusted incrementally caused the slightly different flow rates between the experiments. The differences in flow rates were small so that they were unlikely to have caused any of the effects discussed below.

Both colloids showed a higher breakthrough from Accusand than from Hanford sand: the steady-state effluent concentration increased by ~0.1 and ~0.2 C/C_0 for Hanford colloid and kaolinite, respectively. A second peak is observed for the colloid breakthrough in Accusand, and we attribute this peak to an experimental artifact. The dynamics of θ, as depicted in Figs. 3c and d, reveals that deposition of both colloids resulted in higher coverages on Hanford sand than on Accusand. In addition, the fractional surface coverages by Hanford colloids on both types of sands were one order of magnitude larger than those of kaolinite. This was likely caused by the more chemical heterogeneous nature of the natural Hanford colloids than the model kaolinite colloids. The slope of the α-θ relationship curves reduced to a constant value at one pore volume (Figs. 3e, f). This indicates a critical point of attachment efficiency (α), at which the decreasing deposition

rate stabilized at a constant value. The attachment efficiency of Hanford colloids leveled off at a larger surface coverage compared to kaolinite. Taking the constant attachment efficiency at the flat portion in Figs. 3e and f as the particle-particle collision efficiency, we see that Hanford colloids stick more easily than kaolinite particles under the same experimental conditions.

Johnson et al. (1996) suggested that geochemical heterogeneity has a profound impact on colloid transport. Capacity of attachment-favorable sites of a collector determines the amount of colloidal particles directly attached on the matrix, and this further influences how many subsequent colloidal particles can be removed from the liquid flowing through the column. Commonly, heterogeneous surfaces possess more favorable settings than relatively uniform surfaces for colloid attachment (Song and Elimelech, 1993a; Johnson and Elimelech, 1995; Johnson et al., 1996; Ren et al., 2000). Hanford sediments have more heterogeneous surfaces, both physically and chemically, than the relatively uniform silica Accusand (Serne et al., 2002; Zhuang et al., 2003). The different types of minerals contained in Hanford sediments, differently exposed crystallographic faces, and irregular surface coatings or cracks have been reported (McKinley et al., 2001; Zachara et al., 2002). Therefore, Hanford sediments likely provided more settings favorable for colloid deposition than the Accusand.

CONCLUDING REMARKS

Comparison of the transport of Hanford colloids and kaolinite through chemically heterogeneous Hanford sand and chemically homogeneous silica sand generated several interesting results. Increased water flow velocity caused more colloids to breakthrough the

Hanford sand and Accusand, and the colloid deposition rate increased as the flow velocity increased. Chemical heterogeneity associated with the Hanford colloids caused stronger particle-particle and particle-matrix interactions than was the case for the more homogeneous kaolinite colloids. Hanford colloids also had higher deposition rates than kaolinite, again due to pronounced chemical heterogeneity. While both hydrodynamic interaction (due to variation of flow velocity) and electrostatic interaction (due to chemical heterogeneity) were involved in the attachment of Hanford colloids, chemical interaction was relatively weak and hydrodynamic interaction probably dominated the attachment of kaolinite particles. Therefore, solution chemistry had more significant effects on the transport of Hanford colloids than kaolinite. The same trend was found on the natural Hanford sand and the model Accusand. This study indicates that several interaction mechanisms might be involved simultaneously during colloid transport, but their relative importance in the overall transport depends on the chemical and physical properties of colloids and transport media as well as the environmental conditions.

ACKNOWLEDGEMENTS

This work was supported by the Environmental Management Science Program, U.S. Department of Energy under Grant No. DE-FG07-99ER62882.

REFERENCES

Ackler, H., R. H. French, and Y. Chiang. 1996. Comparisons of Hamaker constants for ceramic systems with intervening vacuum or water: from force laws and physical properties. J. Colloid Interface Sci. 179: 460-469.

Compere, F., G. Porel, and F. Delay. 2001. Transport and retention of clay particles in saturated porous media: Influence of ionic strength and pore velocity. J. Contamin. Hydrol. 49:1-21.

Elimelech, M., and C.R. O'Melia. 1990a. Kinetics of deposition of colloidal particles in porous-media. Environ. Sci. Technol. 24:1528-1536.

Elimelech, M., and C.R. O'Melia. 1990b. Effect of particle-size on collision efficiency in the deposition of Brownian particles with electrostatic energy barriers. Langmuir 6:1153-1163.

Gamerdinger, A.P., and D.I. Kaplan. 2001. Colloid transport and deposition in water-saturated Yucca Mountain tuff as determined by ionic strength. Environ. Sci. Technol. 35:3326-3331.

Goldenberg, L.C., I. Hutcheon, and N. Wardlaw. 1989. Experiments on transport of hydrophobic particles and gas-bubbles in porous-media. Transport Porous Media 4:129-145.

Grolimund, D., M. Borkovec, K. Barmettler, and H. Sticher. 1996. Colloid-facilitated transport of strongly sorbing contaminants in natural porous media: A laboratory column study. Environ. Sci. Technol. 30:3118-3123.

Grolimund, D., M. Elimelech, M. Borkovec, K. Barmettler, R. Kretzschmar, and H. Sticher. 1998. Transport of in situ mobilized colloidal particles in packed soil columns, Environ. Sci. Technol. 32:3562-3569.

James, S.C., and C.V. Chrysikopoulos. 2000. Transport of polydisperse colloids in a saturated fracture with spatially variable aperture. Water Res. Resour. 36:1457-1465.

Jin, Y., Y. Chu, and Y. Li. 2000. Virus removal and transport in saturated and unsaturated sand columns. J. Contam. Hydrol. 43:111-128.

Johnson, P.R., and M. Elimelech. 1995. Dynamics of colloid deposition in porous media: Blocking based on random sequential adsorption. Langmuir 11:801-812.

Johnson, P.R., N. Sun, and M. Elimelech. 1996. Colloid transport in geochemically heterogeneous porous media: Modeling and measurements. Environ. Sci. Technol. 30:3284-3293.

Ko, C.H., S. Bhattacharjee, and M. Elimelech. 2000. Coupled influence of colloidal and hydrodynamic interactions on the RSA dynamic blocking function for particle deposition onto packed spherical collectors. J. Colloid Interf. Sci. 229:554-567.

Kretzschmar, R., K. Barmettler, D. Grolimund, Y.D. Yan, M. Borkovec, and H. Sticher. 1997. Experimental determination of colloid deposition rates and collision efficiencies in natural porous media. Water Resour. Res. 33:1129-1137.

Kretzschmar, R., M. Borkovec, D. Grolimund, and M. Elimelech. 1999. Mobile subsurface colloids and their role in contaminant transport. Adv. Agron. 66:121-193.

Lenhart, J.J., and J.E. Saiers. 2002. Transport of silica colloids through unsaturated porous media: experimental results and model comparisons. Environ. Sci. Technol. 36:769-777.

Logan, B.E., D.G. Jewett, R.G. Arnold, E.J. Bouwer, and C.R. O'Melia, 1995, Clarification of clean-bed filtration models, J. Environ. Eng. 121:869-873.

McCarthy, J.F., and J.M. Zachara. 1989. Subsurface transport of contaminants-mobile colloids in the subsurface environment may alter the transport of contaminants. Environ. Sci. Technol. 23:496-502.

McDowell-Boyer, L.M. 1992. Chemical mobilization of micro-sized particles in saturated porous media under steady flow conditions. Environ. Sci. Technol. 26:586-593.

McDowell-Boyer, L.M, J.R. Hunt, and N. Sitar. 1986. Particle-transport through porous-media. Water Resour. Res. 22:1901-1921.

McGechan, M.B., and D.R. Lewis. 2002. Transport of particulate and colloid-sorbed contaminants through soil, Part 1: General Principles. Biosystems Engineering 83:255-273.

McKinley, J.P., C.J. Zeissler, J.M. Zachara, R.J. Serne, R.M. Lindstrom, H.T. Schaef, and R.D. Orr. 2001. Distribution and retention of ^{137}Cs in sediments at the Hanford site, Washington. Environ. Sci. Technol. 35:3433-3441.

Mills, W.B., S. Liu, and F.K. Fong. 1991. Literature review and model (COMET) for colloid/metals transport in porous media. Ground Water 29:199-208.

O'Melia, C.R. 1990. Kinetics of colloidal chemical processes in aquatic systems. In: Aquatic Chemical Kinetics: Reaction Rates of Processes in Natural Water (ed. Stumm, W.) Wiley-Interscience, New York, pp. 447-474.

Rajagopalan, R., and C. Tien. 1976. Trajectory analysis of deep-bed filtration with the sphere-in-cell porous media model. AIChE J. 22:523-533.

Ramsay, J.D.F. 1988. The role of colloids in the release of radionuclides from nuclear waste. Radiochim Acta 44/45:165-170.

Ren, J.H., A.I. Packman, and C. Welty. 2000. Correlation of colloid collision efficiency with hydraulic conductivity of silica sands. Water Resour. Res. 36:2493-2500.

Ryan, J.N., and M. Elimelech. 1996. Colloid mobilization and transport in groundwater. Colloid Surf. A 107:1-56.

Ryan, J.N., M. Elimelech, J.L. Baeseman, and R.D. Magelky. 2000. Silica-coated titania and zirconia colloids for subsurface transport field experiments. Environ. Sci. Technol. 34:2000-2005.

Saiers, J.E. and G.M. Hornberger. 1996. The role of colloidal kaolinite in the transport of cesium through laboratory sand columns, Water Resourc. Res. 32:33-41.

Serne, R.J., B.N. Bjornstad, H.T. Schaef, B.A. Williams, D.C. Lanigan, D.G. Horton, R.E. Clayton, A.V. Mitroshkov, V.L. LeGore, M.J. O'Hara, C.F. Brown, K.E. Parker, I.V. Kutnyakov, J.N. Serne, G.V. Last, S.C. Smith, C.W. Lindenmeier, J.M. Zachara, and D.S. Burke. 2002. *Characterization of Vadose Zone Sediment: Uncontaminated RCRA Borehole Core Samples and Composite Samples*; Pacific Northwest National Laboratory, US Department of Energy, PNNL-13757-1: Richland, Washington.

Song, L.F., and M. Elimelech. 1993a. Dynamics of colloid deposition in porous-media-Modeling the role of retained particles. Colloid Surf. A 73:49-63.

Song, L.F., and M. Elimelech. 1993b. Calculation of particle deposition rate under unfavorable particle-surface interactions. J. Chem. Soc. Faraday Trans. 89:3443-3452.

Wan, J., and T. Tokunaga. 1997. Film straining of colloids in unsaturated porous media: Conceptual model and experimental testing. Environ. Sci. Technol. 31:2413-2420.

Yao, K.M., M.T. Habibian, and C.R. O'Melia. 1971. Water and wastewater filtration: concepts and applications. Environ. Sci. Technol. 5:1105-1112.

Zachara, J.M., S.C. Smith, C.X. Liu, J.P. McKinley, R.J. Serne, and P.L. Gassman. 2002. Sorption of Cs+ to micaceous subsurface sediments from the Hanford site, USA. Geochimica et Cosmochimica Acta 66:193-211.

Zhao, H., Y. Deng, J.B. Harsh, M. Flury, and J. Boyle. 2004. Alteration of kaolinite to cancrinite and sodalite by simulated Hanford Tank Wastes and its impact on cesium retention, Clay and Clay Minerals, (in press).

Zhao, H., J.B. Harsh, M. Flury, and K. Mashal. 2002. Alteration of mineralogical and surface properties of Hanford sediments contaminated with tank waste, Abstracts, 222nd ACS National Meeting, August 26-30, Chicago, Illinois.

Zhuang, J., M. Flury, and Y. Jin. 2003. Colloid-facilitated cesium transport through water-saturated Hanford sediments and Ottawa sand. Environ. Sci. Technol. (in press).

Table 1. Some basic properties of the experimental porous media and colloids*

Materials	CEC cmol/kg	Fe_0 mg/kg	OM g/kg	d_g, d_c mm	Mineralogy
Hanford sand	6.6	6461	1.0	1.02	mica, illite, smectite, vermiculite, quartz, feldpars, pyroxene
Accusand	0.6	28.7	0.4	0.44	quartz
Hanford colloid	6.7	56709	-	6.27×10^{-4}	mica, illite, smectite, vermiculite, quartz, cancrinite, sodalite
Kaolinite	2.0	1300	-	1.92×10^{-3}	kaolinite

*CEC: cation exchange capacity; Fe_0: free Fe-oxide; OM: organic matter; d_g: geometric diameter of sand grains; d_c: Z-averaged hydrodynamic diameter of the colloidal particles measured in 2 mM $NaNO_3$ by dynamic light scattering with a Malvern Zetasizer 3000HSA (Malvern Instruments Ltd., England); Mineralogical composition was analyzed with X-ray diffraction.

Table 2. Experimental conditions and parameters

Column Exp.	Sand	Colloid	ε (–)	v (cm/h)	I (mM)	D_p (10^{-13} m^2/s)	N_{pe} (–)	K_a (h^{-1})	η (–)	α (–)	L_T (m)
1	Hanford	Hanford	0.38	2.13	1	6.72	3412	0.20	0.36	0.03	0.74
2	Hanford	Hanford	0.37	4.54	1	6.72	7081	0.35	0.17	0.05	0.89
3	Hanford	Kaolinite	0.41	2.17	1	2.19	11485	0.14	2.07	0.004	1.09
4	Hanford	Kaolinite	0.37	4.54	1	2.19	21684	0.23	1.25	0.004	1.35
5	Hanford	Hanford	0.37	4.54	10	6.72	7081	7.00	0.17	1.00	0.04
6	Hanford	Kaolinite	0.37	4.45	10	2.19	21254	0.72	1.28	0.01	0.43
7	Accusand	Hanford	0.33	5.03	1	6.72	3018	0.29	0.20	0.01	1.19
8	Accusand	Kaolinite	0.32	4.88	1	2.19	8696	0.13	1.39	0.001	2.52

*ε: porosity; v: pore water velocity; I: ionic strength; D_p: colloid diffusion coefficient; N_{pe}: colloid Peclet number; K_a: deposition rate; η: collector efficiency; α: attachment efficiency; L_T: travel distance.

Figure Captions:

Fig. 1. Effect of flow velocity on transport of Hanford colloids and kaolinite through Hanford sand-packed columns in $NaNO_3$ solution (1 mM, pH 10).

Fig. 2. Effect of ionic strength on transport of Hanford colloids and kaolinite through Hanford sand-packed columns in $NaNO_3$ solution (pH 10).

Fig. 3. Transport of Hanford colloids and kaolinite through Hanford sand and Accusand in $NaNO_3$ solution (1 mM, pH 10).

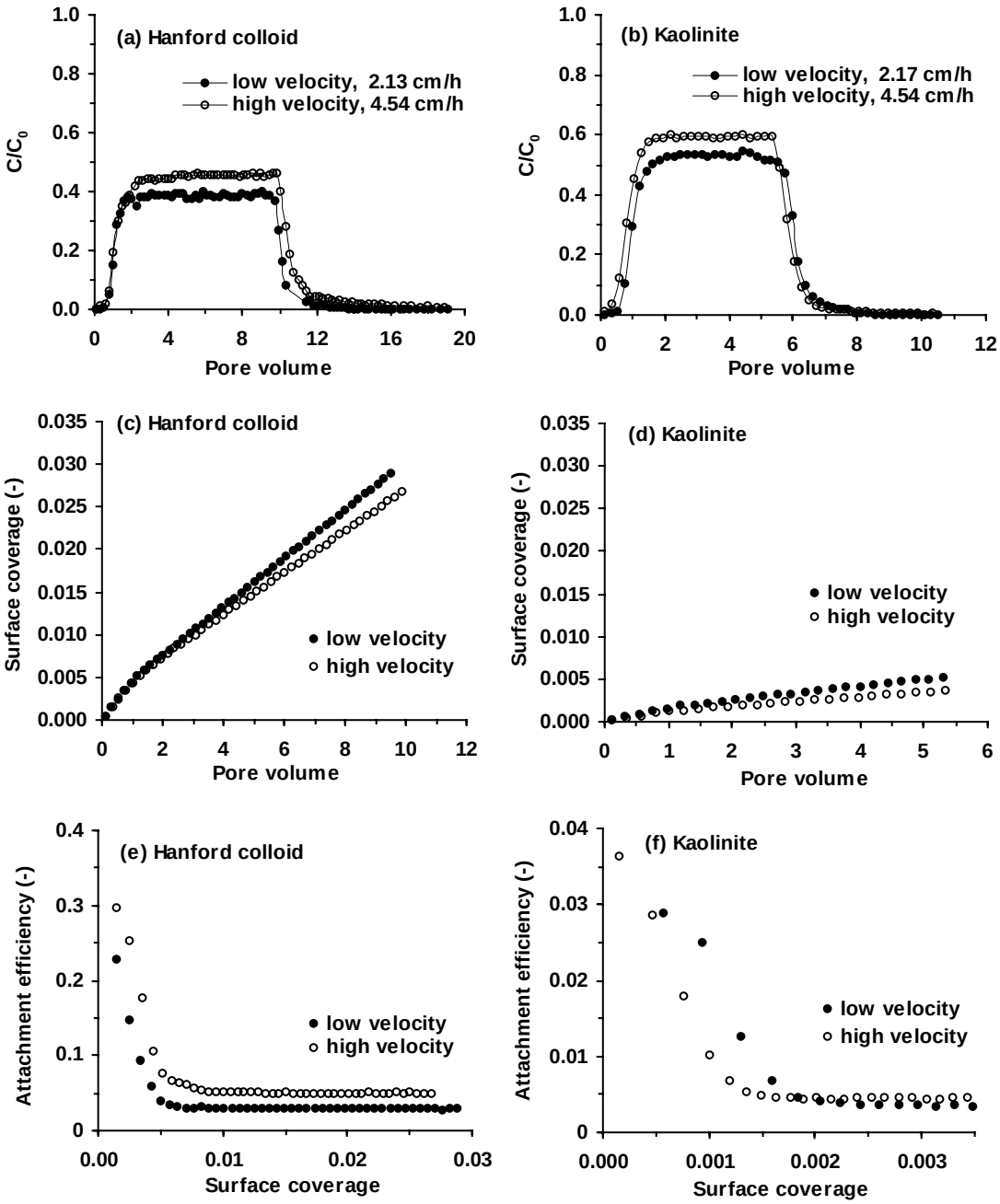
(a) Hanford colloid
low velocity, 2.13 cm/h
high velocity, 4.54 cm/h
C/C0
Pore volume
(b) Kaolinite
low velocity, 2.17 cm/h
high velocity, 4.54 cm/h
C/C0
Pore volume
(c) Hanford colloid
Surface coverage (-)
low velocity
high velocity
Pore volume
(d) Kaolinite
Surface coverage (-)
low velocity
high velocity
Pore volume
(e) Hanford colloid
Attachment efficiency (-)
low velocity
high velocity
Surface coverage
(f) Kaolinite
Attachment efficiency (-)
low velocity
high velocity
Surface coverage

Figure 1

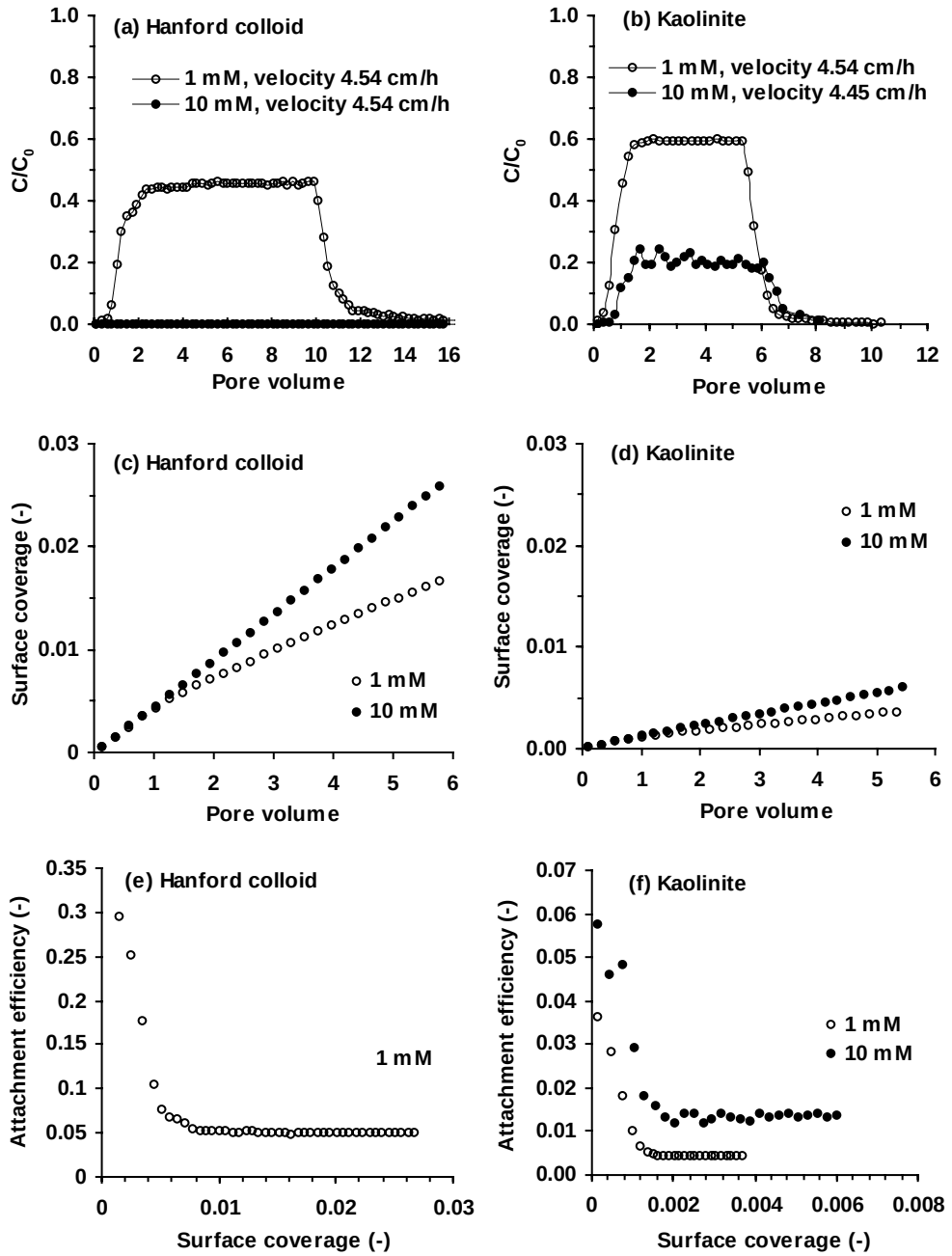
(a) Hanford colloid
1 mM, velocity 4.54 cm/h
10 mM, velocity 4.54 cm/h
C/C0
Pore volume
(b) Kaolinite
1 mM, velocity 4.54 cm/h
10 mM, velocity 4.45 cm/h
C/C0
Pore volume
(c) Hanford colloid
Surface coverage (-)
1 mM
10 mM
Pore volume
(d) Kaolinite
Surface coverage (-)
1 mM
10 mM
Pore volume
(e) Hanford colloid
Attachment efficiency (-)
1 mM
Surface coverage (-)
(f) Kaolinite
Attachment efficiency (-)
1 mM
10 mM
Surface coverage (-)

Figure 2

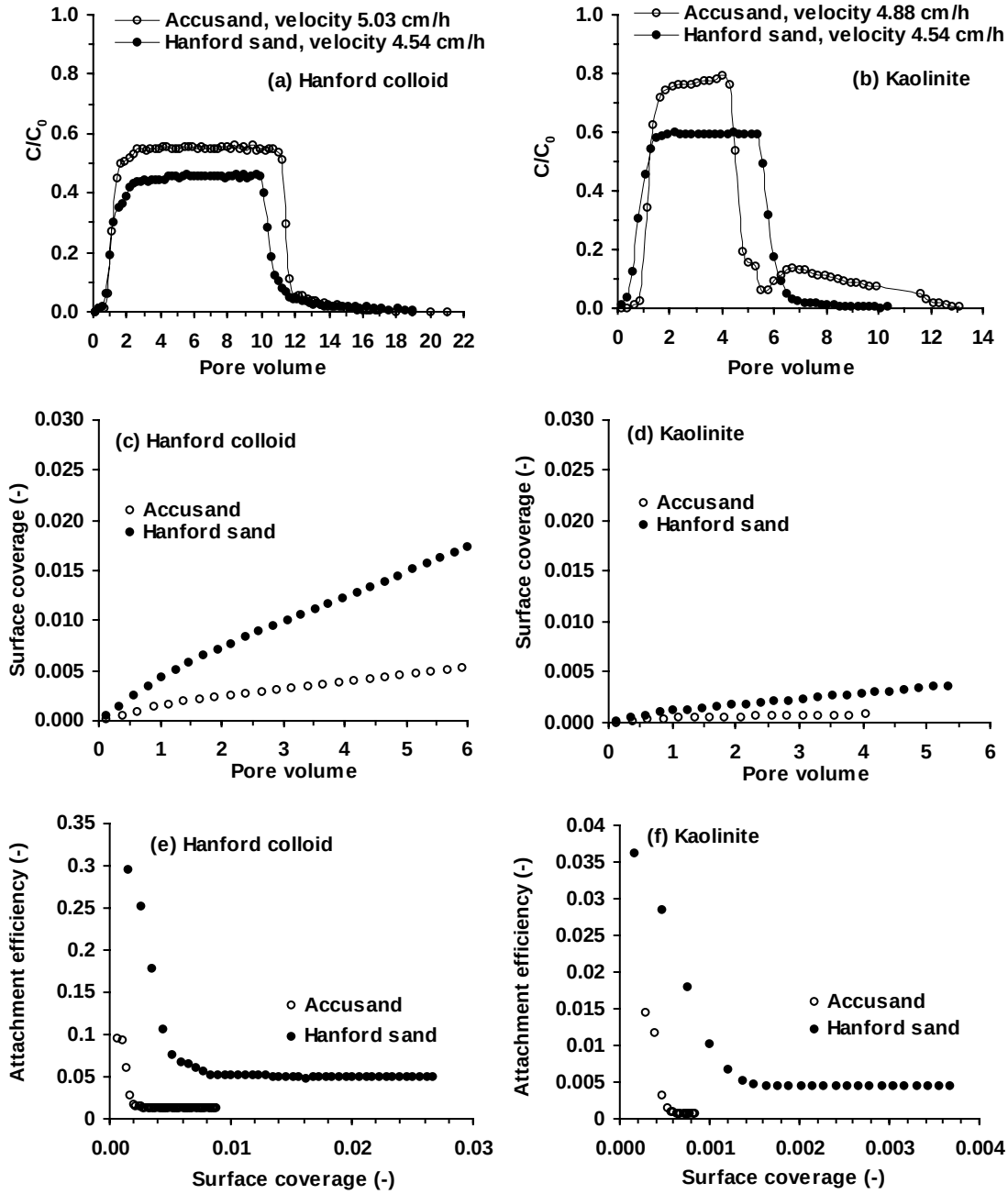
Accusand, velocity 5.03 cm/h
Hanford sand, velocity 4.54 cm/h
(a) Hanford colloid
C/C0
Pore volume
Accusand, velocity 4.88 cm/h
Hanford sand, velocity 4.54 cm/h
(b) Kaolinite
C/C0
Pore volume
(c) Hanford colloid
Accusand
Hanford sand
Surface coverage (-)
Pore volume
(d) Kaolinite
Accusand
Hanford sand
Surface coverage (-)
Pore volume
(e) Hanford colloid
Accusand
Hanford sand
Attachment efficiency (-)
Surface coverage (-)
(f) Kaolinite
Accusand
Hanford sand
Attachment efficiency (-)
Surface coverage (-)

Figure 3